Effect of Mechanical Loading Conditions on Near-neutral pH Stress Corrosion Cracking (NNpHSCC) Initiation and Early-stage Growth for Bent Pipeline

by

Giao Nguyen Hoang Vo

A thesis submitted in partial fulfillment of the requirements for the degree of

Master of Science

in

Materials Engineering

Department of Chemical and Materials Engineering

University of Alberta

ABSTRACT

Near-neutral pH Stress Corrosion Cracking (NNpHSCC) continues causing failures of steel pipelines despite the use of preventative measures such as protective coating and cathodic protection. In pipelines with bends, the issue is more profound as stress is concentrated around the bends and the protective coating layer is more prone to failure there. In this study, axial loads of 50%, 25% and 15% of Specified Minimum Yield Strength (SMYS) were applied to pipe sections bent to 20- and 40-degree angles under a near-neutral pH condition. Pit and crack distribution, as well as pit and crack depth were analyzed. Smaller maximum stresses are found to have a more profound effect on pit and crack initiation at the center of bend. While smaller bending angles experienced less compressive stress and hence pitting initiates more readily on the surface, larger bending angles suggested a more drastic change in residual stress, resulting in more pits and cracks growth. The crack distribution between the two changes near the center of bend, but no difference was found along the length of the pipe. The study also suggested that despite having a compressive residual stress near the center of bend, pits and cracks can still be initiated from the breakage of mill scale exposing the surface of the pipe, and cyclic loading changes the stress distribution along the pipe length and depth, which aids in pit and crack initiation.

Keywords: Circumferential Near-neutral Stress Corrosion Cracking, Axial Bending, Crack Initiation and Stage I Growth, Residual Stress Distribution

PREFACE

This thesis is an original work by Giao Nguyen Hoang Vo. No part of this thesis has been previously published.

ACKNOWLEDGEMENTS

This work could not have been accomplished without the help and support of many individuals. I would like to acknowledge and give my warmest thanks to Dr. Weixing Chen, Dr. Reg Eadie and Dr. Jing Liu for their guidance, assistance, and patience in advising me during this project. I also would like to thank my research associate, Dr. Zhezhu Xu for his assistance with many topics in this project, as well as his guidance in the troubleshooting phase of this project. I also would like to express my appreciation to my SCC research group, Hamed Shirazi, Hiroyuki Tanaka, Dr. Shidong Wang and Greg Nelson for their help in this project.

On a personal note, I would also like to give special thanks to my parents, Dzung Nguyen and Tung Vo, and my family and friends for their continuous support throughout my study.

TABLE OF CONTENTS

LIST OF TABLES

LIST OF FIGURES

LIST OF SYMBOLS AND ABBREVIATIONS

SCC	Stress Corrosion Cracking
NNpH	Near-Neutral pH
NNpHSCC	Near-Neutral pH Stress Corrosion Cracking
NNpHCF	Near-Neutral pH Corrosion Fatigue
EAC	Environmentally Assisted Cracking
CF	Corrosion Fatigue
HIC	Hydrogen-Induced Cracking
SMYS	Specified Minimum Yield Strength
CP	Cathodic Protection
SSRT	Slow Strain Rate Test
API	American Petroleum Institute
CSA	Canadian Standards Association
SMTS	Specified Minimum Tensile Strength
HAZ	Heat Affected Zone
PE	Polyethylene
A-SCC	Axial Stress Corrosion Cracking
C-SCC	Circumferential Stress Corrosion Cracking
FEA	Finite Element Analysis
NDE	Non-Destructive Evaluation
DDT	Distributed Dislocation Technique

SEM	Scanning Electron Microscopy
FEM	Finite Element Method
f	Cyclic loading frequency
R	Cyclic loading amplitude

CHAPTER 1

INTRODUCTION

Pipelines have been one of the most common transportation methods in the oil and gas industry because of their cost-effectiveness in transporting large quantities of flowing matter. With growing technology, pipelines are designed to carry a greater variety of materials with a varying range of inner pressures and temperatures. Over a long distance, pipelines pose a threat to the surrounding environment and people, therefore, they are regulated within standard operations to ensure safety of humans and protect the public and the environment. Coating is a common practice to protect the outer pipeline surface from coming into contact with the surrounding environment, and the use of coating is effective to elongate the pipeline service time. However, after some time in service, coating is defected, and the pipe surface underneath is exposed. In order to protect the exposed pipe surface, cathodic protection is an effective method to prevent corrosion. This method uses a sacrificial anode that is more reactive than the pipe materials that will react and produce ions to the pipe, keeping it from corroding. Normally, two or more preventative methods are used altogether to protect the pipe surface.

Despite the use of one or more preventative methods, pipeline rupture remains an issue that still needs to be addressed. One of the common issues seen in pipelines with damaged coating is stress corrosion cracking (SCC). In this type of environmentally assisted cracking, the susceptible pipeline material underneath the protective coating layer is exposed to the corrosive environment on the outside, along with a stress source, resulting in crack growing and in worse cases, pipe ruptures. Stress factors typically include internal pressure, external force, residual stress, soil movement, etc. In some cases, external forces and soil movement cause the pipe to bend, creating a residual stress at the local bending point.

In North America, stress corrosion cracking is commonly found in near neutral pH environments, and the type of SCC is named near-neutral pH stress corrosion cracking (NNpHSCC). NNpHSCC continues to be an issue after being discovered in the 1980s, because the mechanism of this type of SCC is generally unclear. However, it is believed that NNpHSCC occurs in three stages: I) crack initiation and early-stage growth by dissolution, II) hydrogen-facilitated crack growth and III) unstable crack growth. Pipeline is believed to spend most of its service life in stage I and II. Little study has been done on longitudinally bent pipelines and how bending interacts with the other stress factors, making it challenging to predict SCC in these conditions.

This study focuses on stage I of NNpHSCC, studying how crack initiation is affected with mechanical loading conditions in bent pipelines. As stage I depends mostly on the anodic dissolution, the mechanical effect is believed to be minimized, however, in bent pipelines, mechanical loading affects the residual stress distribution within the pipe, and hence, changes the early-stage initiation. The study aims to understand how changing the maximum load during cyclic loading will affect the residual stress distribution in outward bending conditions. This will provide knowledge on how different mechanical loading conditions affect the crack initiation in NNpH environments.

CHAPTER 2

LITERATURE REVIEW

In this chapter, previous research on near-neutral pH stress corrosion cracking (NNpHSCC) is discussed. An overview of pipelines in Canada, as well as the common issues found in pipelines in Canada are presented. The definition of stress corrosion cracking (SCC) is provided with the two types of SCC. This chapter also includes the factors that affect NNpHSCC, and corrosion fatigue as the highlighted mechanism. Additionally, how residual stress contributes to the stress experienced by the pipeline, as well as crack initiation and growth are also discussed.

2.1 Pipelines in Canada

Oil and gas are a big industries in Canada, more specifically in Alberta, and research on oil and gas pipelines has taken place for many years to ensure pipeline safety and protect the people and environment. There are many subfields within the pipeline integrity field, and many methods have been incorporated to prevent pipeline incidents and protect pipelines, including protective coating, cathodic protection, corrosion inhibition, and inspection [1]. Moreover, research on pipeline integrity issues has developed significantly with more applications and environments being introduced to pipelines. Many new technologies were developed to study pipeline integrity, and the number of failures per length of pipeline related to pipelines in North America has greatly decreased [1].

Pipeline in Canada is an effective method to transport natural gas and high vapour pressure products. Pipeline integrity is crucial to ensure safety of humans and the environment. As pipelines age every year with harsh weather conditions, they are more prone to leakage and failures, and companies need to actively increase the capacity of pipelines to keep original pipelines that are

more than 60 years old in use [2]. Pipelines are susceptible to many degradation mechanisms, one of which is general corrosion. However, corrosion has been a commonly studied issue that is well understood and managed, but another issue arises with stress corrosion cracking (SCC). Cracking is a serious issue in pipelines, because it can happen in an instant, resulting in costly damage and can be dangerous to humans and the environment. Evidence of SCC in Canada has not been in attention until after 1980, where the type of SCC found was not the same as the typical SCC found elsewhere - SCC occurs not at a high pH but the environmental pH is rather low [2]. This SCC mechanism gained attention from TransCanada Pipelines Limited and much research was then carried out to have a better understanding of the so-called near-neutral pH SCC [2].

2.2 Stress Corrosion Cracking

Stress corrosion cracking (SCC) refers to an environmentally assisted cracking (EAC) mechanism where there are three factors involved and interacting with each other: environment, susceptible material and tensile stress [2]. There are three types of environmentally assisted cracking, including stress corrosion cracking (SCC), corrosion fatigue (CF) and hydrogen-induced cracking (HIC). SCC is one of the problems that cause material degradation that involves corrosion of susceptible materials. The process involves corrosion and straining of a metal from a stress factor, being either applied or residual stress. The stress that causes SCC is relatively low, below the specified minimum yield strength (SMYS) of the susceptible metal [3]. SCC is found in many settings worldwide, with heavy influence on the gas pipeline transportation field [2].

SCC occurs when the three factors are present and interact with one another. Without the presence of one factor, the initiation of SCC will not happen. Figure 1 outlines the three factors that cause SCC and some examples of each factor involved.

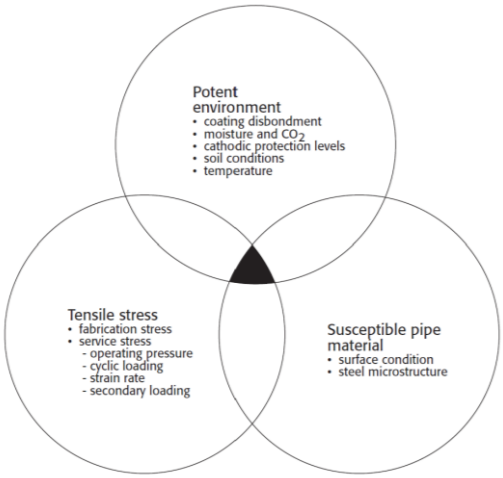

Figure 1: Stress corrosion cracking conditions [2].

Each material is susceptible to SCC in a different environment. If a metal is not susceptible to SCC in a certain environment, then it is unlikely that SCC will occur in that environment [3]. Table 1 lists the metals and their susceptible environments to SCC.

SCC is typically found in colonies where all the smaller cracks grow in one direction [2]. These cracks can grow after some time in service, and may cause problems such as leaks or ruptures. However, as it requires three factors to happen, SCC is typically more rare than other types of failures. The mechanisms of SCC can be categorized into two types: dissolution-based and mechanical fracture-based [3].

Table 1: Metal list and their SCC-susceptible environments [3]

Metal	Environment
Aluminum alloys	NaCl-H_2O_2 solutions NaCl solutions Seawater Air or water vapor
Copper alloys	Ammonia vapor and solutions Amines Water or water vapor
Gold alloys	$FeCl_3$ solutions Acetic acid-salt solutions
Inconel	Caustic soda solutions
Lead	Lead acetate solutions
Magnesium alloys	NaCl-Na_2CrO_4 solutions Rural and coastal atmospheres Seawater Distilled water
Nickel	Fused caustic soda
Steels	NaOH solutions NaOH-Na_2SiO_4 solutions Calcium, ammonium, and sodium nitrite solutions Mixed acids ($H_2SO_4 - HNO_3$) Acidic H_2S solutions Seawater Carbonate-bicarbonate solutions
Stainless steels	Acidic chloride solutions NaCl-H_2O_2 solutions Seawater H_2S NaOH-H_2S solutions Condensing steam from chloride waters
Titanium alloys	Red fuming nitric acid Seawater Methanol-HCl

In dissolution-based, a small crack in a favorable environment that supports growing at the crack tip will propagate. The dissolution is more severe at grain boundaries or around precipitates. The difference in chemistries and electrochemical potentials between 2 phases also provide a path for SCC to progress [3]. The corrosive environment forms a corrosion product (passive film) on these paths, slowing down the process by creating a barrier between the base metal and the corrosive environment. When these passive films rupture, these high-risk areas are exposed to the solution again and dissolution continues. Moreover, as cracking progresses inside the metal, more slip planes and grain boundaries are allowed to connect, creating more pathways for SCC cracks [3].

In mechanical fracture-based, the stress at the crack tip is believed to increase causing fracture. Cracks progress by dissolution, but the fracture is mostly mechanical. Several models are developed to explain this mechanism, including the adsorption-induced brittle fracture model and the film-induced cleavage model. The adsorption-induced brittle fracture model explains that bonds are weakened by adsorption, which decreases the stress necessary to initiate cracking [3-6]. There is also another similar model, in which the resolved shear stress is the resulting stress factor that is influenced by adsorption. According to these models, the crack propagates continuously until blunted by plastic deformation or reaching a different region. In the film-induced cleavage model, the internal stress arising from the growing passive film when present alongside tensile stress will cause brittle failure. When the film ruptures, crack is blunted by plastic deformation. This model explains the cleavage structure on the fracture surface of SCC, as well as crack arrest and crack propagation [3-6].

Hydrogen also contributes to SCC, and it can be a culprit causing crack growth in SCC. Hydrogen enters the steel through many ways, including electroplating, welding, pickling, heat

treatment, exposure to gases containing hydrogen, as well as corrosion. Hydrogen is adsorbed into the metal as atomic hydrogen, which is a product of many corrosion reactions. When existing in steels in a molecular form, hydrogen causes blisters. In its atomic form, hydrogen causes the steel to lose its ductility, become brittle and fracture after being exposed to hydrogen. Hydrogen-induced cracking refers to the brittle fracture of a ductile material under cyclic loading after being exposed to hydrogen [3]. Despite having similar features, HIC and SCC mechanisms cannot be understood as one. In many cases, hydrogen is the leading culprit for cracking even without external stress or corrosion [3,7]. HIC and SCC differ by a variety of factors, including the nature of corrosion, crack initiation sites, etc. [7]. While SCC relies on a favorable environment, pitting and crack initiation from pits, and passive film on the fracture surface, HIC relies on any metal treatment processes that allow hydrogen to enter the steel, as well as service conditions with high pressure and hydrogen surrounding [7]. There are some overlaps between the two, however, the relationship between the two is complicated.

There are two distinct types of SCC that are found on the outside of the pipeline, with different mechanisms and crack profiles: high pH SCC and near-neutral pH SCC.

2.2.1 High pH Stress Corrosion Cracking

High pH stress corrosion cracking refers to the SCC that happens in a basic pH range. Many papers report different pH levels that this type of SCC is found, but the mechanism of high pH SCC is generally understood. High pH SCC occurs at pipe sections with coating breakage at an electrochemical range between -600 to -750 mV ($Cu/CuSO_4$) and a pH range of more than 9.3 [2].

When the outer coating of steel pipelines breaks, the steel underneath is exposed to the corrosive environment. Cathodic protection (CP) works to protect the steel surface from corrosion,

hence severe corrosion is typically not observed in this type of SCC. However, the CP activity leads to a different corrosive environment for the exposed steel. When the coating flakes, the trapped water underneath has a different composition compared to the environmental groundwater, causing the basic pH range seen in high pH SCC but not in groundwater [8,9]. The solution that causes high pH SCC is found to be high in carbonate-bicarbonate concentration, more specifically bicarbonate. The environment that causes high pH SCC in steel pipelines depends on the cathodic protection current density, the CO_2, Na^+ and K^+ present in soil or groundwater to form the carbonate-bicarbonate solution, as well as the permeability of the coating [8-11].

The cracks found in high pH SCC are intergranular. These cracks are small and sharp, commonly primarily on the longitudinal direction of the pipe (axial cracks), and heavy corrosion is generally not found on the crack face [10]. Based on the mechanisms of SCC, it is found that high pH SCC occurs from the passive film rupture at the crack tip. The dissolution is highly focused at the tip of the crack, with no secondary corrosion found, keeping the crack small and sharp [2]. The passive film Fe_3O_4 is formed in the potential range of high-pH SCC, and ruptures at high strain rate locations such as grain boundaries [12]. This explains the intergranular nature of high pH SCC cracks.

In service, pipeline failures caused by high pH SCC have been reported to occur near compressor stations in service [2]. This type of SCC happens in areas with higher temperatures (above 75^{o}C), and the mechanism is found to be temperature dependent. As such, high pH SCC crack growth rate decreases as temperature drops, following the Arrhenius behaviour [2,10]. The Faraday equation alongside the potentiodynamic curves can be used to predict the crack growth rate of these high pH SCC cracks. Figure 2 shows the crack growth profile of high pH SCC [13]. The tensile hoop stress that causes high pH SCC is found to be above 60% of SMYS [12]. For the

aforementioned reasons, high pH SCC does not occur often in pipeline systems, particularly in cold climates.

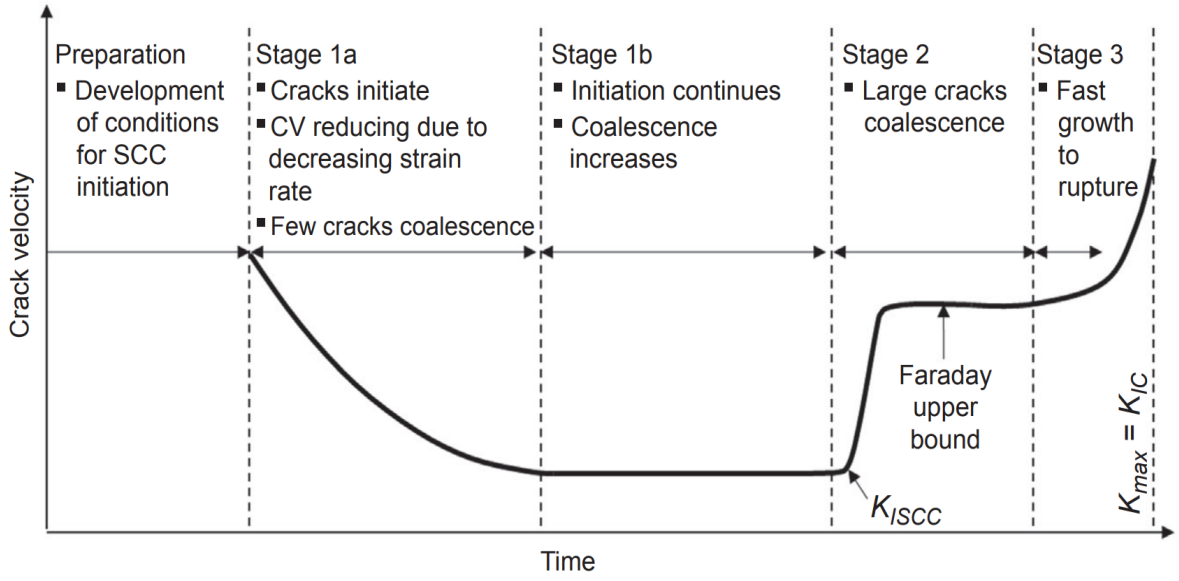

Figure 2: Crack velocity as a function of time in a high pH environment. Note that in stage I and II, crack growth rate is limited by dissolution rate [13].

2.2.2 Near-Neutral pH Stress Corrosion Cracking (NNpHSCC)

Near-neutral pH stress corrosion cracking (NNpHSCC) refers to the SCC that happens in a range of pH from 5.5-7.5 (slightly acidic to slightly basic). The study of this type of SCC is about 20 years behind high pH SCC, but many researchers have been working towards understanding NNpHSCC. NNpHSCC is typically found on pipe sections with disbonded coating at an electrochemical range of -760 to -790 mV ($Cu/CuSO_4$) [2]. Unlike high pH SCC, the steel surface underneath the coating is exposed to groundwater but not CP, since the coating is usually shielding

the CP. The pH range at NNpHSCC sites reflect the lack of CP, and the solution is a diluted bicarbonate solution formed from the presence of CO_2 in groundwater [2].

Because of no CP activity, NNpHSCC sites normally show signs of heavy corrosion. The corrosion product detected is often iron (II) carbonate, which can be found in the field at anaerobic sites [8]. There are other possible reactions to form more stable passive firms though very unlikely in a diluted bicarbonate solution [14]. Previous studies believe that the mechanism for this type of SCC is mainly dissolution with hydrogen being introduced to the steel, however, many papers over the years have proven that this might not be the case [2,15-19]. While the mechanism of crack initiation appears to be dissolution and pit to crack transition, the crack growth mechanism in a NNpH environment does not depend on dissolution, but rather is caused by corrosion fatigue, as crack pressure fluctuation plays a key factor in NNpHSCC crack growth [2,13,16,19].

Cracks produced by NNpHSCC are transgranular, wide with large openings. In most cases, secondary corrosion on the crack side wall can be found, and in dense areas, cracks merge into one another to create a bigger crack. The NNpHSCC cracks are found in both longitudinal and transverse (circumferential) directions, at high tensile stress locations or near weld seams [2]. Cracks are initiated at corrosion pits and dissolution at the bottom of pits results in early-stage crack growth. The crack growth mechanism in NNpHSCC can be found in Figure 3 [13]. At the end of stage I, crack becomes dormant from lack of favorable conditions for further growth. Most of the crack growth progresses in stage II, with the aid of fatigue cycles and hydrogen. Crack initiation for NNpHSCC depends mostly on the material and the dissolution in diluted bicarbonate solution, while crack growth depends mostly on the materials and stress factors [13]. Therefore, stress factor is very important in NNpHSCC to support crack propagation after initiation. Cracks are typically formed in a cyclic loading condition causing the corrosion fatigue condition, and the

maximum applied load in the hoop direction can be as low as 46% of SMYS [8,11,12]. However, in these cases, there is almost always another stress factor that increases the stress experienced by the near-neutral pH corrosion fatigue (NNpHCF) area, causing cracking [12]. Residual stress is a popular stress factor that causes an increase in stress in pipelines. Residual stresses can come from temperature changes, soil movement, field bends, etc. and the resulting stress needs to be looked into [20].

Moreover, unlike high pH SCC there is no found evidence that this SCC type is related to temperature change. NNpHSCC is typically found in colder climate regions such as Canada. These zones have higher CO_2 dissolved in groundwater, making an ideal environment for NNpHSCC to develop [2].

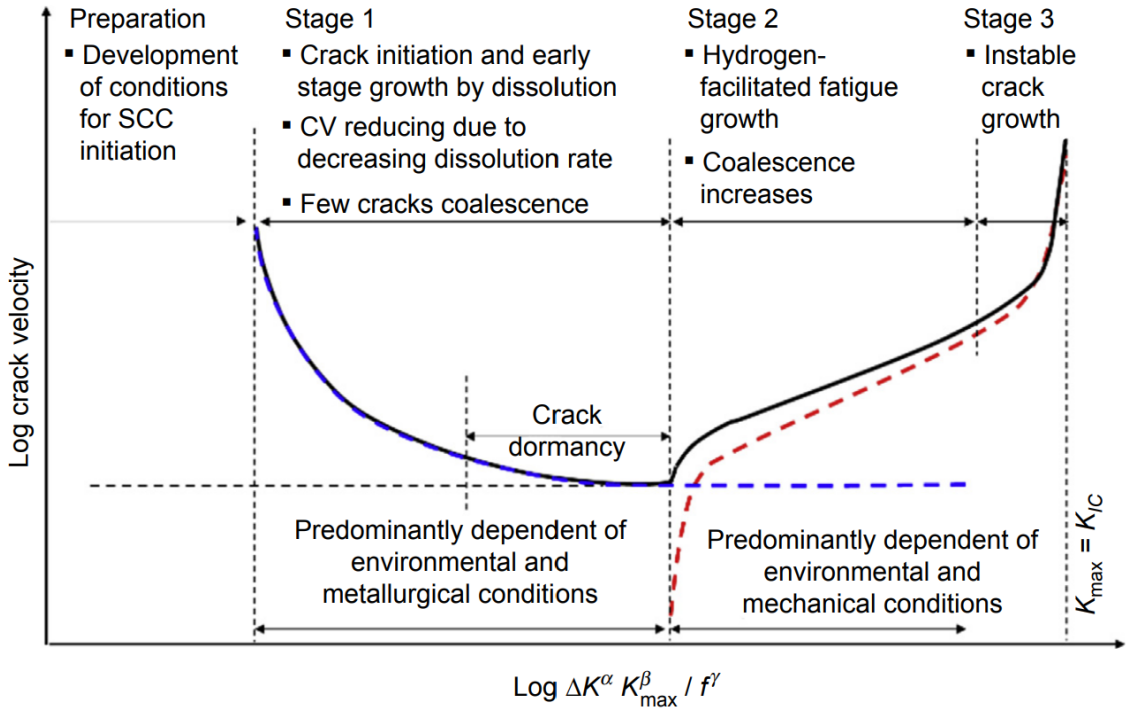

Figure 3: Cracking mechanism in NNpHSCC [13].

2.3 Factors affecting NNpHSCC

As mentioned in section 2.2, there are three main factors that, when happening altogether, would result in SCC. The same can be said for NNpHSCC. This section will discuss the three factors that cause NNpHSCC and how this type of SCC has been studied in the past.

2.3.1 Near-neutral pH environments

Since NNpHSCC was a serious failure mechanism in Canadian pipelines in 1985, many studies have been carried out to understand this type of EAC. Groundwater and soil samples near failure sites were analyzed, and researchers have mimicked the groundwater conditions using many laboratory-made solutions. The goal of these studies is to find a "recipe" that closely resembles the composition and ionic compounds as seen near NNpHSCC sites with a similar pH and electrochemical range. Both soil and groundwater chemistry have been found to have an influence on crack propagation, however, the parameters that are detrimental to SCC have not been clear in these studies [8,21]. Many solutions were proposed for the prediction of NNpHSCC with compositions assembling soil and trapped water chemistry, and the SCC studies carried out using these synthetic solutions have been quite successful [21]. Out of the earliest studies are NS4 and NOVA Trapped water solutions (NOVA TW), which gained popularity amongst researchers and were used in many experiments. The compositions of these two solutions are shown in Table 2, along with the average compositions of water found near the NNpHSCC sites and compositions found in the soil extracts from these locations [8,21]. While NS4 and NOVA TW are made based on the trapped water compositions seen in cracks, the cracks in these experiments are found to grow only in more aggressive conditions and in high pH environments, different from the less severe loading conditions found in the field. Moreover, hydrogen migration did not occur in these

synthetic groundwater solutions, which was believed to be a cause of SCC crack growth [7,21]. In another study using the soil extract solution, it was found that hydrogen resulting from bicarbonates in the solution correlated with slow strain rate tensile (SSRT) tests [21].

Table 2: Compositions of soil extracts, groundwater at NNpHSCC sites and two synthetic lab solutions, NS4 and NOVA TW [8,21].

Ionic species	Ionic concentration (mg/L)			
	Water samples, Central Canada (average)	Soil extracts, 6 samples observed (range)	NS4 solution	NOVA TW solution
Ca^{2+}	56	9.2-194	49.5	100
Mg^{2+}	22	2.7-205	12.9	102
K^{+}	78	<1.0-7.94	64.0	7.9
Na^{+}	86	8.0-464	132.2	119.6
$CO_3^{2-} + HCO_3^{-}$	350	29.9-283	350.8	1110.2
Cl^{-}	30	2.5-18.8	145.5	7.13
SO_4^{2-}	29	3.1-2160	51.1	19.3

The pH of these synthetic solutions depends on how much bicarbonates are presented. In a study by Wilmott and Diakow, the laboratory made solutions are found to have higher pH than the actual groundwater [22]. This shows that the actual groundwater found in NNpHSCC sites are saturated with CO_2, and having CO_2 sparging continuously into the laboratory-made solution also

removes traces of dissolved O_2 in the solution [21,22]. The presence of CO_2 also prevents high pH SCC from happening by keeping the pH low.

The solution used for NNpHSCC study poses an importance to simplify small-scale, laboratory studies of this type of SCC. There are multiple environments and soil conditions that cause NNpHSCC, as well as the type of clay and micro organisms existing at SCC sites. The standard solution allows for a more controlled environment for the experiment and provides a reliable source for SCC study. Seeing how cracking tendency of steel samples in slow strain-rate tensile tests are affected by the pH of the electrolyte solution, Chen et al. had prepared a list of 4 synthetic solutions, differ by the amount of $CaCO_3$ added, which results in change in pH in these solutions [21]. The study compares the solutions with NS4 and NOVA TW solutions for corrosion rates. While the mass loss in these solutions are similar to NS4 and NOVA TW in the first few days of the experiment, after 25 days, there was a clear gap between them, where the mass loss in NS4 and NOVA TW is around two times smaller than the synthetic soil solutions developed by Chen et al. [21]. The decrease in mass loss rate as the test proceeds suggests that in NS4 and NOVA TW, a passive film has formed on the corrosion surface which slows down the corrosion. In order to closely imitate how cracking occurs in the field, it is important to note that in NNpHSCC, the electrochemical corrosion curve has no passivation zone, and therefore, the formation of a passive film is not applicable. Chen et al. also showed how corrosion rate changes with pH, where lower pH results in higher corrosion rate compared to higher pH solutions [21]. Crack length and width are also a discussion of synthetic solutions. The cracks observed in Chen et al.'s and Gu et al.'s studies for NOVA TW and NS4, respectively, are similar in size and length [21,23]. These early solutions show a wide crack with blunted tip, while cracks formed in C2 solution are narrower and dissolution focused because of the readily corrosive environment.

Because of these differences in laboratory synthetic solutions, literature on crack growth mechanism and crack blunting needs to be discussed to further understand the environment used to study NNpHSCC.

2.3.2 Materials

Carbon steel is a common material used in pipelines in Canada because of its availability and low production cost. Steels used for pipelines are regulated by API (American Petroleum Institute) or by CSA (Canadian Standards Association), where steels are categorized based on their respective minimum yield strength in ksi or in MPa. There are other steel designation systems such as SAE which is based on compositions, and ASTM, which places steel based on their mechanical properties. Lower-grade pipelines were developed back in the 1950s, and recent technology is being developed for higher-grade pipelines with higher yield strength and more desirable properties. Table 3 shows the main chemical composition and mechanical properties of commonly used pipeline steels specified in the API standard [24]. As seen in the standard, the main compositions of these pipeline grades are very similar to each other. Higher grade pipelines differ in the amount of micro alloys being added and the manufacture and treatment processes, resulting in an increase in yield strength and tensile strength of these pipeline grades. For example, with pipeline grades X60 and higher, the plate used to produce pipeline undergoes cold rolling to achieve a better strength [25].

Table 3: Chemical composition and mechanical properties of commonly used pipeline grades [24]

Steel grade	Composition, wt%				Specified Minimum Yield Strength (SMYS), MPa	Specified Minimum Tensile Strength (SMTS), MPa
	C	Mn	P	S		
X46	0.28	1.40	0.030	0.030	320	435
X52	0.28	1.40	0.030	0.030	360	460
X60	0.28	1.40	0.030	0.030	415	520
X65	0.28	1.40	0.030	0.030	450	535
X70	0.28	1.40	0.030	0.030	485	570

NNpHSCC has been found to appear on carbon-manganese steels where the microstructure is a ferrite/pearlite matrix [10]. The newer, more homogenous pipeline steels are found to be less susceptible, as cracking is less likely to occur in one homogenous phase. In Kushida et al.'s study, the bainitic ferrite/bainite structure is found to be less susceptible to SCC than a ferrite/pearlite matrix [26]. Lower grade pipeline steels have larger grain microstructures and have been found to have SCC occurring, however, SCC is also found on newer grade pipeline steels [25,27,28]. Alloying elements within these newer grade steels plays a role in SCC resistance, but alloys also change the mechanical properties of steel, creating a challenge to assess how alloying affects SCC occurrences [28]. Therefore, it is inconclusive whether microstructure and composition are factors that cause SCC. However, areas within the welding zone or near the heat affected zone (HAZ) on

pipeline show a higher occurrence of SCC [10,25]. This happens because this area has a low fracture toughness, and comes from a residual stress factor caused during the welding process.

Researchers believe that SCC is only rarely seen on newer, higher grades pipelines because the pipe is recently installed with less service time [10,25,29]. Figure 4 and 5 show the SCC occurrences versus pipeline grades and ages, respectively [29]. X60 is found to have the most SCC occurrence because this pipeline grade is the most popular grade and is used in a variety of services. From Figure 4, it is not conclusive that any grade of pipeline steel is more susceptible to SCC than another. The yield strength and tensile strength of these pipeline grades come from the microstructure, which was not found to have a factor on SCC occurrence. Therefore, controlling the susceptible materials might be the most challenging part in SCC control, because there is no clear relationship between different steel grades and SCC. Moreover, pipelines of 31-40 years old show the most SCC occurrences. This does not necessarily mean that older pipelines are not susceptible to SCC, but there might not be enough data to observe SCC on these older pipelines, as SCC might have already occurred sometime during service or pipeline failure occurs from another reason. Older pipelines also have a higher chance of disbonded coating that reveal the pipe surface under coatings to the corrosive environment, causing SCC to happen. It is also found that the type of coating plays an important role on SCC occurrences. Pipelines with polyethylene (PE) tape coatings are found to have more SCC, as PE tapes are prone to disbond and break easily during groundwater and soil movements [29]. Without coating breakage, chances of steel pipelines being exposed to the surrounding environment are much lower, and hence SCC does not occur.

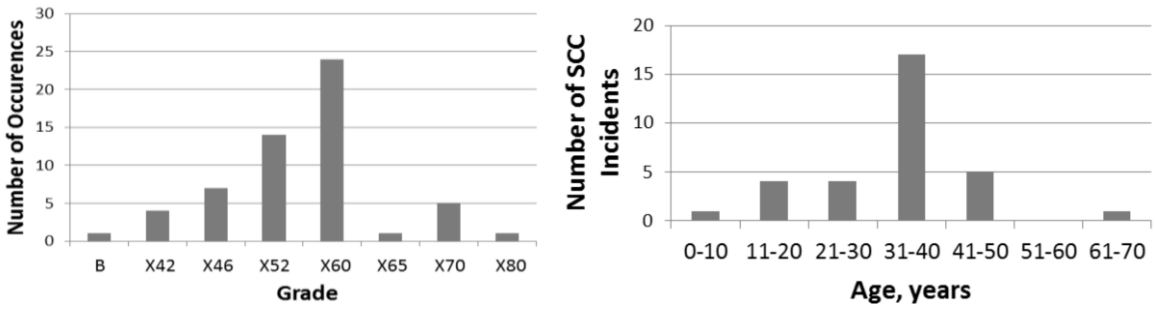

Figure 4 and 5: C-SCC occurrences according to pipeline grades and ages [29]

2.3.3 Stresses and corrosion fatigue

The stresses in SCC can come from many sources, including internal stress, bending stress, field stress, etc. [20]. The internal stress of the pipe comes from the inner flowing fluid, where the fluid comes into contact with the pipe wall, causing hoop stress, and to a lesser extent, axial stress. Hoop stress on SCC is one of the most widely studied stresses, because along with other stresses in the same direction, it causes axial SCC (A-SCC). Circumferential SCC (C-SCC), however, occurs in the transverse direction, calling for the study of stress in the axial direction instead. Internal fluids when coming to the pipe ends will exert pressure on the pipe wall, causing axial stress [20]. This axial stress is about half of hoop stress on the pipeline [20]. For safety reasons, the internal pressure is often kept below the Specified Minimum Yield Strength (SMYS) of the pipeline grade carrying the fluid. However, if other stresses are also accounted for, the maximum stress in the hoop direction might exceed 100% of SMYS, making the axial stress higher than about 50% of SMYS. In the study by Leis and Eiber, the hoop stress causing NNpHSCC was found to be as low as 46% of SMYS, without the presence of other stresses [12]. This indicates that, at an axial stress as little as about 20% of SMYS – half of the 46% hoop stress, SCC can occur in a NNpH environment.

The actual hoop stress causing SCC in the field is a good starting point for the study of how stress affects crack initiation and propagation in a NNpH environment. Because of how cracking occurs in NNpHSCC, many studies have used a SSRT test to study this SCC condition. SSRT tests are fast, and the testing conditions are often harsh, causing failure of the test specimen, which does not closely represent the actual condition seen in service for NNpHSCC [30,31]. The initiation stage of NNpHSCC mostly relies on creating crack-like defects from corrosion pitting or from the imperfect pipe surface. Therefore, applying a mechanical stress equal to or above the yield strength does not represent the condition very well. Moreover, fatigue growth was found to be the dominating growth model for NNpHSCC crack propagation [31]. This indicates that the NNpHSCC cracks grow under a cyclic loading condition, rather than a constant stress application.

Corrosion fatigue happens when there is a cyclic stress present in a corrosive environment, causing failure [3]. There is a difference between corrosion fatigue and SCC, which is that SCC is supposed to happen under static tensile stress, while corrosion fatigue occurs under a cyclic load. The maximum stress observed in corrosion fatigue is often low, however, the corrosive environment shortens the service life of the material, and after a number of stress cycles, the material approaches failure. The corrosion fatigue mechanism is represented by the stress - cycle curve, where the number of cycles to failure increases with lower stress [3]. The loading cycles are applied perpendicular to the direction of crack growth, causing cracks to propagate under mode I conditions [20].

In the field condition, corrosion fatigue is a reasonable model as pipelines experience fluctuations in internal pressure. Figure 6 shows the pressure fluctuations as seen in gas pipelines [32]. It can be seen that the average load experienced by these gas pipelines is around 60% of SMYS, however an upper design limit is considered for fluctuation. The cycles required to develop

a crack into a certain length also changes depending on the main type of cyclic loading. This also relies on the amplitude of the cycles, typically expressed as R. The R value is the ratio of minimum peak stress divided by the maximum peak stress ($R = \sigma_{min}/\sigma_{max}$). In all cases, underloading as explained below generally poses a more aggressive condition for crack propagation [32].

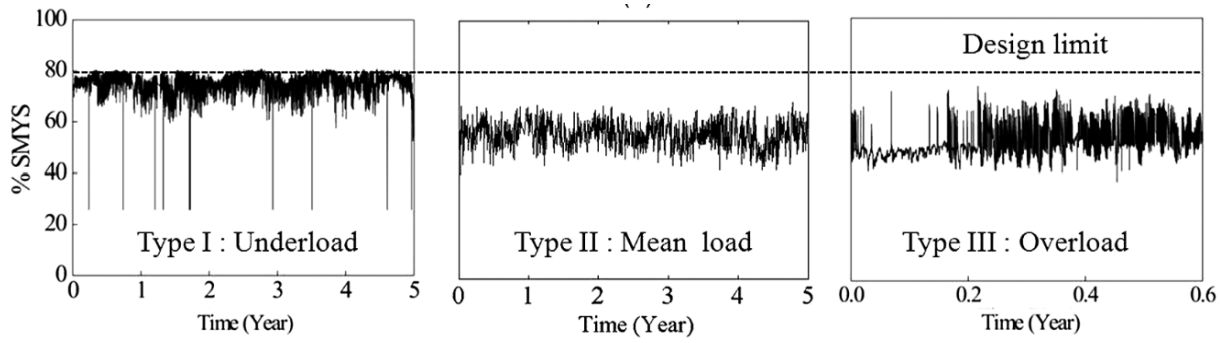

Figure 6: Pressure fluctuation as seen in gas pipelines [32].

In order to thoroughly understand how constant stress and cyclic load may apply to NNpHSCC, many experiments have introduced a "hold" period during cyclic loading to reduce the number of cycles, and the "hold" is often done at the maximum stress [32-35]. It was observed that crack growth rate decreases with a "hold" period, and in some cases, no crack growth is observed during the "hold" period, which indicates that corrosion fatigue is the key mechanism to NNpHSCC crack growth [32,35]. The loading frequency is also a factor to be considered in the study of crack initiation and growth in NNpH environments. In the crack growth and fatigue model, frequency is equivalent to loading cycles, and the crack growth rate can be determined based on the number of cycles applied. However, since stage I of NNpHCF, crack initiation, depends largely on dissolution and the environment, it is crucial to allow time for corrosion reactions to occur. Moreover, pipelines in service are more susceptible to "SCC" after about 30

years, which indicates that the pipelines have been under cyclic loading long before any signs of SCC. Therefore, in Wang et al.'s studies, a pre-cyclic loading period is introduced [36,37]. The frequency of pre-loading cycles and time is calculated to account for more than 10 years of service for the pipeline [36]. The actual frequency found in service for gas pipelines is about 10^{-7} to 10^{-5} Hz [37]. Generally, developing an appropriate loading cycle for the study of NNpHSCC is required to closely imitate the field conditions.

Welding is also another significant source of stress that causes NNpHSCC. Welding is a joining method involving heat that is very commonly used in pipeline manufacturing. The two ends of a steel plate are connected by melting a filler metal to act as a "glue" and allow the metal to solidify. Heat expands the base metal, and the cooling down process from such a high temperature creates a tensile stress on the area near the weld joint. This area is often known as the heat affected zone (HAZ), and the microstructure of HAZ is affected by the heating and rapid cooling from welding, making HAZ more susceptible to cracking. In fact, cracking is often observed along the seam welds in the field [2]. The local stress at welding joints is to be considered in NNpHSCC studies that involve girth welds.

2.4 Residual stress distribution on pipelines with bends

Residual stress is an important source of stress that causes NNpHSCC, alongside applied stress in gas pipelines. Residual stress can come from soil movement, pipe bending, causing axial stress and C-SCC. There are three types of residual stress, differing by the length scale. Type I residual stress refers to the large-scale residual stresses (macro scale). This type occurs over a long distance, and residual stress is considered macro when it occurs over a distance of a few grains or larger. All the stresses that occur on pipelines including temperature change, pipe manufacturing, pipe bending, etc. are considered type I residual stress. Type II residual stress is the microscopic

residual stress that occurs within the grain. This type of residual stress could arise from the microstructure variation in the metal matrix. The last type of residual stress is type III, where atomic scale residual stress comes from segregation or different composition at grain boundaries [20]. The residual stress most associated with NNpHSCC is type I residual stress, which changes the stress experienced by the pipeline system and consequently, affects the mechanism of NNpHSCC.

Pipelines are subjected to field bending when these stresses are present, and the bending location experiences a tensile or compressive residual stress depending on the direction of bending. In order for a pipe to be bent and plastically deformed, a bending force must be applied, which puts the bending locations in stress. The concave surface experiences compressive stresses and the convex surface experiences tensile stresses at the bent location. However, when the applied load is removed and the pipeline is allowed to spring back, the stress profile within the pipe section changes. The concave surface that was originally compressive, after spring back, becomes tensile near the surface and vice versa. The stress profile in bending is shown in Figure 7, and the stress profile after springback is shown in Figure 8 [29]. The total stress in the pipeline balances out, and this applies to bent sections as well. The level of compressive stress in the bent section should be equal to the level of tensile stress in the sample, making the total stress zero. The residual stress profile from concave to convex surface also varies from tensile to compressive, but these stresses will balance each other out, and the stress profile in all directions should add up to zero.

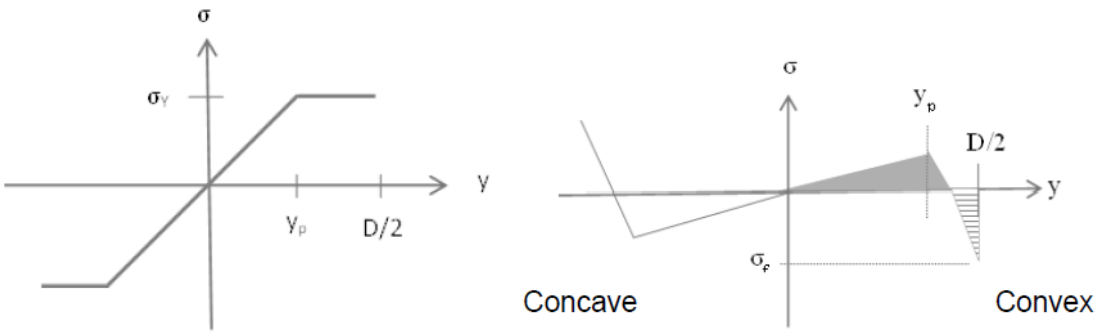

Figure 7 and 8: The stress profile in original bending from concave to convex (left) and the stress profile after spring back (right) [29].

The role of residual stress in the mechanism of NNpHSCC was not fully understood until Van Boven et al. and Chen et al.'s studies [33,34]. In their studies, Van Boven et al. study the effect of residual stress on pitting and crack initiation as well as crack dormancy. Bent samples were used in the study, and the residual stress was measured by neutron diffraction. In many studies, high tensile residual stress locations were found to be more susceptible to SCC [2,3,10]. Tensile stress is important at the crack tip because it is the driving force for crack propagation and mode I fracture. As discussed, the concave surface of the sample experiences tensile residual stress and the convex surface experiences compressive residual stress. Van Boven et al. found that in their testing samples, the residual stress ranges from -300 MPa to 300 MPa, ranging from convex to concave samples. Of the residual stress profile, corrosion pits are found more towards the tensile residual stress, however, pitting still happens at compressive stresses, though at a much lower amount. Pitting is very important in stage I NNpHCF as this stage focuses on dissolution, and cracking initiates from surface defects or at the bottom of corrosion pits. Figure 9 shows the pits distribution of bent samples ranging from a compressive (negative value) residual stress to a tensile (positive value) residual stress [33]. Based on the number of locations with a 300 MPa residual

stress, the highest residual stress will have the highest chance of pitting [33]. This agrees with the understanding about how tensile stress impacts SCC. Pits found in NNpH conditions are wide and have a small depth to length ratio.

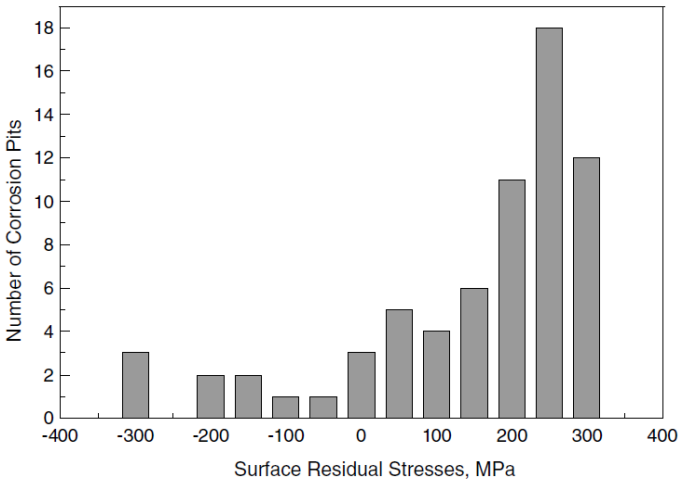

Figure 9: Pits distribution on a residual stress profile. Note that the values in this graph are not normalized [33].

The relationship between cracking occurrence and residual stress is also explored. Higher residual stress results in more pitting occurrence, however, this is not the case for cracking. Cracking is observed to happen only at a small range of tensile residual stress. Cracking peaks at around 200 MPa stress, and happens in smaller amounts at residual stresses higher and lower than 200 MPa. However, as residual stress moves out of this "cracking range", cracking does not occur. Figure 10 demonstrates the cracking and pitting behaviour of steel samples at a tensile residual stress range [33]. These findings aid in the study of NNpHSCC mechanism as residual stress is considered an important aspect in cracking in NNpHSCC.

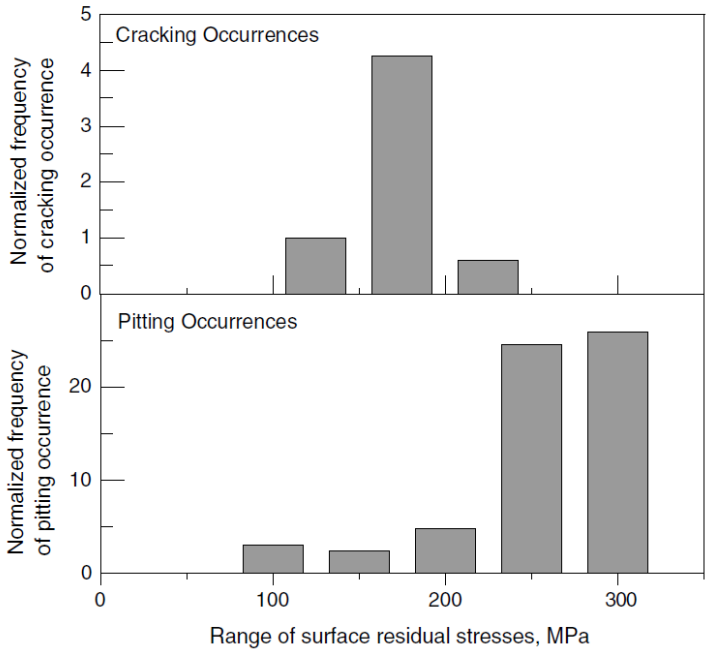

Figure 10: Pitting and cracking vs residual stress [33].

In the field, it is common to have both residual stress and applied stress from internal pressure or other sources. These stresses interact with one another and change the stress profile within the pipeline. High tensile residual stress locations are prone to pitting, but not necessarily to cracking. With an applied tensile stress, the resulting residual stress can increase or decrease depending on the initial stress level. Therefore, even though the residual stress at a certain point before applied stress might not be in the "cracking range", the applied stress can bring the stress profile into the "cracking range". With compressive residual stress, a tensile applied stress might be large enough to cause a tensile stress in the pipeline. In Van Boven et al.'s study, after cyclic conditioning is applied to compressive residual stress samples, the residual stress becomes less compressive, and at some points, tensile [33]. This tensile stress after cyclic loading can result in cracks initiating from pitting if this stress fits in the cracking range as seen in Figure 10. This

makes the prediction of NNpHSCC cracks more challenging, as there are many other possibilities for cracking to occur and lowering the local stress does not necessarily eliminate the risk of SCC.

2.5 Crack initiation and growth

Cracking on materials generally initiates from a microscopic defect. In SCC, these defects could originate from corrosion pitting, scratches, notches or intergranular attack [3]. These defects increase the stress concentration at the defect location, and with the right conditions, crack can initiate and grow from these defects. In the early days of research on how cracks can be initiated from corrosion pits, a study by Hoeppner presents a model that explains the transition from pitting to cracking that leads to failure. The model includes: i) pits initiation, ii) pits propagation, iii) initiation of mode I crack at a corrosion pit site, iv) propagation of mode I crack, v) initiation of fracture instability, and vi) unstable crack propagation [38]. The model uses the knowledge of pitting rate and fatigue threshold to predict the pit size and the number of cycles during cyclic loading to produce cracks. According to Hoeppner, the stress intensity factor at a surface flaw depends on the size and shape of the flaw. Using Weibull fit to the corrosion fatigue data, the stress intensity calculation can be used to predict crack initiation. Generally, if the stress intensity range of pit growth is more than the threshold, cracking will initiate from the existing pit [38].

Similar to Hoeppner, a few other approaches are also used to understand the crack initiation [39-43]. Fang et al. study the pit to crack transition with cyclic loading tests in both air and NNpH environments [40]. According to Fang et al., NNpHCF cracks progress from pits to blunt cracks, and then blunt cracks propagate into sharp cracks. The corrosion fatigue onset is believed to depend on loading frequencies, as well as the behaviour of the short cracks. Cracking occurs after pitting in the form of blunt cracks, and while these blunt cracks act as stress concentrators, sharp cracks initiate when a threshold is achieved. While applying cyclic loading in air after corrosion produces

microcracks, they suggested that cyclic loading in a NNpH solution initiates cracks after about 1000 cycles fewer than in air. This occurs because electrochemical attack prefers plastically deformed zones, making a more ideal environment for short cracks to initiate. Cracking is also found to increase with a higher depth to width ratio, but shape factor also plays a role in crack initiation. Moreover, while examining field specimens, a mixture of blunt and sharp cracks are not found, showing that blunt cracks are not a result of corroded out sharp cracks [40].

Multiple researchers have used a threshold fatigue stress to predict crack initiation from pits, but the idea is similar [39,40]. The driving force for corrosion pits is from dissolution, which decreases as the pit grows deeper. The driving force for crack propagation, however, comes from mechanical conditions, as the stress intensity factor of crack changes with the crack length, and the surface curvature, which produces the source of residual stress at the surface. This driving force increases with the propagation of crack, dominating the corrosion pit. This approach is shown in Figure 11, and is critical to the study of crack initiation from corrosion pits till this day [39]. Crack initiation from pits is also evidenced to increase with applied stress. If the maximum applied stress increases, the likelihood of crack initiation also increases. The conclusion is true in both static and cyclic loading conditions [39]. From the model, deeper pits are expected to nucleate more cracks. However, this was found to be not true, as under a constant load, pits of up to 400 μm do not have any cracks nucleating, and pits smaller than 50 μm - the expected minimum pit size for crack initiation - show nucleation of crack. Time is found to be a factor for early crack initiation, and shorter duration might be insufficient to cause crack initiation from pits [39]. Moreover, areas with concentrated pits do not necessarily have cracks initiated [39]. These findings are in line with Van Boven et al.'s study on how cracks are not present at highest pitting locations with the highest stress. Chen et al. discussed in their study that cracking depends on the stress state at the bottom

of a corrosion pit [34]. At the bottom of pits, the depth is different and the stress concentration is also different compared to at the surface. These studies have shown that the residual stress along the depth profile varies at the same location along the length of the specimen. Therefore, the residual stress level at the bottom of pits might be different, hence cracking does not occur even at larger pits or at locations with high residual stress on the surface [33,34].

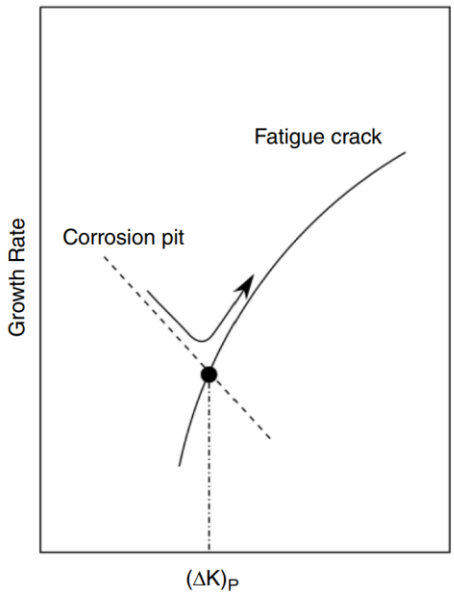

Figure 11: Crack initiation from corrosion pit model [39].

The cracks formed at the bottom of pits in NNpHSCC are microcracks that have a cone or balloon-like morphology, which is distinct from a crack from the fracture mechanics view [33]. Figure 12 illustrates the microcracks found in Van Boven et al.'s study [33]. These microcrack morphologies allow researchers to understand more about the mechanism of NNpHSCC and how residual stress affects crack growth. Cracks initiate from a pit on the surface, and propagate into the material before reaching dormancy. The crack tip is blunted, which is shown by the cone-shape or balloon-shape at the end. There are also cases where crack is re-initiated after blunting, as shown

in Figure 12-d. Van Boven et al. measured the residual stress profile in the length and depth of a bent sample, and there is a difference in residual stress level in the depth direction. As cracks propagate into the material, they reach a zone with a different residual stress than the surface residual stress where pits are initiated. Therefore, it is important to consider the residual stress at the location of the microcracks in the sample before predicting the growth of microcracks.

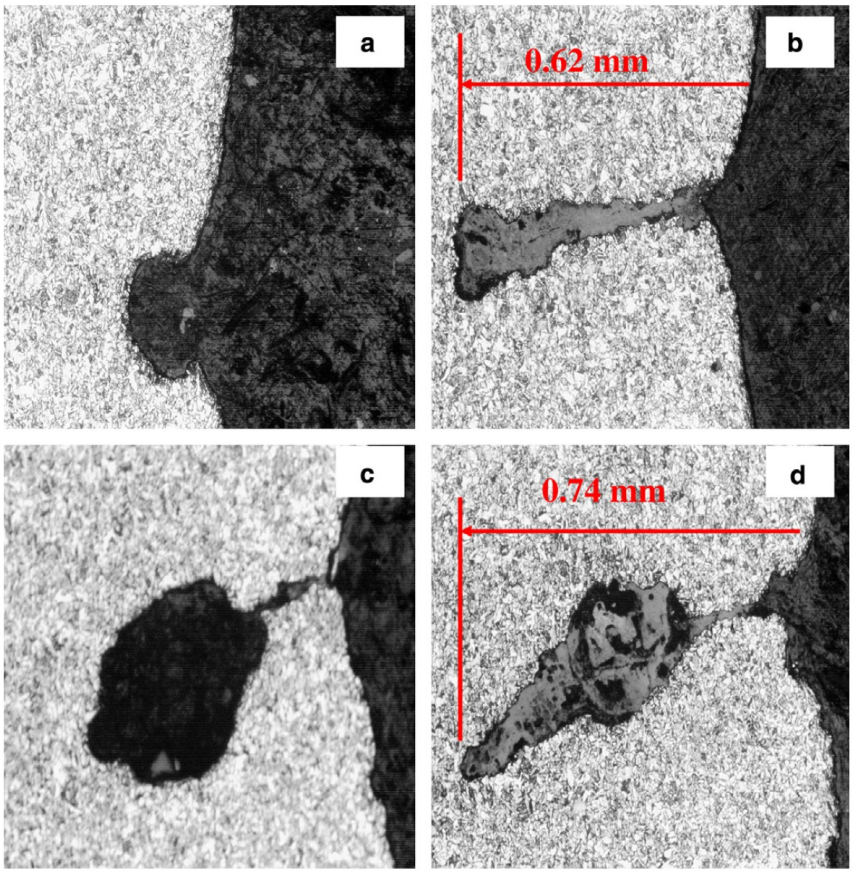

Figure 12: Microcracks forming at the bottom of corrosion pits [33].

Turnbull et al. used both simulation and experimental approaches to understand the pit to crack transition [41]. In order to develop a crack model that shows a constant growth rate, the study uses finite element analysis (FEA) on a pipeline geometry with an existing pit, alongside the

experimental aspect with control exposure time of samples in the testing environment. Three different cracking manners are found near the corrosion pit, instead of just initiating from the bottom of pit. Figure 13 shows the three cracking manners [41]. The study shows that FEA is an appropriate method to predict pit size distribution when comparing to the experimental results, however, the pit/crack morphology as seen in Figure 13 cannot be predicted with this model and X-ray tomography would be the better method to resolve this limitation. X-ray tomography shows that many cracks can grow from one pit, and over time, these cracks can coalesce. Moreover, because plastic strain is localized just below the pit mouth, cracking develops around the mouth area, causing a crack that extends beyond the pit base and breaks into the surface. Turnbull et al. conclude that the pit to crack transition is rather complex, and the conventional belief of crack depth being the same as pit depth during transition from pit to depth cannot fully describe the pit to crack transition [41].

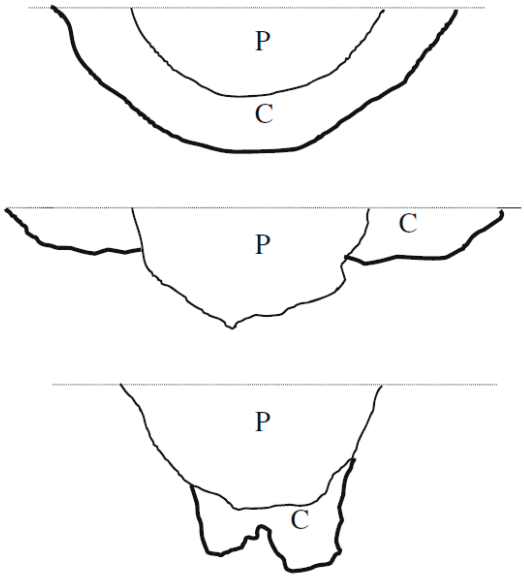

Figure 13: The possible manners of pit (P) and crack (C) showing pits with crack extending beyond pit base and breaking surface, pits extending beyond crack, and crack emanating from pit base but not extending to surface [41].

Many non-destructive evaluation (NDE) methods are used to detect SCC damage, and standard procedures such as ASME B31G or API 579 are used in the integrity assessment of corroded structures [44,45]. Fracture mechanics calculations are typically used to predict crack growth using pit size as the initial flaw size within the standards, but these methodologies do not correctly predict cracking behaviour. Therefore, Balbin et al. presented a microstructural model to study the pit to crack transition and corrosion fatigue life [42]. The model uses distributed dislocation technique (DDT) to simulate the growth of a short crack in the material. Three pit shapes are considered: V-shaped pits, U-shaped pits, and semi-elliptical pits. Balbin et al. used an algorithmic approach to understand crack initiation, and validated the model with experimental data [42]. Other researchers, such as Chen et al., also approached the problem with a more calculation-based method [43]. These studies attempted to capture the pit to crack transition time, as well as predict the crack morphology. The advantages of these approaches are that they are flexible, and can be used to estimate the fatigue life of the corroded specimen, providing any experimental study a reference time and expected results. However, with modeling and computational methods, the results are still quite approximate, and the predicted mechanism might not accurately explain the complication of NNpHCF crack initiation and growth.

CHAPTER 3

EXPERIMENTAL METHOD

As discussed in the previous chapters, dissolution and corrosion fatigue govern the crack initiation (stage 1) and second stage growth in NNpHSCC. While there has been some research on the mechanical loading conditions that cause SCC in steel pipeline, the understanding of how cyclic loading affects the residual stress along the pipeline and their relationship to stage I NNpHSCC is still limited. This study focuses on how different mechanical loading conditions affect the crack initiation and early stage growth of pipeline steel in NNpHSCC. The distribution of pitting reveals the distribution of residual stress along the length of the specimen. By comparing the pitting distribution of these mechanical loading conditions, one can determine the effect of these conditions on the residual stress profile. With these analyses, the minimum stress that causes pitting, and possibly crack initiation can also be determined.

3.1 Materials

The steel sample used in this study was machined out of a X52 pipe section that had been in service for an unknown amount of time. The composition of X52 steel is given in Table 3 in chapter 2. The machined sample has a dog-bone shape with pin holes at both ends. The length of the sample was machined from the longitudinal direction of the pipe. Figure 14 shows the sample design.

After fabrication, the samples were bent lengthwise at three points: at the centerline and at the end of the gauge length. The two bending conditions are +20 and +40 degrees (outward bending). The bending was done so that the roof of the specimens is on the outer surface of the original pipe. After bending, the samples were covered with tuck tape at the two ends, on the back

and sides, exposing only the corrosion surface. This surface is the outer surface of the original pipe section. Figure 15 shows how bending and coating is done.

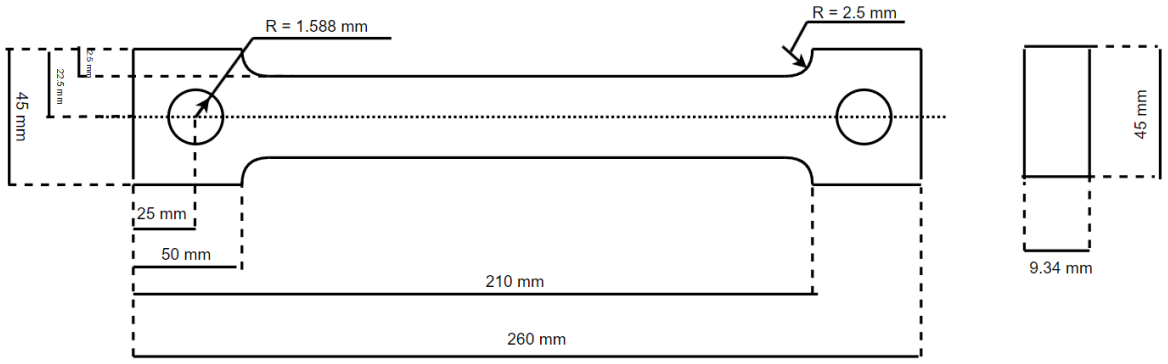

Figure 14: Dog-bone sample design with two pin holes on both ends.

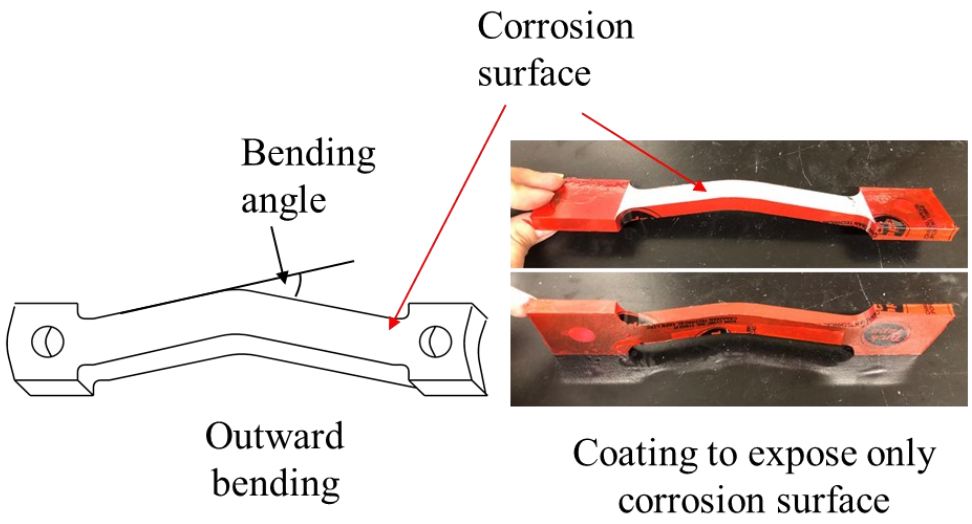

Figure 15: Specimen bending and coating. The bending angle is indicated. The corrosion surface is the outer surface of the original pipe.

The corrosion surface was kept as is, without further polishing. This was to ensure that the mill scale was still present from the original pipe section to provide some shielding on the surface, causing a local corrosion effect. Moreover, as crack initiation tends to occur at surface defects, leaving the surface as is would ensure that the existing defects aid in the initiation of SCC cracks.

3.2 Corrosion without loading test

The solution used for this test is a synthetic soil solution, C2. The composition of this solution is shown in Table 4. The solution is continuously sparged with a mixture of 5% CO_2 + N_2 balanced for 72 hours before testing to remove any oxygen in the solution and stabilize the solution pH. The pH of the solution before testing is about 6.3.

Table 4: Composition of C2 solution used in this experiment.

Composition	Amount (g/L)
$MgSO_4$	0.0274
$CaCl_2$	0.0255
KCl	0.0035
$NaHCO_3$	0.0195
$CaCO_3$	0.0606
pH (sparged with 5% CO_2 + N_2)	6.29

The corrosion cells were large plastic cylinders made so that two specimens could fit into one cell. The cells were sealed with a rubber stopper and silicon so no air can enter or exit the corrosion chamber. Two plastic tubes were connected to the rubber stopper to allow the 5% CO_2 + N_2 gas mixture to flow in and out of the corrosion cell. A schematic of the set up of this experiment is shown in Figure 16. After adding the testing specimens, the solution was added to fully submerge the specimens in the C2 solution before sealing. The cell was then connected to the gas cylinder containing 5% CO_2 + N_2 gas, and gas was continuously being sparged into the cell throughout the test. Generally, there were two testing chambers connecting to each other, and to one gas cylinder. To ensure no leakage point and a constant bubbling speed, the corrosion cells were connected to an outlet beaker filled with water to prevent back flow of gas. The bubbling speed inside the corrosion chambers and in the outlet beaker should be about the same if there is no leakage. Corrosion tests without any cyclic loading were done on all the testing specimens, for a duration of 90 days. Throughout the test duration, the solution was kept the same in the testing chamber, and no solution replacement was done on any of the testing samples.

After this experiment, the specimens were rinsed with ethanol to wash off the C2 solution residue, and split into two batches. One batch would go into the cyclic loading test, and the other batch was analyzed as control samples.

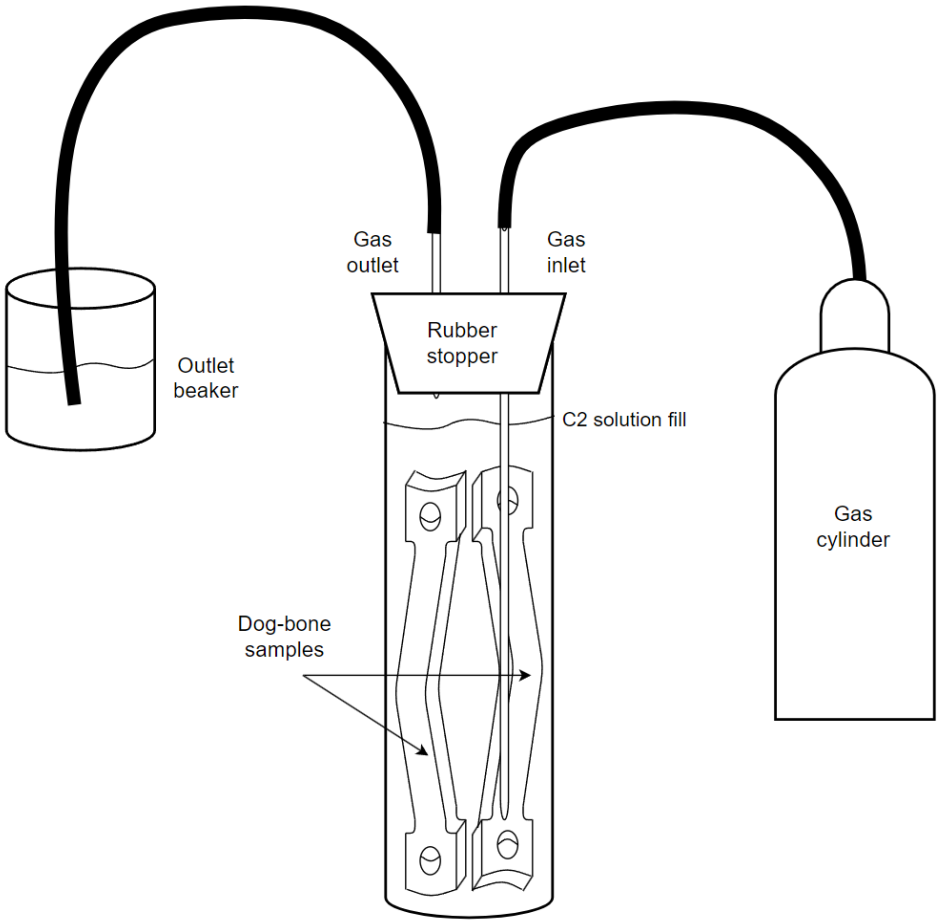

Figure 16: Corrosion test setup.

3.3 Cyclic loading test

The solution used in this experiment was C2 solution, and the composition is found in Table 4 of the previous section. After the corrosion test, the samples' tape coatings were removed and reapplied, as shown in Figure 15. Each testing sample was then fit into an acrylic cell sealed at two ends, and the cells then went through a mechanical loading test. Each testing cell can fit one specimen, and two plastic tubes were connected to each cell to allow gas inlet and outlet through the cell. The cells were connected in a continuous series to ensure they had the same mechanical loading conditions. The two testing cells were connected using a steel connector and two steel

pins. The two-cell setup was then loaded onto the MTS hydraulic machine, model 810. The machine has a load capacity of 100 kN, and is controlled by the 8500 Instron Controls. The mechanical loading test setup can be found in Figure 17.

Each mechanical loading test was run at a testing frequency f = 1E-04 Hz, which is equivalent to 8.64 cycles per day. The frequency used in this experiment was based on the field condition, the critical frequency for crack growth, as well as the time considered for the experiment. The actual fatigue loading frequency that pipelines experience in the field is found to be less than f = 1E-08 Hz [33]. However, as conditions in the field occur within years, a higher frequency was considered in the lab setting to accelerate the process. In studies done by Wang et al. and Nelson et al., the critical frequency ideal for crack growth conditions is f = 1E-3 Hz [36,46]. It was found by Zhao et al. that any frequencies larger than f = 1E-03 Hz is in the high-frequency regime and crack growth rate increases as frequency decreases. In the low-frequency regime (f < 1E-03 Hz), crack propagation does not change significantly with fluctuating loading frequencies [32]. The frequency used in this study was chosen in the low-frequency regime in order to allow time for pitting and crack initiation throughout the test duration. The R value was set to be 0.2 for a more aggressive loading condition, and the maximum stress ranges from 15 - 50% of SMYS. This maximum load matched the conditions in the field, where axial stress is one half of hoop stress, and the hoop stress that NNpHSCC occurs can be as low as about 40% of SMYS. All mechanical loading tests ran for a duration of 90 days.

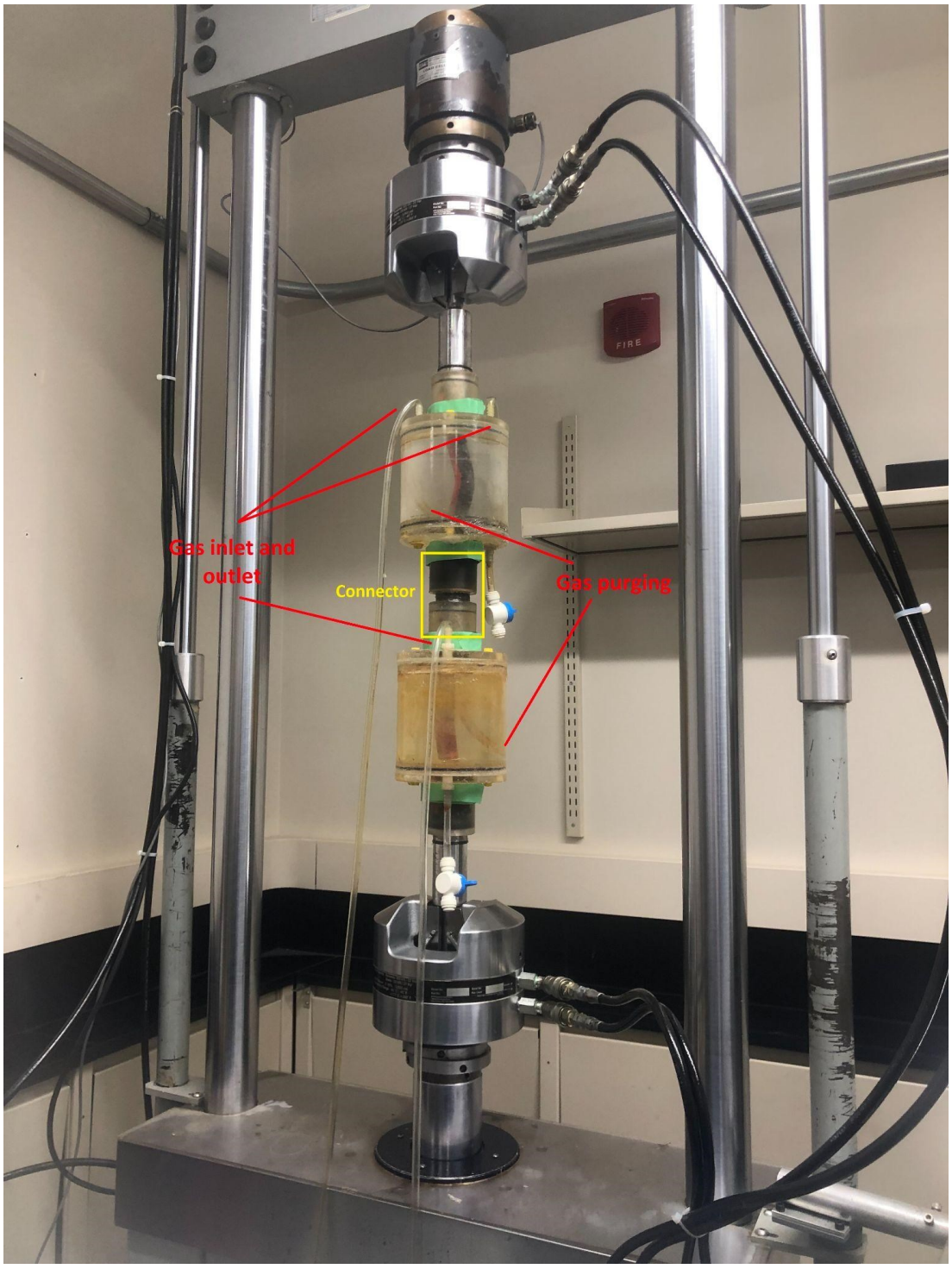

Figure 17: Mechanical loading test setup.

Table 5 outlines the testing conditions of the specimens. It can be noted that the cyclic loading test only happened after the samples had gone through a 90 days pre-corrosion test. Each mechanical loading condition was done on one +20 and one +40 degree bending sample. Moreover, there is no duplicate testing on any conditions, because the samples are symmetrical lengthwise through the center of bending, and with one full length specimen, two different results can be obtained. Except for sample #1 which had the same residual stress distribution throughout and had not undergone any corrosion testing, each sample yielded two sets of results.

Table 5: Testing matrix for both experiments.

Sample	Bending angle	Corrosion without loading test (90 days)	Cyclic loading test (90 days)	Maximum load (% of SMYS)
1	0	no	no	N/A
2	+20	yes	no	N/A
3	+40	yes	no	N/A
4	+20	yes	yes	50%
5	+40	yes	yes	50%
6	+20	yes	yes	25%
7	+40	yes	yes	25%
8	+20	yes	yes	15%
9	+40	yes	yes	15%

After the test, the samples were removed from the testing chamber, rinsed with ethanol to wash off any C2 residue, and the tape coating was removed. The samples were then ready for characterization.

3.4 Characterization

The testing specimens in this experiment were analyzed using a destructive analysis method. The two ends were sawed off, leaving only the gauge length of the sample. The gauge length was then sectioned lengthwise into 4 parts, and all four were analyzed. Figure 18 shows how the samples were sectioned. The samples are symmetrical lengthwise through the center of bending, so section 1 and 2 can be considered a separate sample from section 3 and 4.

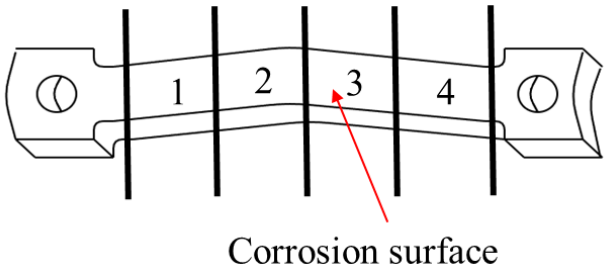

Figure 18: Initial sectioning. The two ends were sectioned off, and the gauge length was sectioned symmetrically.

The pit depth on the corrosion surface was measured by grinding and polishing the side surface, making sure that the interface between the top surface and side surface were not damaged. The side surface was ground up to 600 grits, and fine polished to 1 μm. The polished surface was then observed using scanning electron microscopy (SEM), where the pits and microcracks were captured. The samples were then sectioned in the width direction, revealing the inner side surface, and the preparation and analysis with SEM were repeated. Each sample was sectioned 10 times,

with an interval of 1 mm per section. Figure 19 shows the sectioning done for 10 slices analysis. Corrosion was expected to be randomly scattered on the corrosion surface, therefore, the 10-slice analysis would provide enough information to study how changing the loading condition might impact the pitting and cracking initiation. After SEM, pits and cracks were counted, and the length of pits and cracks were also measured.

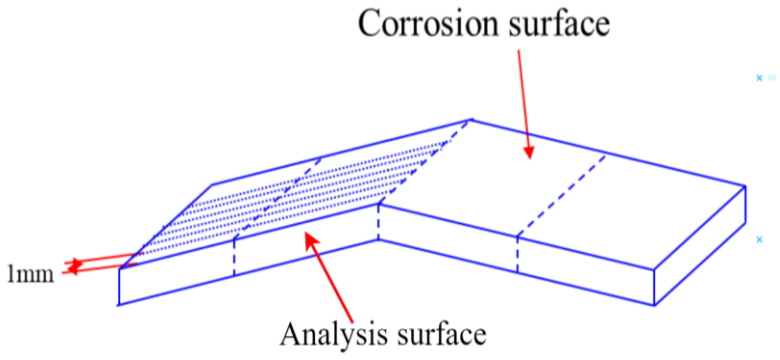

Figure 19: Sectioning of sample for SEM analysis

CHAPTER 4

RESULTS AND DISCUSSION

4.1 Effect of residual stress on pit and crack formation

All the samples in this experiment underwent a corrosion without cyclic loading phase before some went through a cyclic loading phase with different maximum loads. Sample #2 and #3 are the control samples that have no applied cyclic loads. The only stress factor in these samples came from bending, which produced residual stress in the samples. These samples were compared with the as-received sample (sample #1) for the number of pitting occurrences, and the pits were also examined.

Figure 20 and 21 show some typical pits found in samples #2 and #3, respectively. Pits caused by dissolution have wide openings, and a high width to depth ratio. Pitting is found all over the surface in both length and width direction, and microcracks are found to develop at the bottom of pits even without an applied stress. Residual stress distribution along the depth direction is the cause of microcracks happening at the bottom of pits. These microcracks are small, and can potentially grow into a detrimental size, but with dissolution being the main mechanism, it is highly unlikely that microcracks can develop and propagate further, as the speed of pit growth decreases the deeper the pit [39]. Sample #1 also shows surface defects and pit-like features, as seen in Figure 22. These features act as pitting sites that trap solutions, causing pitting to occur at such locations.

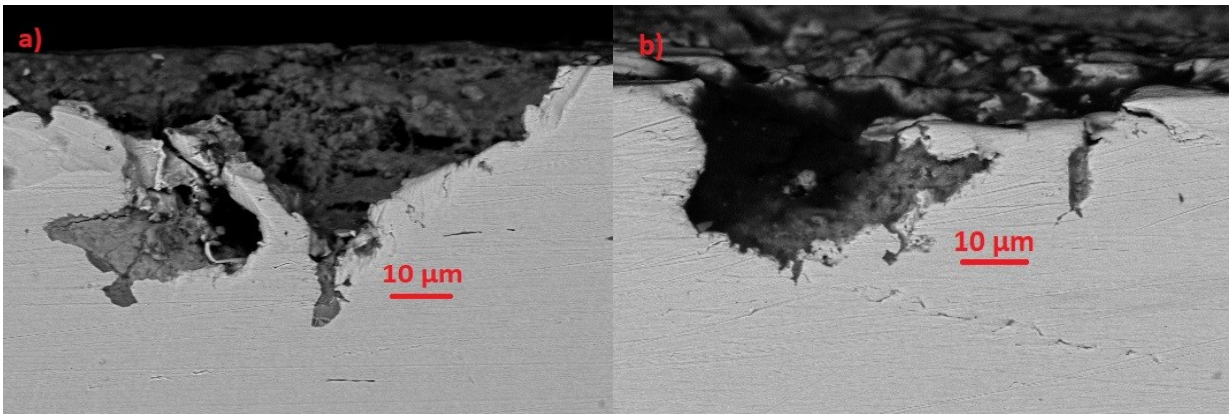

Figure 20: Pitting on sample #2 near center of bend a) on the first half (section II), b) on the second half (section III)

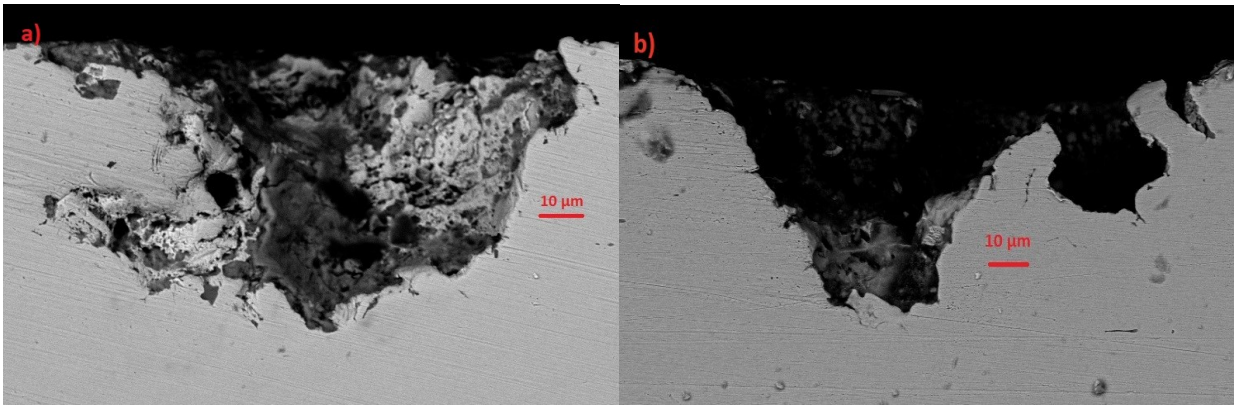

Figure 21: Pitting on sample #3 near center of bend a) on the first half (section II), b) on the second half (section III)

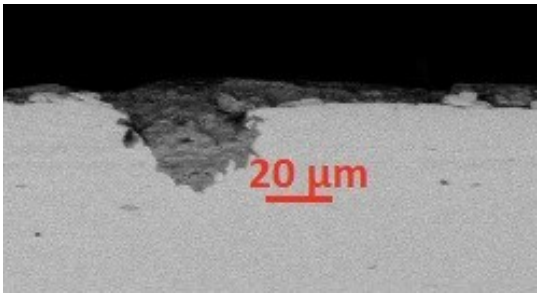

Figure 22: As received surface defects seen on sample #1

The number of pits of all sizes are compared between samples #1, #2 and #3 to study the effect of bending and dissolution on stage I NNpHSCC in steel pipeline. Figure 23 shows the number of pits found in all three samples. Sample #1 also had signs of pitting, which indicated that there were existing pits before the pipe was formed and in service, before hot rolling.

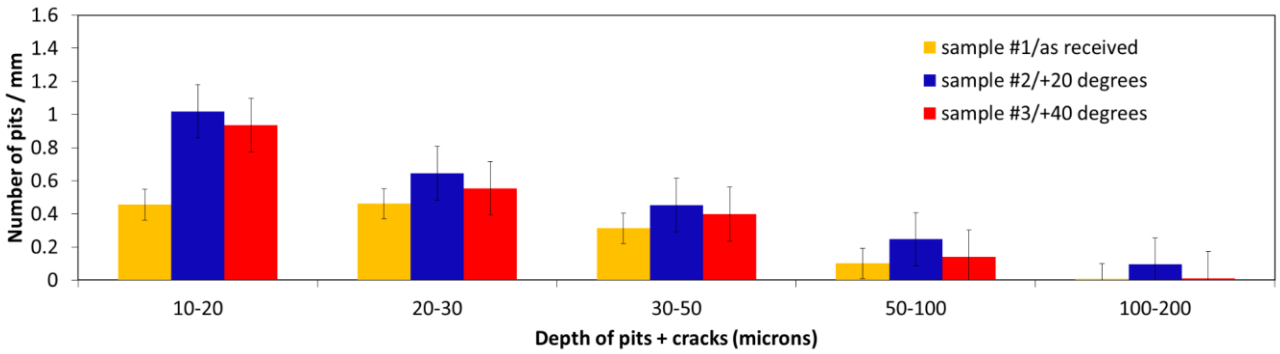

Figure 23: Number of pits of all sizes on samples #1, #2 and #3.

Dissolution is found to initiate more pits on the surface, and aids in the propagation of pits. The number of 10 - 20 µm sized pits show a sharp increase after the corrosion experiment. Since larger pits develop from the smaller sized pits, the difference in number of pits in the 10 - 20 µm range compared to control samples shows how corrosion causes pitting in a NNpHSCC solution. Many small pits are initiated on the surface as a result of corrosion. Not only does corrosion initiate pitting at the sample surface, corrosion also induces growth of already existing pits and defects. The number of pits larger than 20 µm indicates that corrosion also induces the initiation of deeper pits even after only 90 days. Moreover, the number of pits and cracks of sizes 50 - 200 µm in corrosion samples increases significantly compared to the as received sample. Smaller defects seen in the as received samples develop and grow deeper into the materials, causing the rise seen in this pit size range. The effect of dissolution is clearest when compared with a non-corrosion specimen

for the pits and cracks occurrences, and it is confirmed that C2 solution used in this study aids with pitting and initiation of stage I NNpHSCC. It can also be noted that the +20 degree bending samples show more pits and cracks of all sizes compared to the +40 degree bending samples. The effect of bending will be explained in a later section.

4.2 Crack initiation and crack tip blunting

Pitting is seen as the first stage of NNpHSCC initiation. The pit and crack morphology in the samples was captured using SEM. On all the samples, with or without cyclic loadings, pits with wide openings were observed along the sample length and width. The pitting size varied, with pits ranging from 10 μm all the way to 200 μm. As defects were also found on the control sample, the SCC susceptibility of the experimental samples increased significantly compared to polished samples. Figure 24 shows some typical pitting morphology found on the surface of all samples. At the bottom of these pits, some cracks were observed to initiate, but some were found to be blunted. The blunted shapes of these microcracks are in line with Van Boven et al.'s study, where often cracks initiation starts, but dissolution takes over, which blunts the crack tip.

Pits appeared in colonies, though there are also some scattered pits along the surface. Most pits found in a colony are shallow, and deeper pits or pits with large cracks initiated at the bottom are generally more rare. With a testing condition that supports stage I NNpHSCC, it was expected that not that many well developed cracks were found, as the dominating dissolution mechanism dominated fatigue crack growth and crack growth became dormant after some time. It is also important to note that crack initiation could be found at the bottom of pits of all sizes, not just deeper ones. Moreover, microcracks could still develop with little to no cyclic loading conditions.

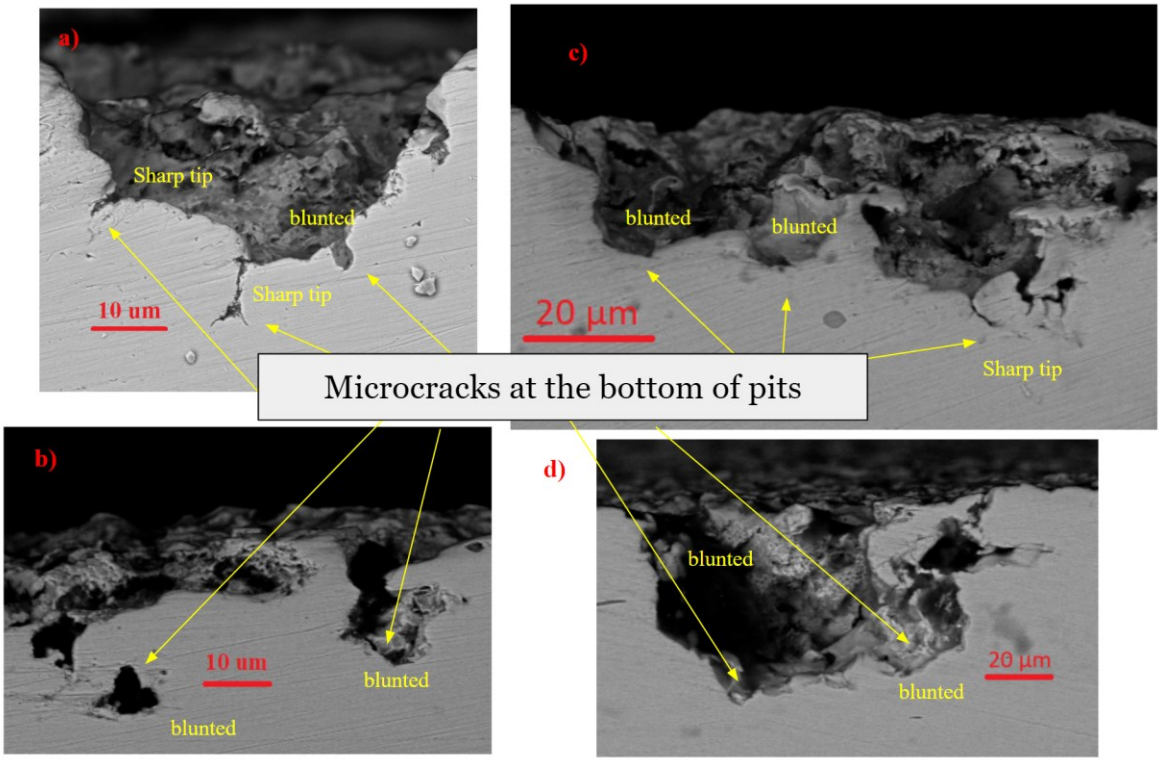

Figure 24: Pitting and crack initiating at the bottom of pits on a) sample #2, b) sample #5, c) sample #6, d) sample #9.

All samples fabricated have an outward bending direction, so the corrosion surfaces on all samples have a compressive residual stress. The residual stress profile changes along the sample length and thickness, which reacts differently with the cyclic loading conditions. At locations where there is compressive stress, cyclic loading can decrease the compressive stress, or turn the local stress tensile. At tensile locations, residual stress decreases after cyclic loading. When there is a local compressive stress, cracking is less prone to happen because the compressive stress does not support a mode I fracture for crack growth. The crack becomes dormant, and the dissolution takes over again. In regions that experience tensile stress, the defects act as a stress concentration point, and tensile stress supports mode I fracture.

The residual stress gradient is largest in the thickness direction, causing the highest strain energy, and pitting occurs to relieve the strain energy in this direction [34]. As pits start to develop, they act as the SCC initiation sites on the surface because anodic dissolution and plasticity from stress concentration effects are localized at this location [47]. Pitting releases the stress state on the surface, causing stress to concentrate at the bottom of pits. As the surface experiences a compressive stress, this stress carries to the bottom of pits, creating elastic strain energy at the bottom of pits as a result of residual stress [48]. Strain energy is released in the form of anodic dissolution, therefore, pits are allowed to grow in the material under compressive residual stress.

4.3 Effect of additional applied cyclic loading

Applying an external stress factor changes the residual stress profile at every location in the sample. In order to compare how different maximum stresses change the residual stress distribution on the surface, pitting distribution was studied. The number of pits of a certain size can give some insights about which condition supports the growth of deeper pits that increases the stress concentration factor in the sample.

4.3.1 Effect of maximum stress on pits and crack depth distribution

The number of pits and cracks of all sizes were plotted between the different maximum stresses to compare how maximum stress affects the number of pitting occurrences. Figure 25 and 26 show the number of pits and cracks of different maximum stresses for +20 degree bending. Figure 27 and 28 show the number of pits and cracks of different maximum stresses for +40 degree bending. Data for both figures was compared to a control sample with no corrosion and no cyclic loading to see the total change in number of pits and cracks. The number of pits plotted is an

average of 10 slices, per mm of sample length. This shows a full picture of the sample section and how changing the maximum stress affects the total number of pits along the entire sample.

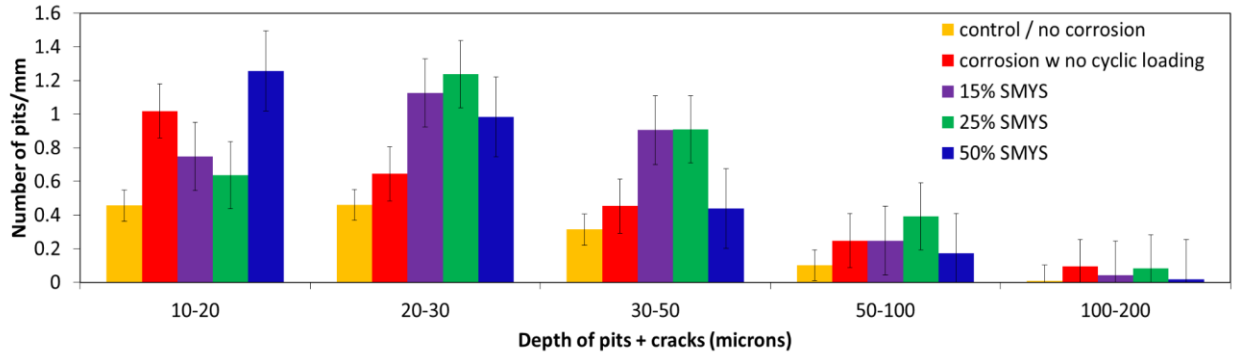

Figure 25: Distribution of depth of pits and cracks for a +20 degree bending angle.

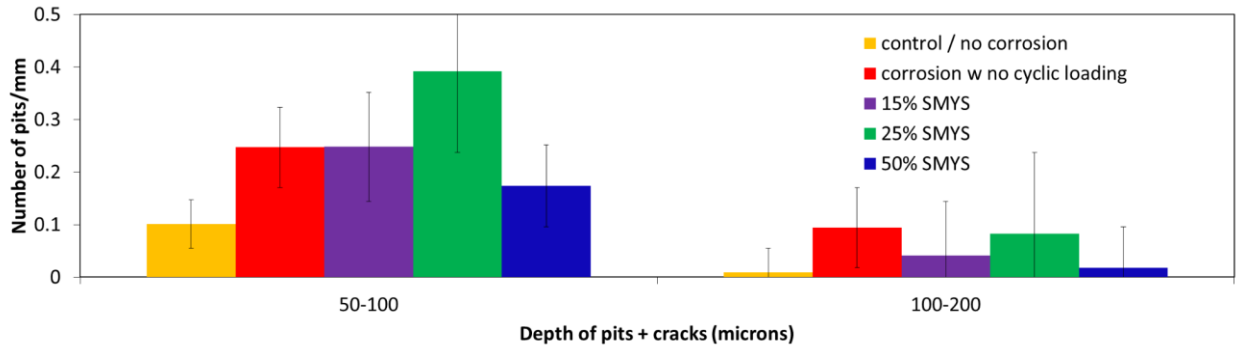

Figure 26: Distribution of depth of pits and cracks for a +20 degree bending angle, with focus on pits of >50 µm only.

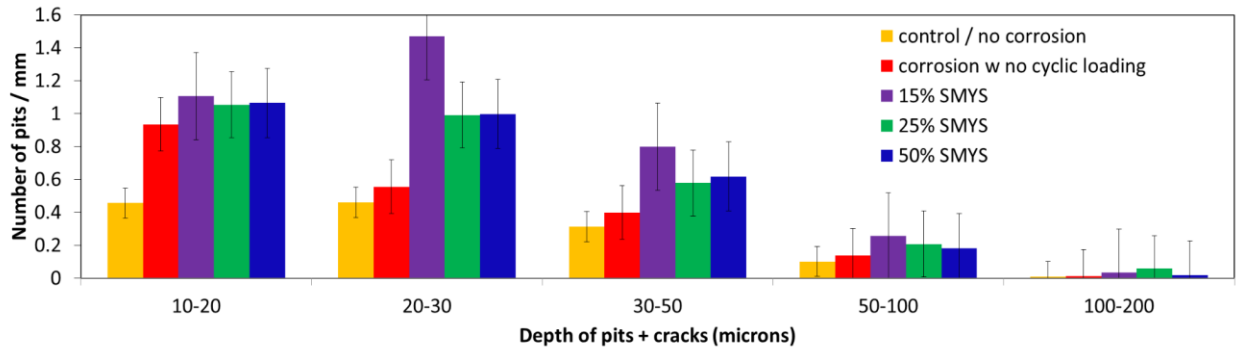

Figure 27: Distribution of depth of pits and cracks for a +40 degree bending angle.

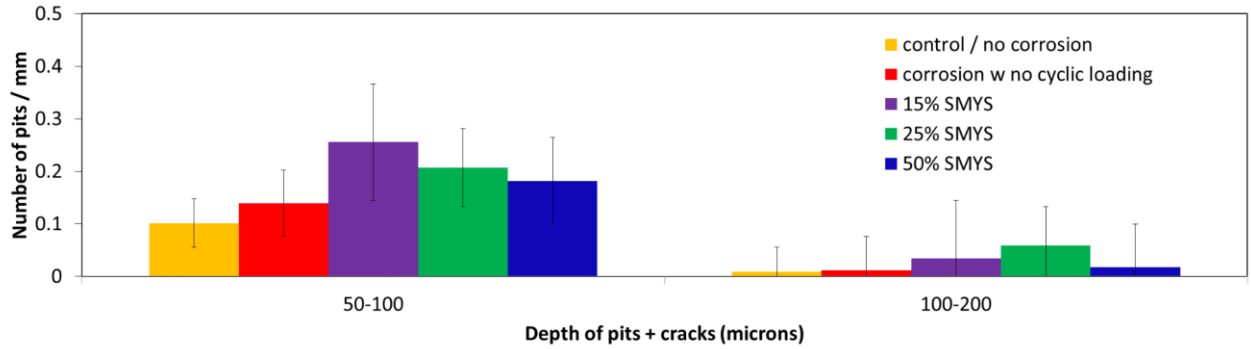

Figure 28: Distribution of depth of pits and cracks for a +40 degree bending angle, with focus on pits of >50 µm only.

In both figures, the 15% and 25% of SMYS have the most pits in the range of 20 - 200 µm. Samples under 50% of SMYS have the most 10-20 µm pits. This shows that lower maximum stresses promote the initiation and development of deeper pits. While the 25% of SMYS dominates the number of pits in a +20 degree bending angle, the number of pits occurring for 15% of SMYS dominates in a +40 degree bending angle. This indicates that maximum stress interacts with residual stress in the different bending angles, causing +20 degree samples to have more pits initiated when 25% of SMYS maximum stress is applied, and +40 degree samples to have more pits initiated when 15% of SMYS maximum stress is applied. Overall, a lower maximum stress

applied promotes deeper pits and more pitting in general in both +20 and +40 bending conditions. This lower maximum stress brings the stress range into the pitting range, which varies with bending angles.

It is also important to note that among the +20 degree bending samples, the sample with only corrosion and no loading (sample #2) has more pits of 10 - 20 μm range than the as received sample and the lower maximum load samples. Sample #2 also has about the same amount of 100-200 μm pits as 25% of SMYS loading (sample #6). Without cyclic loading to increase the tensile stress within the sample, these results contradict the understanding of compressive residual stress having the least pits initiated. Other factors, such as dissolution during mechanical loading test and pit coalescence might have occurred and will be discussed in a later section.

The results shown in Figure 25 and 27 also show how mechanical loading affects the development of pits. When comparing the as received / no corrosion sample (sample #1) with sample #2 and #3 which only undergoes a 90 days corrosion test without cyclic loading, the difference in number of pits show how dissolution contributes to an initial pit development. After undergoing a 90-day corrosion experiment, all the other samples go through cyclic loading for another 90 days. The decrease in smaller pits of 10 - 20 μm and increase in larger pits of 20 - 200 μm indicates that pits and microcracks propagate under cyclic loading test. The difference in number of pits and cracks on each maximum load indicates that mechanical stress does have a role in stage I NNpHSCC, and although dissolution is believed to be the main mechanism of this stage, mechanical stress also contributes by changing the stress profile within the samples.

4.3.2 Effect of maximum stress on pits distribution along sample length

One way to study how different maximum stresses affect the stress profile and distribution within bent samples is to observe how different maximum stresses change the number of pits along

the sample length. Figure 29 shows the pit distribution on sample #1, the control sample, before any corrosion or cyclic loading test. The distribution seen on the control sample can then be compared with the samples that went through corrosion and cyclic loading. As mentioned in section 4.3.1, there are signs of pitting and surface defects on the control sample. However, the distribution of those defects is expected to be randomized, and as seen in Figure 29, there is no area with concentrated pits. By incorporating the control sample into the results, any pit concentrating areas, as well as any pattern in the pit distribution with bending and change in maximum load can be determined. Figure 30a-d shows the pit distribution of +20 degree bending samples in an increasing order of maximum stress. Figure 31a-d shows the pit distribution of +40 degree bending samples in an increasing order of maximum stress. The red dotted line in both figures indicate the distribution as seen on the control / no corrosion sample. As mentioned, each side of the sample can be viewed as a different specimen, and the results from both sides show a symmetrical distribution of pits, which is expected because the specimens are symmetrical through the center of bend.

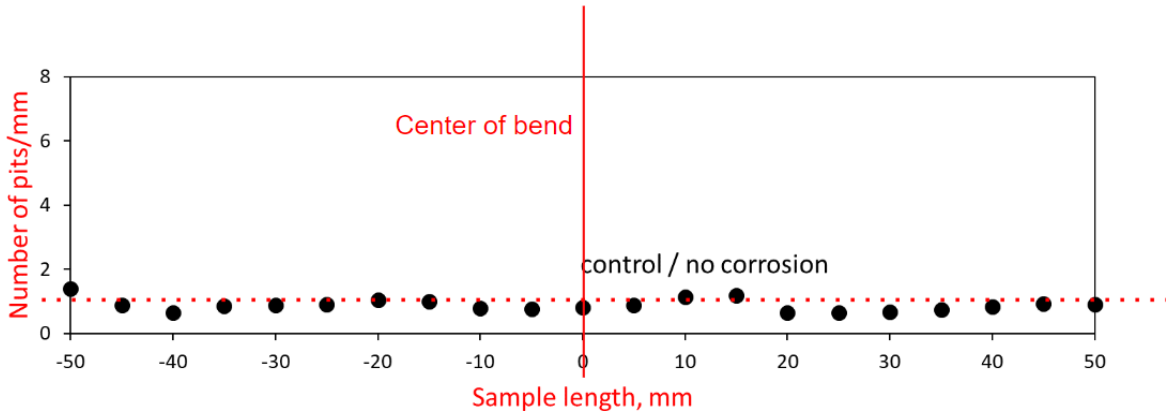

Figure 29: Pits distribution along sample length for the control / no corrosion sample.

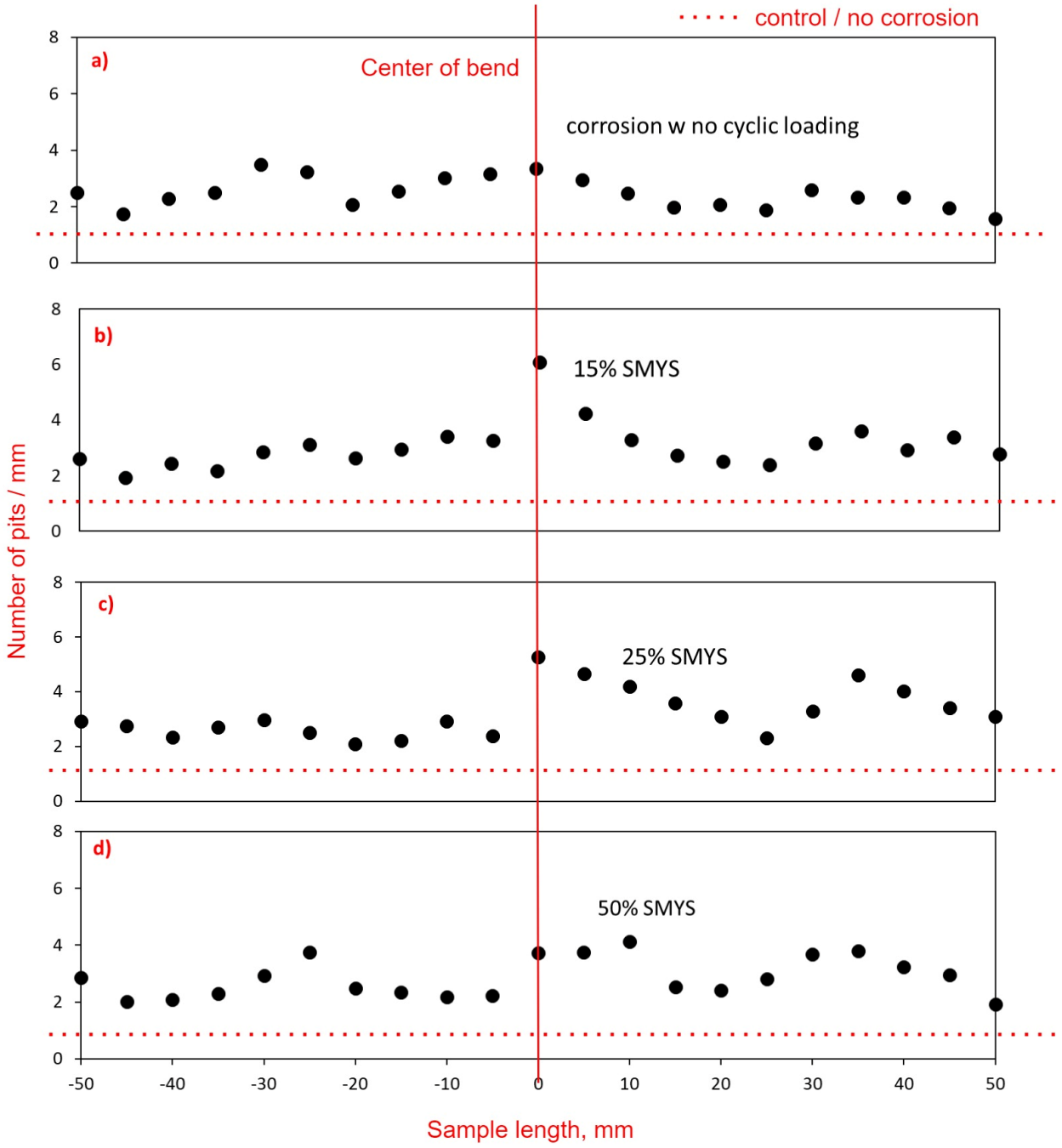

Figure 30: Pits distribution along sample length for +20 degree bending, a) corrosion with no cyclic loading, b) 15% of SMYS maximum stress, c) 25% of SMYS maximum stress, and d) 50% of SMYS maximum stress.

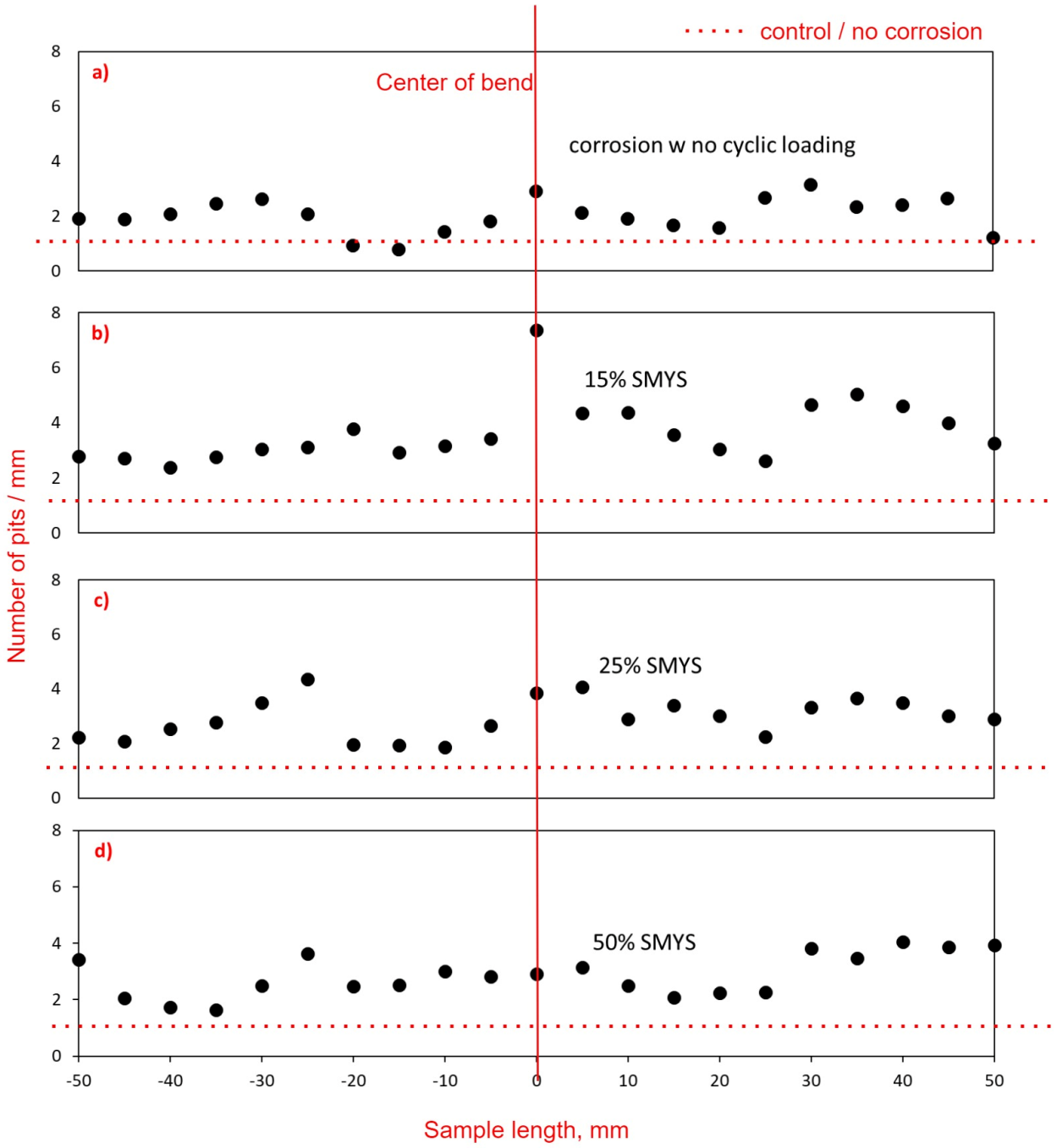

Figure 31: Pits distribution along sample length for +40 degree bending, a) corrosion with no cyclic loading, b) 15% of SMYS maximum stress, c) 25% of SMYS maximum stress, and d) 50% of SMYS maximum stress.

In both figures, there are pits found all along the surface, indicating that pitting occurs even at compressive stress locations. The samples with mechanical loading all show a clear peak at the center of the bend. Before mechanical loading is applied, the center of bend has the highest compressive residual stress. For +20 degree bending angle, the corrosion without cyclic loading sample shows the lowest number of pits at the center of bend. The 15% of SMYS sample has the most pits at the center of bend, and the number of pits at the bent center decreases with increasing maximum stress. There also appears to be an increased number of pits half way along the sample on both halves of the sample, indicating that the quarter point might have a stress concentration. Similar to +20 degree bending, in +40 degree bending angle, an increase in the number of pits at the center of bend also occurs with a decrease in maximum load, and the quarter point is also observed in these samples. The occurrence of concentrated pitting at the quarter locations is initially suspected to appear because of the sectioning of samples, however, most of the samples are sectioned about 10 mm away from this location, meaning that the heavy pitting does not occur because of sectioning. The pit distribution results indicate that lower maximum stress supports the initiation of pits at the center of bend.

From these experimental results, the effect of mechanical loading on an outward bent sample can also be seen. Figure 30-a and 31-a show the samples before any mechanical loading is applied. Similar to the loaded samples, the samples without cyclic loading show a peak at the center, though the peak is more subtle than those with cyclic loadings. This is because compressive stress locations are still subjected to pitting, however, the number of pitting occurrences in compressive areas is relatively low, as seen in section 2.4. It can be seen that overall, there is an increase in the number of pits along the surface length after mechanical loading tests. The change is not profound along the surface, but at the center of bend, the pit concentration increases

significantly. This sharp increase at the center of bend shows that mechanical loading decreases the compressive stress in the sample altogether. As discussed in section 2.4, pitting can still occur at compressive residual stress locations, but the number of pits appear to be much lower compared to a tensile area. As tensile stress increases, the number of pits also increases. While it is still unclear whether the residual stress after applying cyclic loading is tensile, it is clear that mechanical loading changes the stress distribution along the sample.

Without an applied load, the shape of these distribution curves would resemble the condition with only corrosion more, and would not show a sharp increase at the center of bend. Moreover, different maximum loads change the shape of the curve, with smaller maximum stress having a more significant effect at the center of bend. Dissolution might be the overarching mechanism for NNpHSCC, but as residual stress plays a role in pit initiation, mechanical conditions contribute a factor in pit development.

The pitting size was also plotted as a function of length to determine if there is a pattern to where larger pits occur. Since each of the 10 sectioned slices has a different pit distribution, comparing the same slice number of different samples can provide information on the stress profile along the length and width direction of the sample. Figure 32 shows the pit size distribution along the specimen length for sample #4, and Figure 33 shows the distribution for sample #9. Three slices are shown for each sample, with slice 1 being on the sample edge, slice 2 1 mm away from the edge, and slice 10 located in the center of the sample. The locations of these slices are marked in Figure 34.

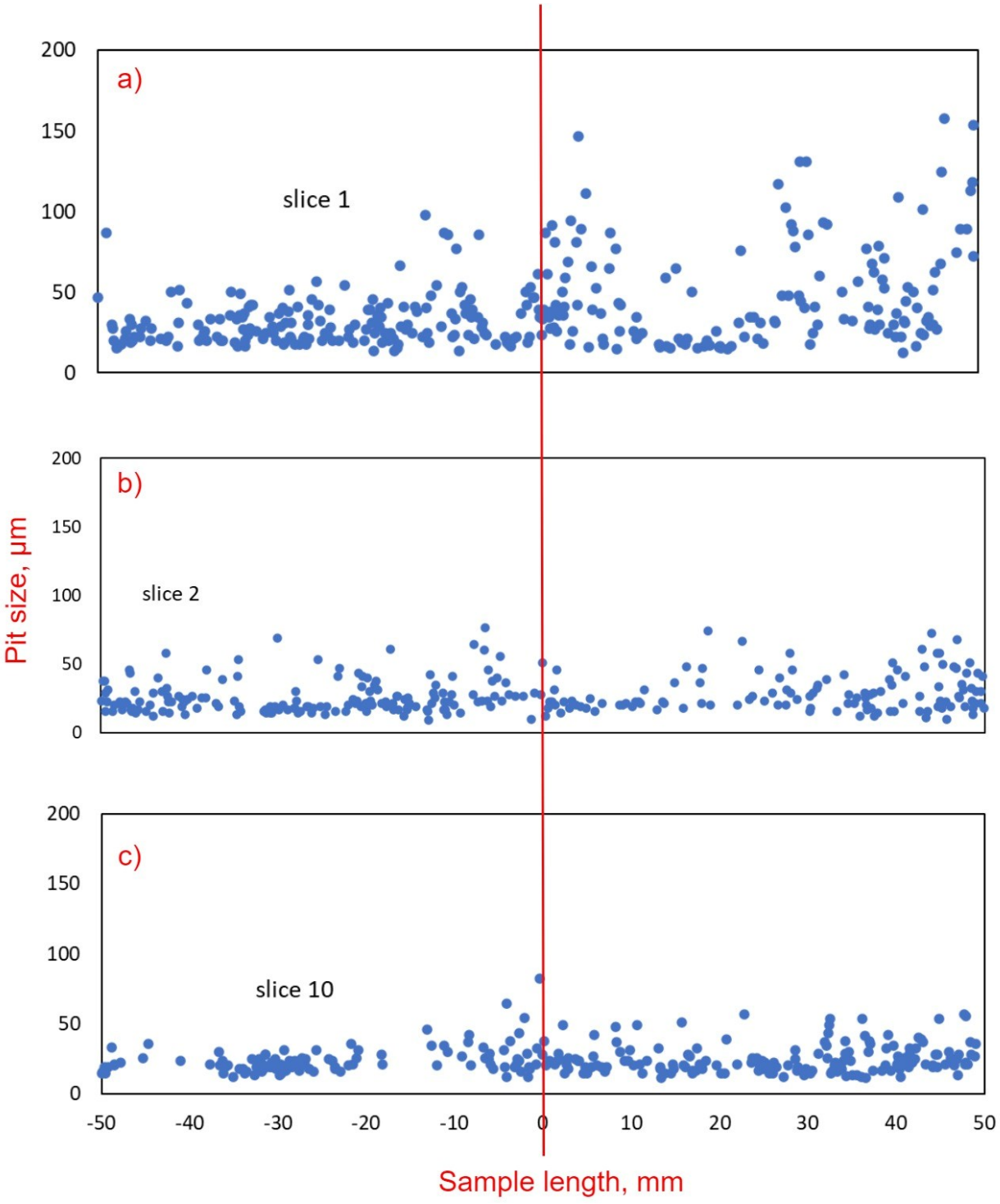

Figure 32: Pit size distribution along sample length for a +20 degree bending sample with 50% SMYS maximum stress, on a) slice 1, b) slice 2, and c) slice 10.

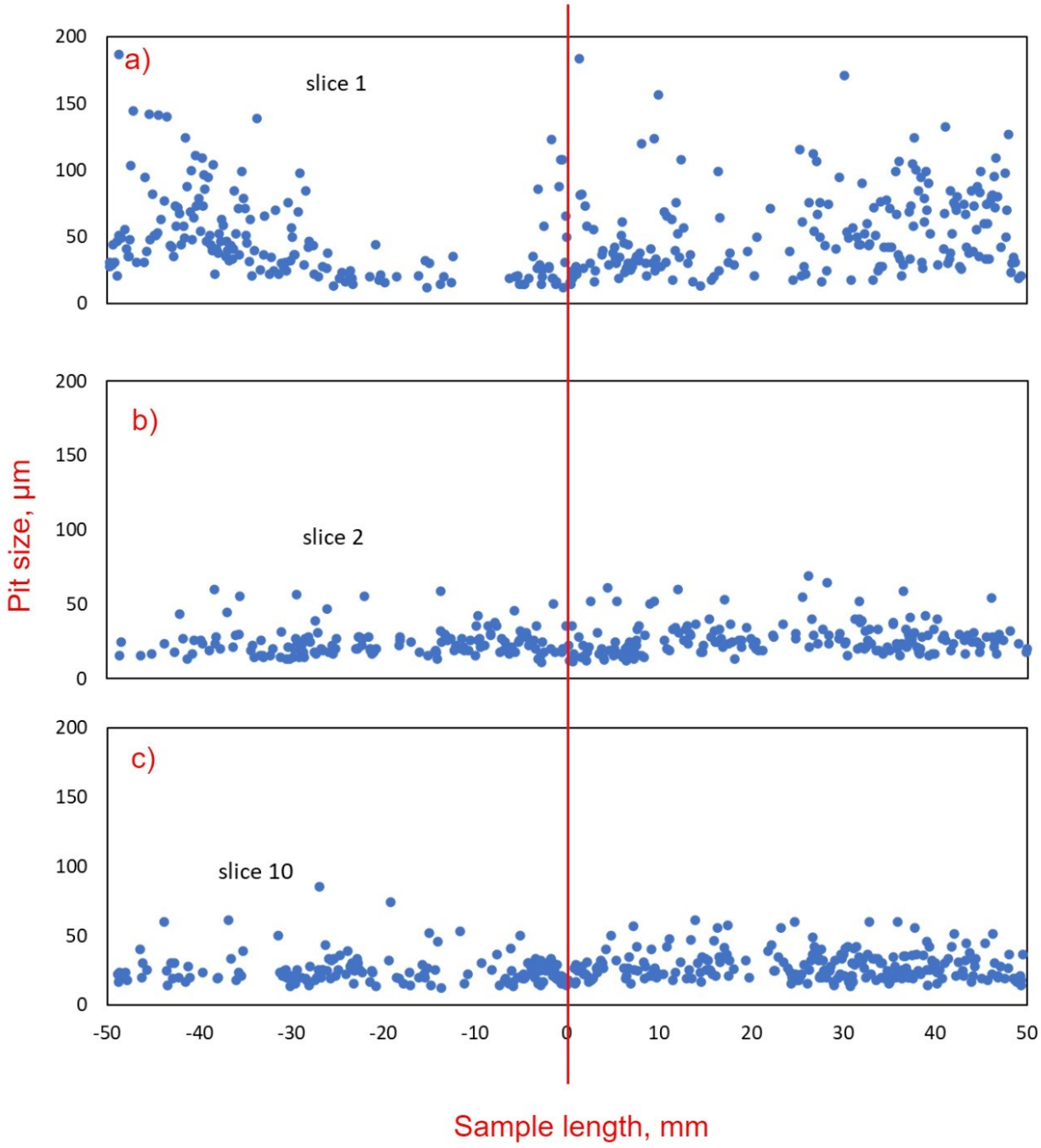

Figure 33: Pit size distribution along sample length for a +40 degree bending sample with 15% SMYS maximum stress, on a) slice 1, b) slice 2, and c) slice 10.

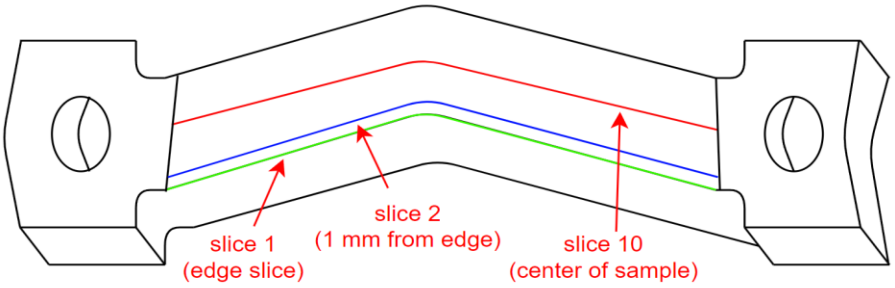

Figure 34: Slices location on the dog-bone specimen

As seen in Figure 32 and 33, the size distribution does not follow any pattern along the sample length. Pits of all sizes are scattered throughout the length of the samples, even though there is a residual stress profile along this direction. It appears that residual stress distribution plays a more significant role on pitting occurrences. It is also important to note that in both sample #5 and #9, the edge slices (slice 1) have more pits of a larger size. Pits that are below 100 µm are found all along the width of the specimens, however, larger pits of more than 100 µm are mostly found on the edge. The effect at the edge will be discussed in section 4.5. In the field, however, pipeline is welded together and this effect does not apply, and welding raises as another stress factor. However, welding will not be considered in this work, as this work focuses more on NNpHSCC occurrences away from weld areas, and welding is a complicated factor and needs to be studied separately.

4.4 Effect of bending angle

In this study, two bending conditions represent two residual stress conditions within the sample. Two outward bending angles of +20 and +40 degree were chosen as they represented the more aggressive bending conditions observed. In the field, it is common to see pipes bent at small

angles such as 10 or 20 degrees, and occasionally 40 degrees. Bending conditions that are more than 40 degrees are considered rare, as bending happens in the field because of soil movement or other applied stresses, but in some cases, it can happen due to the local change in elevation at the pipe location. In order to understand how bending affects cracks initiation and growth in NNpHSCC, samples with the same mechanical loading conditions and different bending angles were compared in terms of number of pits and cracks depth, as well as how these pits and cracks were distributed along the specimen length.

4.4.1 Effect of bending angle on pits and crack depth distribution

The number of pits and cracks of all sizes were plotted between the two bending angles to compare the number of pits developed with each bending angle. Figures 35-38 show how changing the bending angle affects samples without cyclic loading, at 15%, 25% and 50% of SMYS, respectively. Before any mechanical loading is applied, the +40 degree samples have more compressive residual stress at the center of bend compared to the +20 degree samples. This is because a more aggressive bending angle experiences more stress after springback, causing a larger residual stress profile within the sample. The results shown in Figure 34 reflect this difference in residual stress. The +20 degree samples have slightly more pits of all sizes compared to the +40 degree samples. From the bending results, it is clear that pitting can still occur under compression, from anodic dissolution [49]. Anodic dissolution appears to be enhanced in a compressive stress state as compared to a tensile stress state, causing corrosion to occur in a compressive stress location [49]. However, compressive residual stresses act against crack initiation, therefore the number of cracks observed can appear a lot lower at compressive locations as compared with tensile locations.

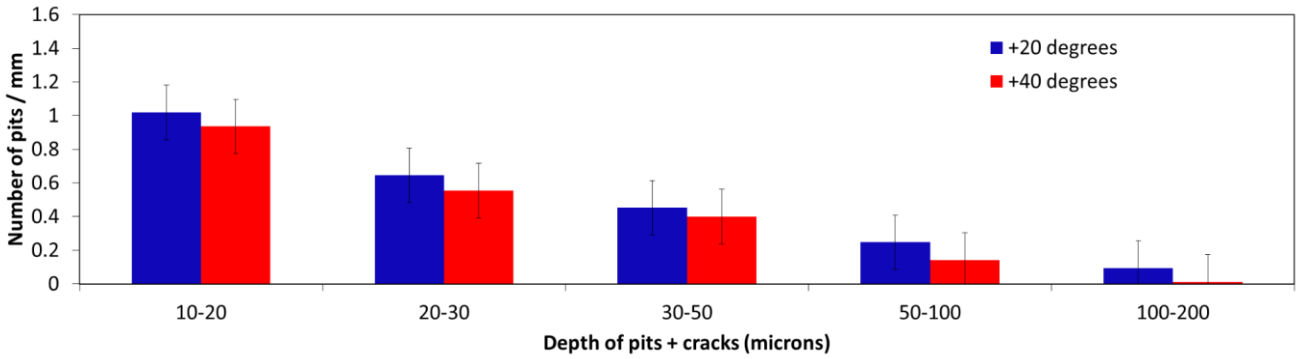

Figure 35: Pits and cracks statistics for corrosion without loading samples (sample #2 and #3)

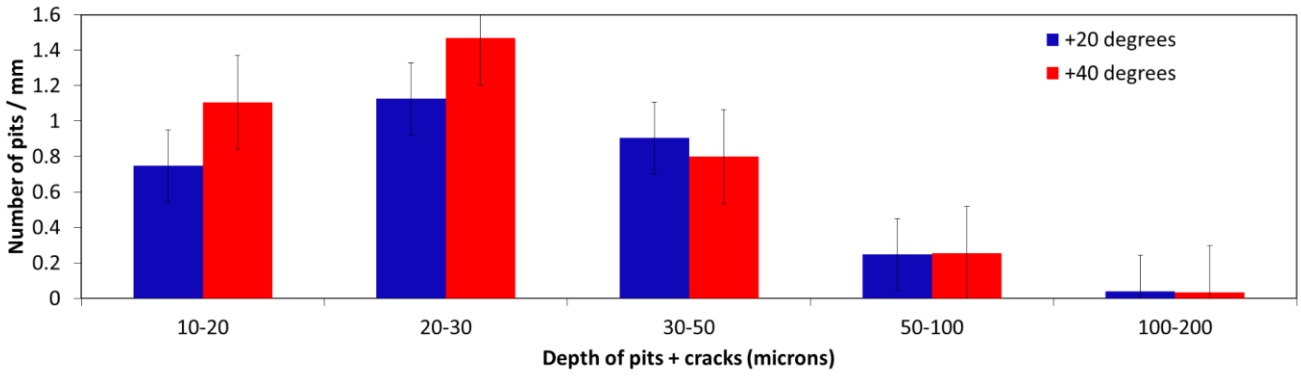

Figure 36: Pits and cracks statistics for 15% of SMYS samples (sample #8 and #9)

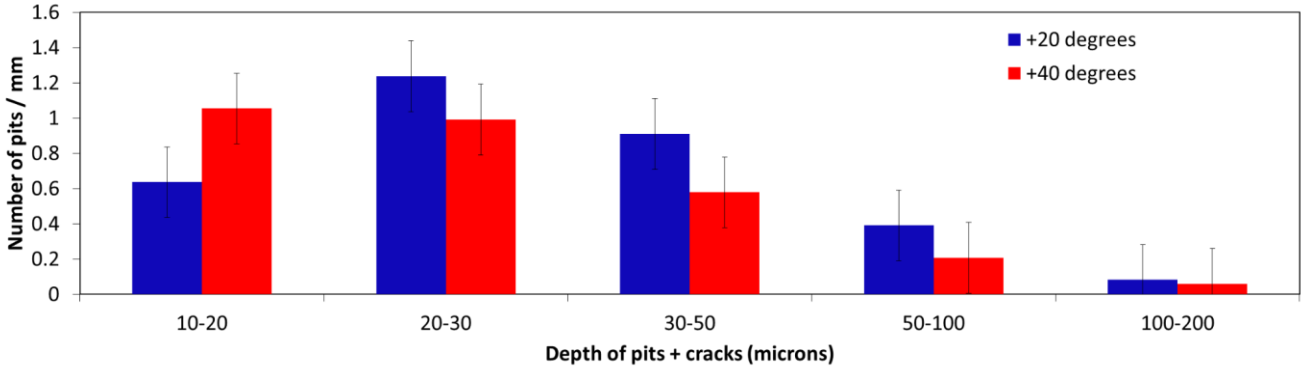

Figure 37: Pits and cracks statistics for 25% of SMYS samples (sample #6 and #7)

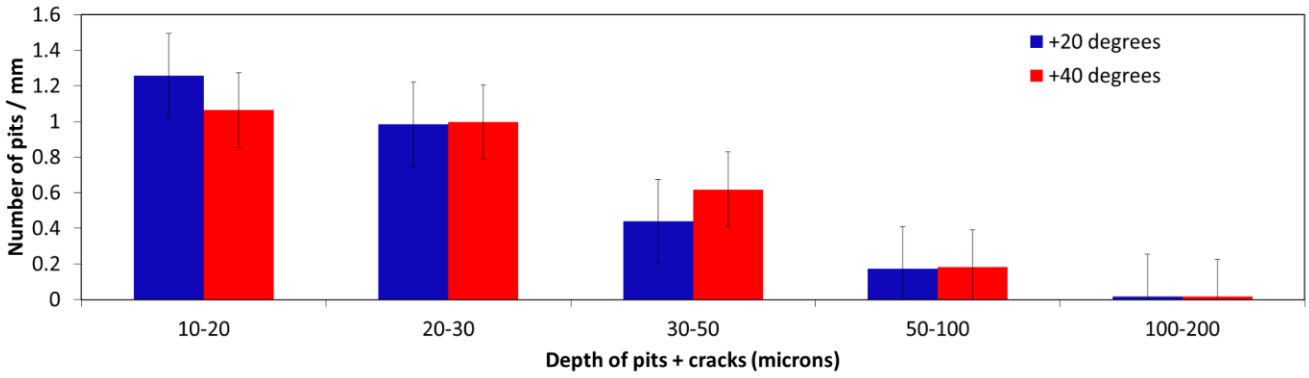

Figure 38: Pits and cracks statistics for 50% of SMYS samples (sample #4 and #5)

The trend seen in the samples with no cyclic loading, however, was not seen in the mechanically loaded samples. For 15% of SMYS cyclic loading samples, +40 degrees dominates in the number of pits and cracks from 10-30 μm. As the larger pit sizes are examined, +20 degrees dominates, but only by a little. There are many possible explanations for why that happened. Mechanical loading changes the residual stress distributions at the sample surface, making more pits initiate at the surface. Cyclic loading changes the stress state in the thickness direction as well, causing existing pits to grow. As pits grow deeper into the materials, they change the local stress state where they appear, causing a change in the speed of growth. In the case of 15% of SMYS, as more pits initiate, it causes a significant stress difference at the surface. However, within the sample's thickness direction, the change caused by pitting occurrences and cyclic loading are not very significant. More so, as more pits are initiated in +40 degree samples, cyclic loading makes +40 degree bending the more severe condition for crack initiation at the surface by bringing the residual stress into the pitting range. This result occurs also from the amount of plastic deformation on both samples. As +40 degree samples are subjected to a larger bending angle, they have more accumulated plastic strains. With tensile stress and plastic strain at these locations, pits initiate more readily, as seen in the results [33].

The same can be said for the 25% of SMYS samples. A larger tensile stress changes the residual stress distribution and the plastic strain at the surface, causing more pits to initiate in the +40 degree samples than +20 degree samples. However, the results are not the same in 50% of SMYS cyclic loading samples. In these samples, the number of 10 - 20 μm pits in +20 degree bending dominates the +40 degree, but for pits larger than 20 μm, +40 degree bending shows a slightly higher number of pits than +20 degree. This result is almost the opposite to the previous results. This likely happens because at a high tensile stress, the residual stress change in the sample is more significant, especially in +40 degree bending angle. A higher maximum stress causes a larger change in +40 degree bending, while in lower bending angles, this effect is minimized. Therefore, pits grow faster in this condition, allowing for a higher number of larger pits seen in +40 degree bending. Moreover, it is clear that 50% of SMYS supports more pit and crack growth compared to lower maximum loads, while lower maximum loads support the initiation of smaller pits.

In conclusion, bending angle changes the residual stress within the sample, and can be an important factor in NNpHSCC crack initiation when the applied stress is known. With varying mechanical conditions, it is more difficult to determine which bending condition would be more detrimental to cause crack initiation in pipeline steel.

4.4.2 Effect of bending angle on pits distribution along sample length

Another way to understand the effect of bending angle on stage I NNpHSCC is to compare the pits distribution along the sample length at the same mechanical loading condition for different bending angles. Figures 39-42 compare the difference in pits distribution along the sample length between +20 and +40 degree bending angle for samples without cyclic loading, at 15%, 25% and 50% of SMYS, respectively. As discussed in section 4.3.2, after bending, samples with +40 degree

bending experience more compressive stress at the center of bend, so pitting is more unlikely to occur at the center of bend. This can be seen in Figure 39. Without any cyclic loading, the +20 degree sample shows more pitting. There is no difference in the pit distribution curves between the two bending angles, because there is no cyclic loading applied to change the residual stress distribution along the specimen length.

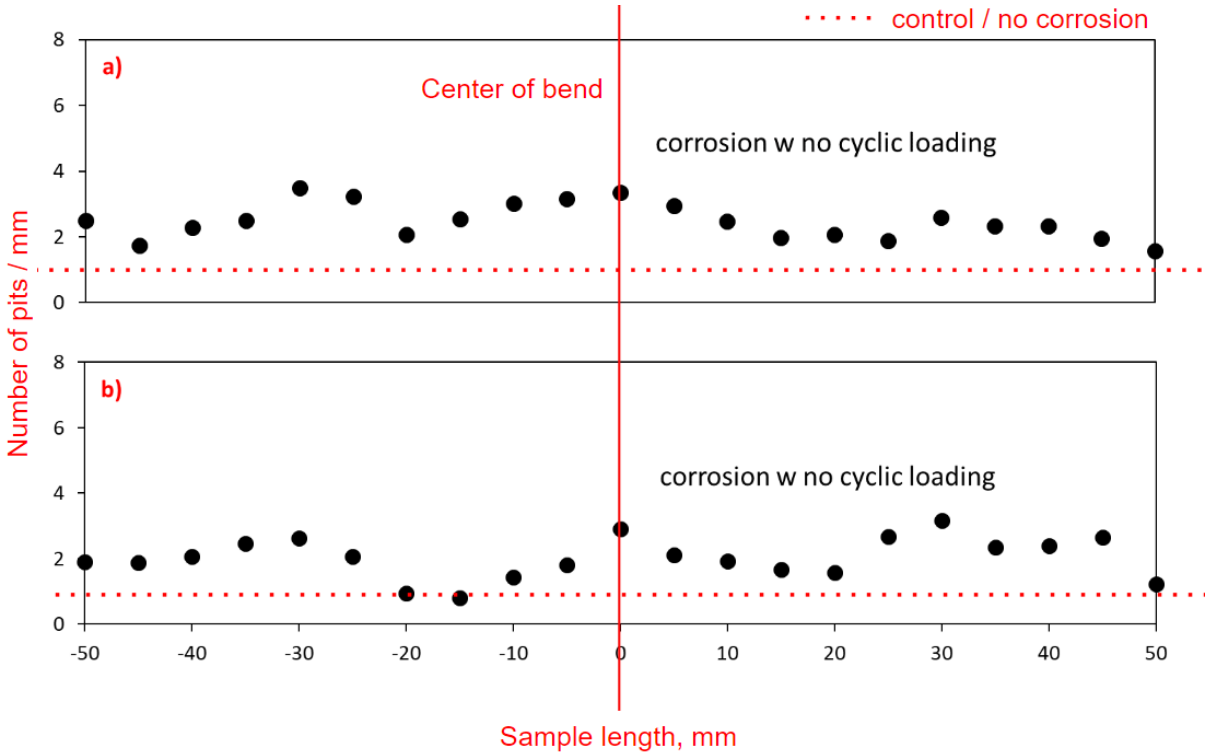

Figure 39: Pits distribution for corrosion without loading, a) +20 degree, b) +40 degree bending

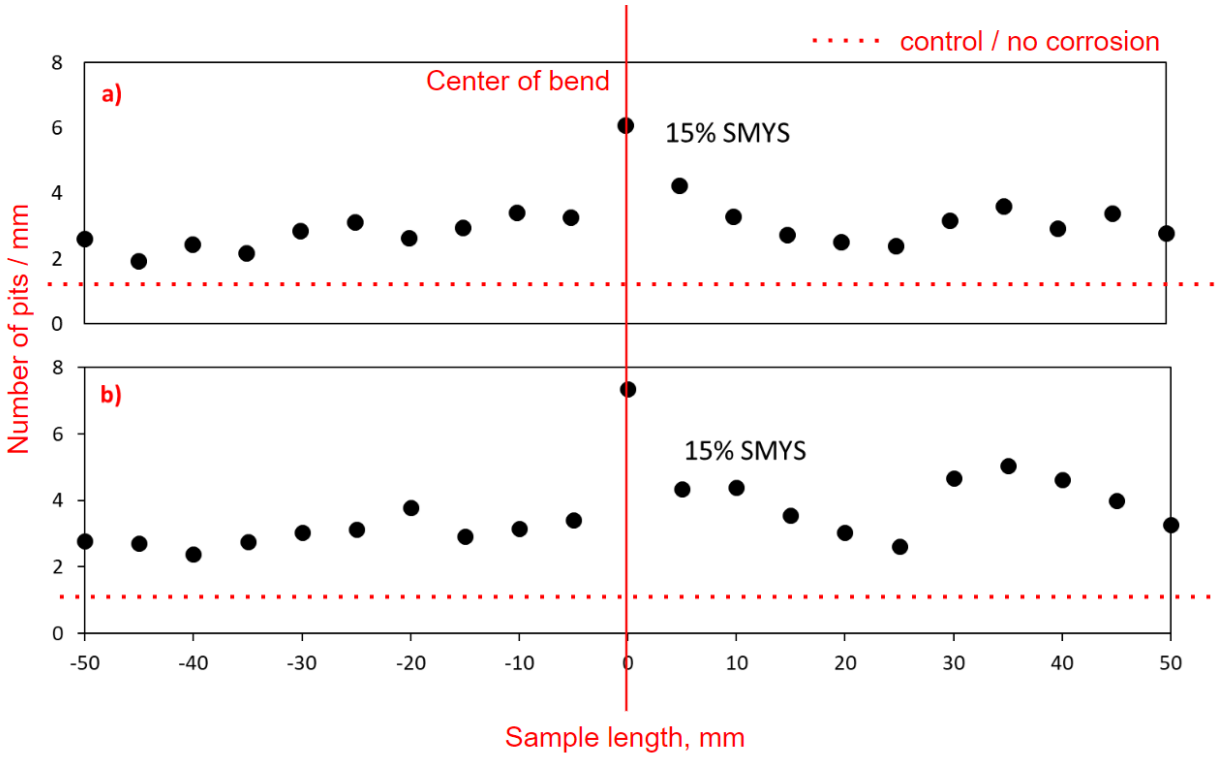

Figure 40: Pits distribution for 15% of SMYS loading for, a) +20 degree, b) +40 degree bending

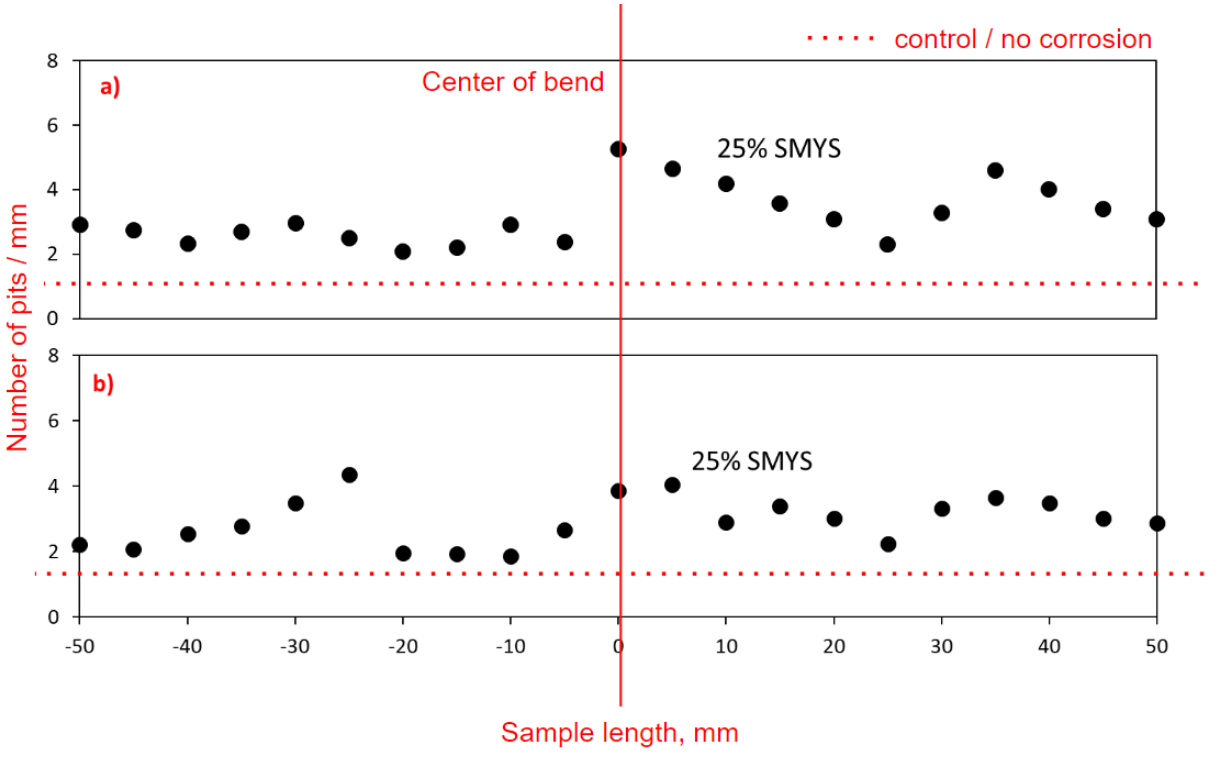

Figure 41: Pits distribution for 25% of SMYS loading for, a) +20 degree, b) +40 degree bending

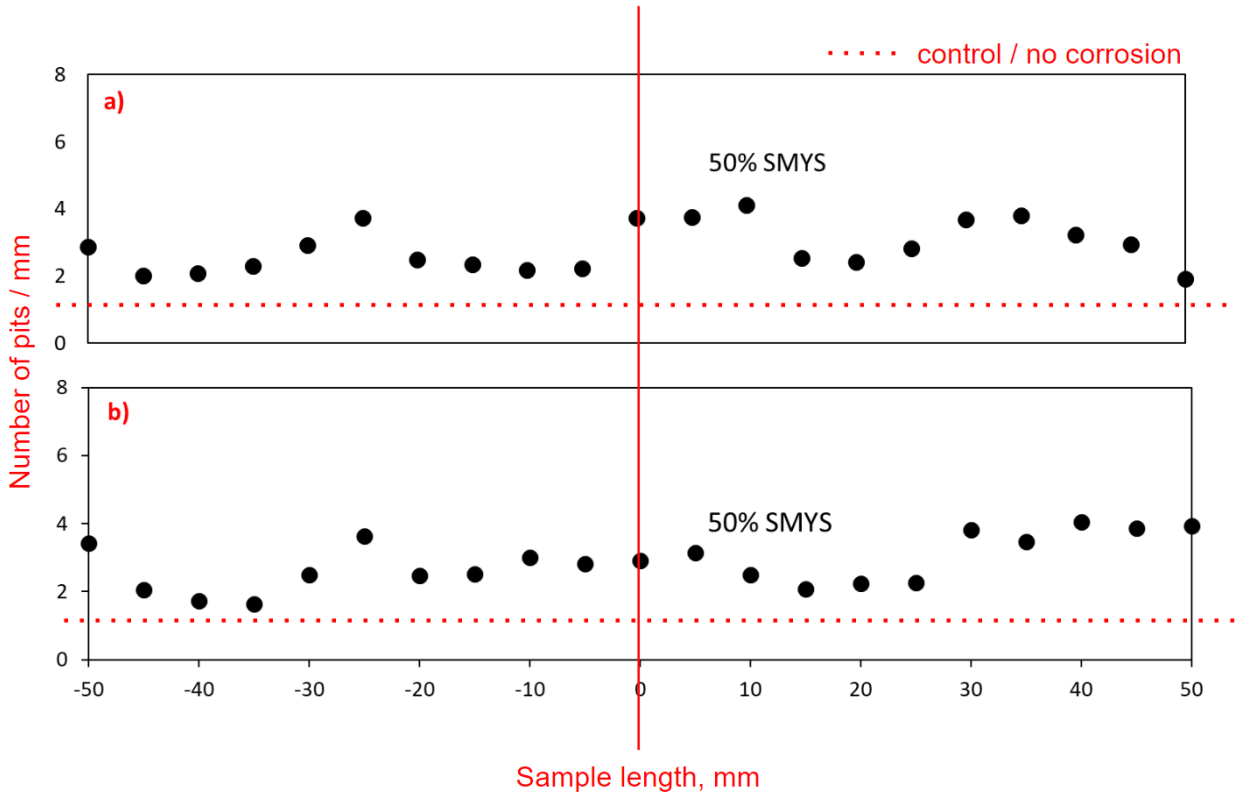

Figure 42: Pits distribution for 50% of SMYS loading for, a) +20 degree, b) +40 degree bending

When cyclic loadings with 15% of SMYS maximum load are applied, +40 degree samples show more pitting at the center of bend than +20 degrees. The number of pits increases along the surface in both cases, but +40 degree bending shows a sharper rise at the center of bend. When some cyclic loading is applied, the residual stress at the center of bend for +40 degree samples approaches the pitting zone, therefore, more pitting is seen at the center of bend. Prior to cyclic loading, +20 degree samples are in the residual stress range that causes pitting. With cyclic loading applied, the residual stress range changes for +20 degrees, therefore, less pitting occurs at the center of bend. When the maximum stress is increased to 25% of SMYS, the residual stress within the samples changes from the 15% of SMYS condition. The +20 degree bending shows more pitting at the center of bend, and the difference is approximately 1 pit/mm. This shows that a higher maximum stress brings the residual stress levels of both bending angles out of the pitting range.

Therefore, +20 degree samples continue having the more aggressive condition. Similarly, in the 50% of SMYS samples, the +20 degree bending dominates +40 degrees at the center of bend. It can be concluded that near the center of bend, +20 degree bending is more susceptible to pitting than +40 degree, especially at higher maximum stress in a cyclic loading cycle. The maximum stress that causes a certain bending angle to have more pitting changes with how residual stress is distributed along the surface. A residual stress measurement for both bending angles before and after cyclic loading would be crucial to understand the effect of both maximum stress and bending angle on NNpH pits and cracks initiation.

4.5 Effect of cutting edge on pits and cracks distributions

As mentioned in section *4.3.2*, the sample edge has a different distribution than the rest of the sample. In order to understand the edge effects, many factors are considered. The sample edge is the interface between the pipeline outer surface and the side. Edging provides a stress concentrator similar to how grain boundaries cause a weaker point in the material matrix. Therefore, edges are expected to have more severe corrosion compared to any other inner slices of the sample.

Secondly, the residual stress near the edge can be an important factor to why more pits occur along the edge. In order to determine if residual stress plays a key role in this distribution, an FEM analysis was done by Z. Xu as part of the SCC Group at the University of Alberta [50]. With this analysis, Xu also performed bending on a stick sample, and used finite element method (FEM) to model the stress distribution on the surface of the sample. The FEM was done on Abaqus, using 3D modelling. After bending, the samples were slightly straightened to imitate the springback condition as seen in bending samples. Figure 43 shows the results from this study on a

tensile surface, done on a sample bent to +40 degree angle. Figure 44 illustrates this sample after being allowed to spring back to +20 degrees.

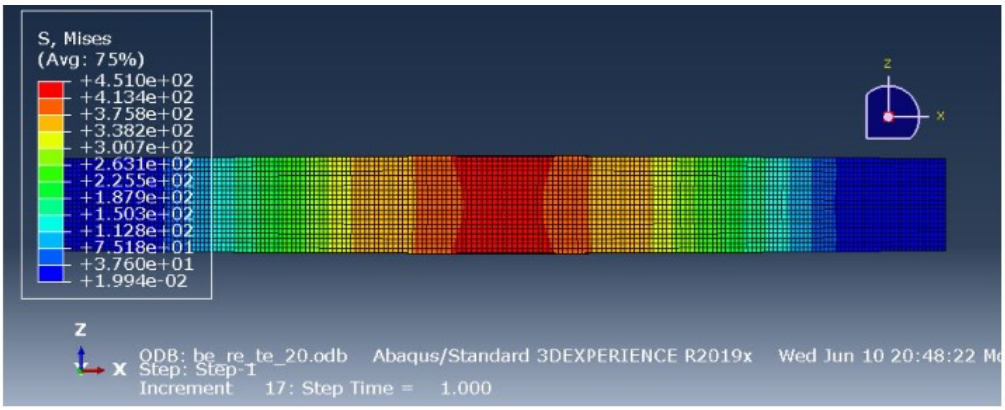

Figure 43: FEM model of a compressive surface bent to 40 degrees [50].

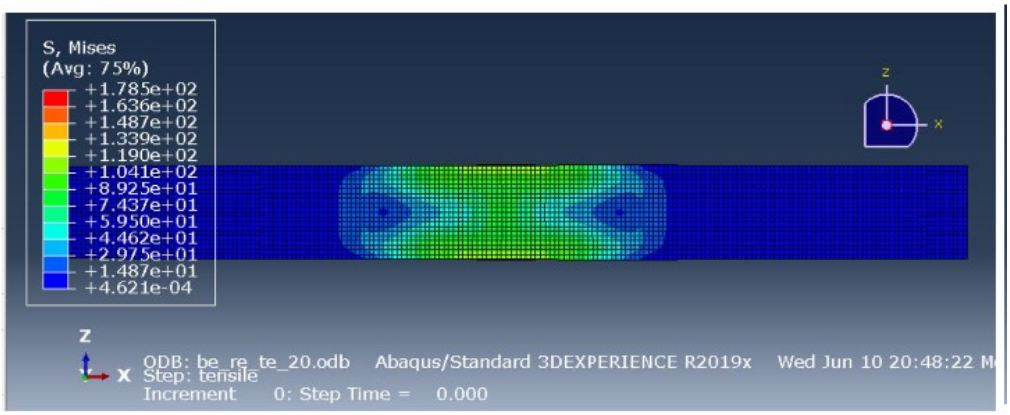

Figure 44: FEM model of a compressive surface bent to 40 degrees and straightened to 20 degrees [50].

As seen in FEM results, the stress is highest at the center of bend, and decreases on both sides of the sample length. As springback is allowed to occur, the stress state changes as the tensile surface becomes compressive and vice versa, and the stress also decreases significantly. After

springback, the stress distribution within the width direction of the sample is not uniform anymore. As seen in Figure 44, the two edges of the sample have a higher stress state compared to the center. The high stress on the edge, however, would be compressive after springback. As the residual stress increases towards the edge, edging shows more pit occurrences compared to the inner surfaces. The FEM results, however, have some limitations and cannot fully describe the real situation. The modelling uses a straight sample, while a machined sample taken from the pipe contains the pipe curvature. The curvature changes the stress distribution in the sample width, making it more challenging to perform modelling. Moreover, Xu attempted to study the effect of springback after bending by straightening the modelled sample to an angle, but it is generally difficult to estimate the amount of springback in any bending, therefore, it is challenging to implement the effect of springback into FEM analysis.

Another explanation for the increased number of pits along the edge would be the effect of plastic deformation after bending. As bending is done on a dog bone sample, the area near the center of bend experiences severe plastic deformation, evident on the edge. Figure 45 shows the edge of the sample after bending. The deformation markings also act as a stress concentrator at the edge, and when coming into contact with a corrosive environment, will corrode readily.

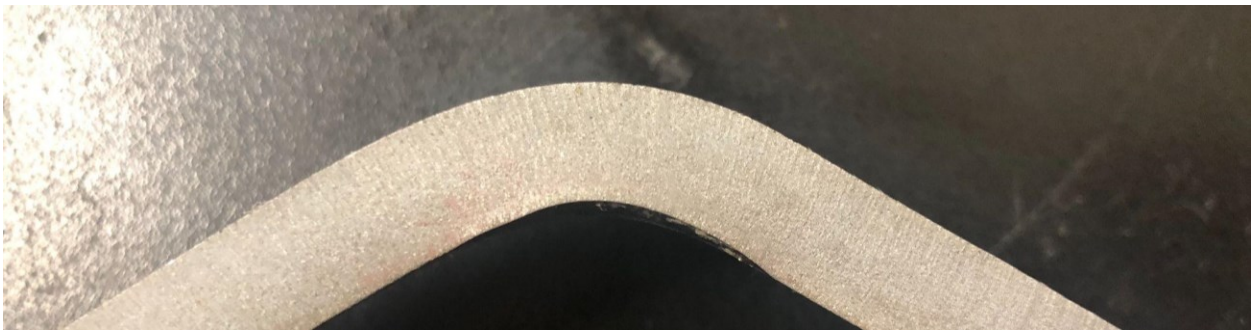

Figure 45: Sample edge after bending.

Because edging is not a condition seen in the field, depth distribution of pits and cracks, as well as pits and cracks distribution are replotted without the edge. Figure 46 and 47 show the number of pits and cracks of different maximum stresses for +20 and +40 degree bending, with and without the edge. Between the samples with and without edge, there is not a lot of difference in whether the edge slice is included. The number of pits from 10 - 50 μm, as well as the pattern seen in different maximum stresses remain unchanged. The number of pits larger than 50 μm in samples excluding edge, however, show a decrease compared to the samples with edge, especially in the control, corrosion with no cyclic loading, and 50% of SMYS. It is also noted that most of the larger pits of sizes 100 - 200 μm are located on the edge of the sample, and as the edge is removed, these larger sized pits are not observed. Without the readily corroded condition on the sample edge and the stress concentrator caused by edging, larger pits and cracks do not develop in this stage. On average, the 9 slices analyzed still yield a similar result to all 10 slices, with the exception of deeper pits of 100 - 200 μm. This result shows the importance of stress concentrator on pit initiation and pit growth in stage I NNpHSCC.

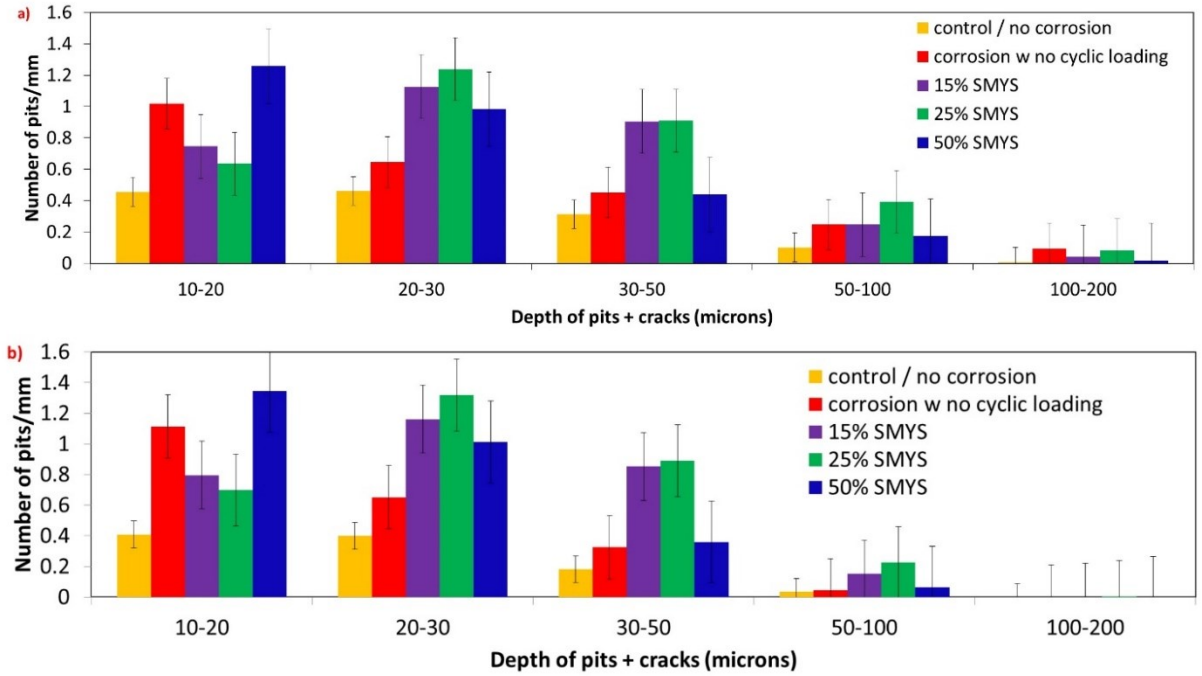

Figure 46: Distribution of depth of pits and cracks for +20 degree bending angle, a) with edge, b) excluding edge.

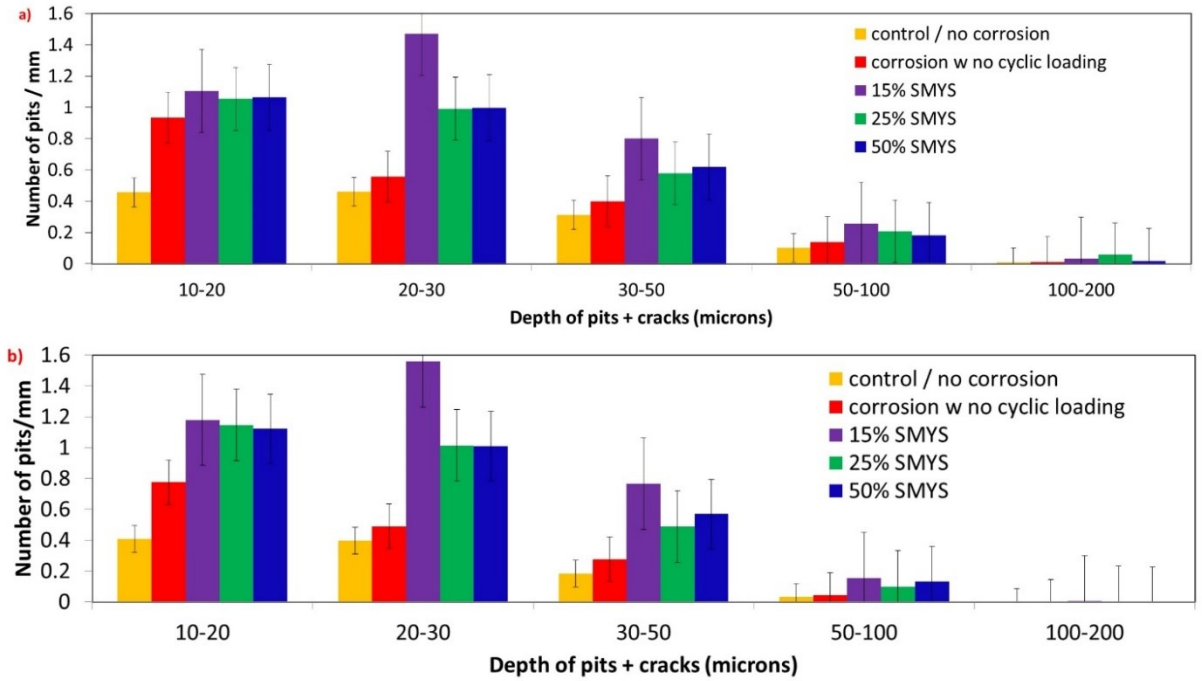

Figure 47: Distribution of depth of pits and cracks for +40 degree bending angle, a) with edge, b) excluding edge.

The pitting distribution along the sample length is also plotted while excluding the effect of edging. Figure 48 demonstrates the distribution differences in sample #6, with and without the edge slice. Similar to the depth distribution, there is also little difference in the distribution along the sample length for samples without the edge slices. The edge contains more pits and cracks of larger sizes, as seen in Figure 32 and 33, but if only the number of pits and cracks along the surface length is considered, the effect of edging is minimized compared to the effect of the maximum loading condition and residual stress on how pits and cracks are distributed along the surface. The comparison in the rest of the samples can be found in the Appendix. Therefore, edging can be a source of experimental error when larger pits are considered. It is important to exclude edge slices when the pit size is analyzed to remove this error source.

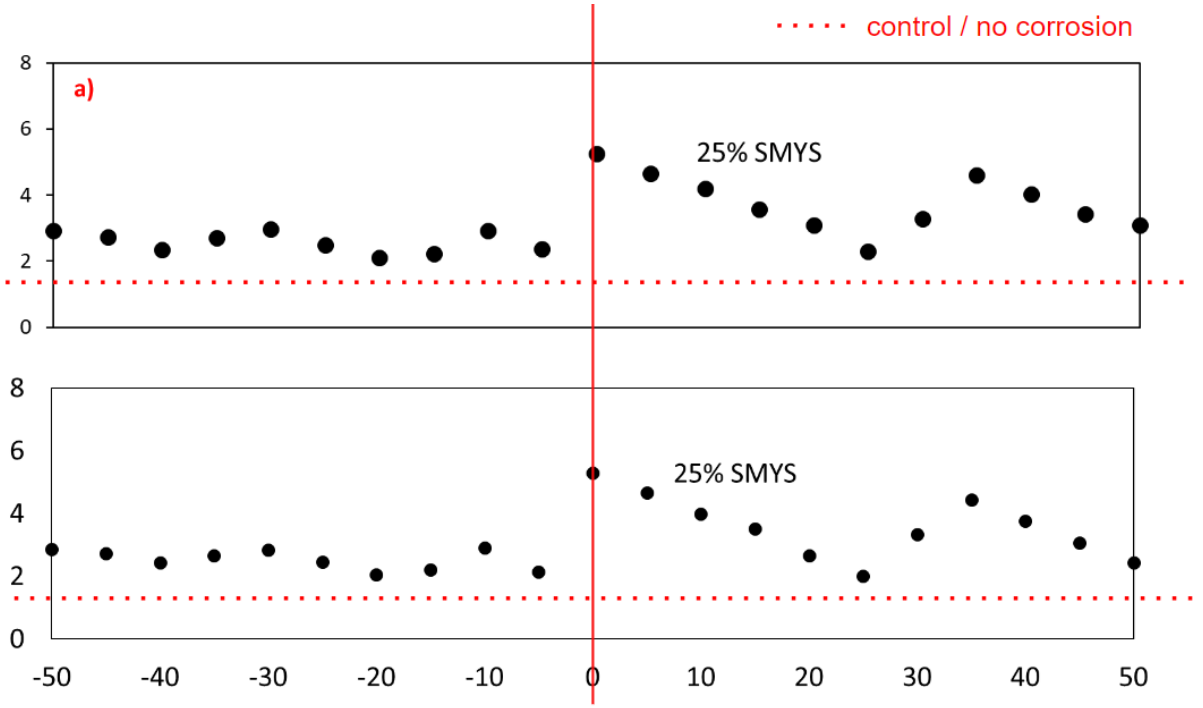

Figure 48: Pits distribution along sample length in sample #6: +20 degree bending, 25% of SMYS cyclic loading, a) including edge, b) excluding edge.

4.6 Discussion

The behaviour of X52 steel with varying maximum stresses depends on a number of factors. While the experiment focuses on the pitting occurrences and how pitting changes with cyclic loading, other factors that happen during the corrosion process can also contribute to how pitting appears and change how cracking occurs. In this section, the actual effect of cyclic loading on residual stress distribution will be discussed. Pits coalescence and mill scale will also be discussed as they both are important factors during stage I NNpHSCC.

4.6.1 Effect of cyclic loading on residual stress distribution

Residual stress is the most important stress factor in this study. Bending provides the source of residual stress, and cyclic loading changes the residual stress distribution caused by bending, either increasing or decreasing the residual stress. For a compressive residual stress (negative values), tensile cyclic loading increases the residual stress (i.e makes it more tensile). Figure 49 shows how residual stress changes after cyclic loading is applied [33]. Note that the study by Van Boven et al. only investigates the effect of cyclic loading in air, which strictly shows how cyclic loading affects residual stress. The pitting shown after dissolution will change because dissolution plays a key factor in pits and crack initiation in this stage, and pitting from dissolution also changes the residual stress distribution in the sample.

While tensile cyclic loading increases the residual stress in a compressive sample, making it less compressive, an applied tensile stress does not do the same to locations that experience a tensile residual stress. In Chen et al.'s study, the residual stresses along the length and thickness directions of a bent sample are measured before and after tensile cyclic loading is applied. The outward bending surface experiences tensile, while the inward bending surface experiences compressive stress, as seen in Figure 50.

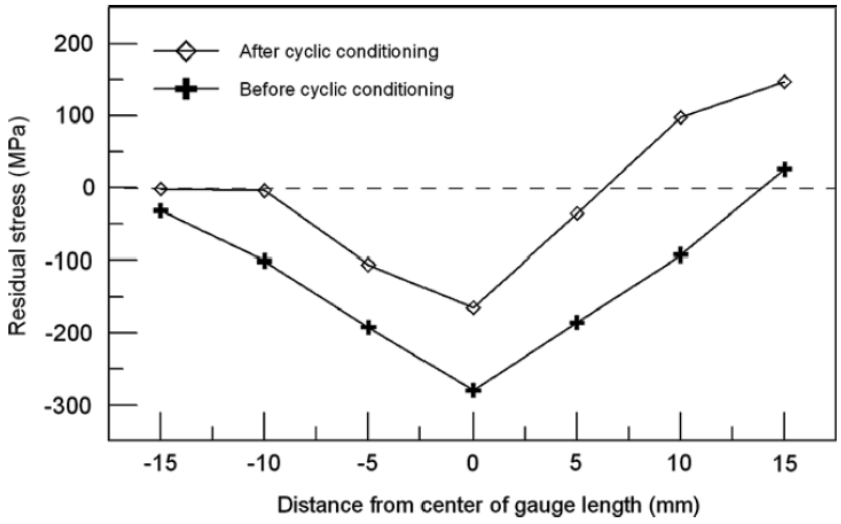

Figure 49: Residual stress in a compressive loaded sample, before and after cyclic loading applied [33].

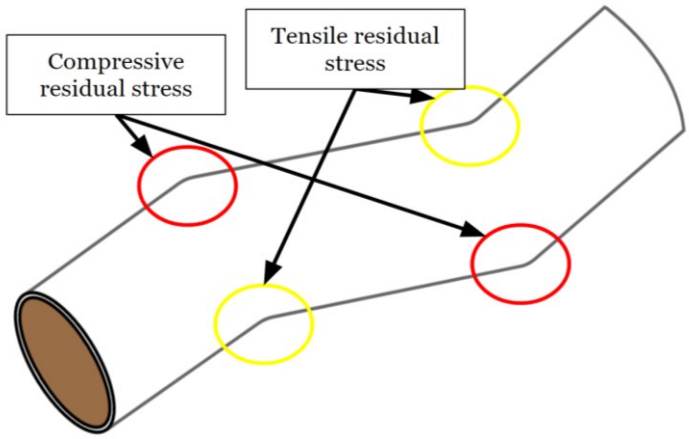

Figure 50: Bent pipeline. At a bent location, one surface experiences tensile residual stress, while the other experiences compressive residual stress.

Figure 51 shows the residual stress distribution along the depth of the sample, before and after cyclic loading [34]. Before cyclic loading, the two opposite surfaces have high tensile and compressive residual stresses. After cyclic loading is applied and removed, the two surface residual stresses decrease in magnitude, bringing the stress profile closer to zero within the sample. At locations with compressive residual stress, this can increase to become tensile, as seen 7 mm away from the center of gauge length, though the total stress within the pipe section balances out, and adds up to a total of 0 MPa throughout the entire sample length [20]. Before cyclic loading, there is high tensile residual stress at the inward bending surface, and therefore, at the outward bending surface, there must be high compressive stress to balance the high tensile residual stress. The local residual stress at a certain location can be tensile or compressive, but the total stress in the pipe when no external load is being applied always comes to zero. Because of this condition, after tensile cyclic loading is applied, the pitting occurrences change within the sample, as seen in the result section. Tensile cyclic loading can cause less pitting and cracking to occur on the surface, as the applied stress decreases compressive stress magnitude within the specimen.

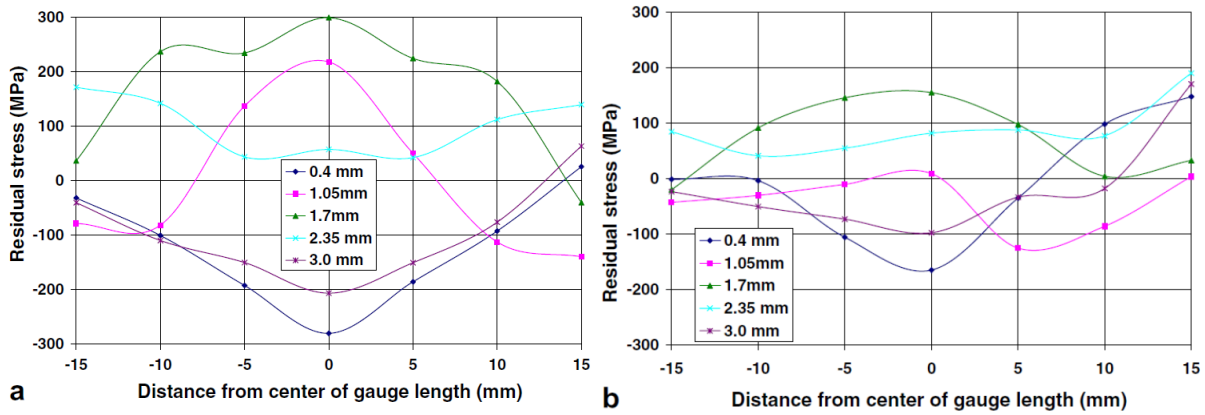

Figure 51: Residual stress distribution a) as received bent sample, b) sample after cyclic loading in air [34].

The aforementioned studies examine the residual stress in the bent specimens after cyclic loading is removed. This condition is similar to the spring back condition, i.e. the stress state in the sample after the original load is removed. However, it is of interest to understand the stress state during cyclic loading, in combination with the effect of dissolution. Without any cyclic loading applied, the residual stress distribution in the sample is the same as the springback condition, and the residual stress at the center of bend is measured [33,34]. When a tensile cyclic load is applied to an outward bending location, the center of bend experiences a compression, while the other points along the surface experience the tension from the load. At a higher maximum stress, the compressive force at the center of bent increases, acting against crack propagation. Therefore, in section 4.3, 50% of SMYS shows the lowest number of pits compared to any lower maximum stress, and unlike the lower maximum load conditions, pits and cracks of 50% of SMYS cyclic loading do not concentrate at the center of bent. When the cyclic loading is removed, however, 50% of SMYS would show the least compressive residual stress at the center of bend because the samples are allowed to relax and spring back. Figure 52 illustrates this phenomenon. Therefore, it is important to understand how materials behave during and after cyclic loading is removed in order to understand the pit initiation pattern, so that the most aggressive condition can be determined and prevented.

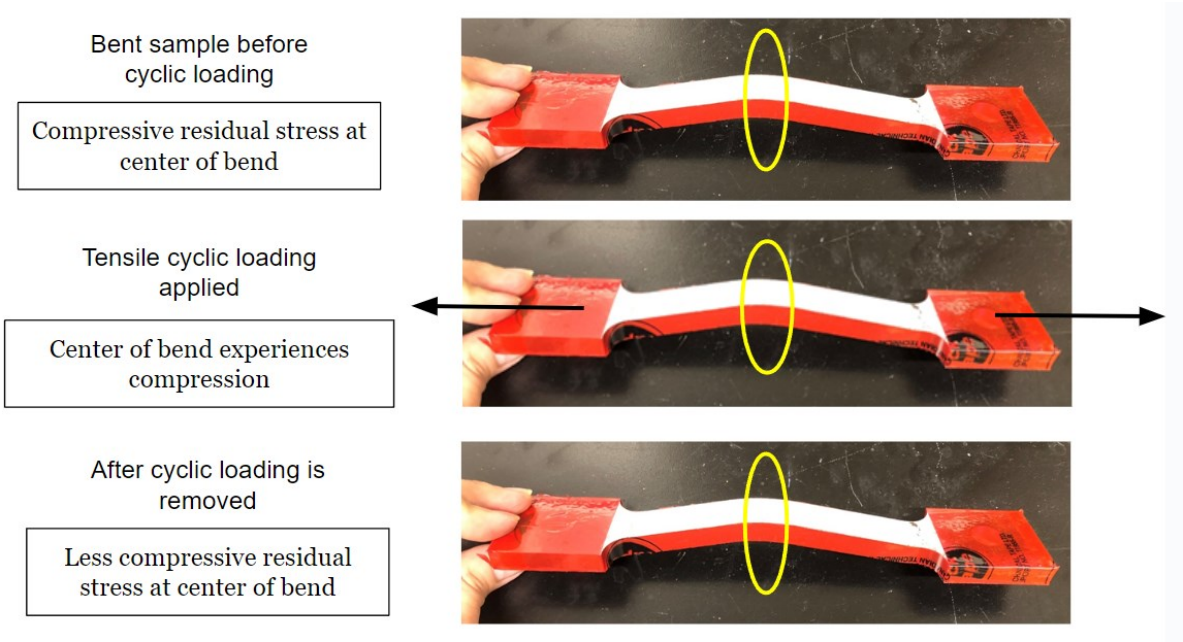

Figure 52: How applied cyclic loading changes stress state at the center of outward bend. When cyclic loading is being applied, the center of bend experiences compression. After cyclic loading is removed, the compressive residual stress decreases at the center of bend.

As most of the samples in this study experience a compressive stress on the corrosion surface, microcracks and crack initiation continues to occur, even though Van Boven et al. discuss that cracking only occurs in a small range of tensile residual stresses. To understand this circumstance, Chen et al. examine the residual stress distribution in the depth direction of SCC and non-SCC areas. Figure 53 shows the results of the experiment [34]. At 0.25 mm depth, which is close to the top surface, SCC areas experience a compressive stress, while non-SCC areas are in tension. As one goes further in depth, the SCC areas show more tensile stress that is in the cracking zone, while the residual stress in non-SCC areas is tensile, but out of cracking range. This happens because the stress distribution in the depth direction balances each other, creating a higher tensile stress as depth increases. Pitting - the first step of NNpHSCC crack initiation - can also occur

under compressive stress, and when the bottom of the pit reaches the depth where residual stress becomes tensile and in the crack initiation zone, cracking can occur. As pit grows, however, the local stress at the bottom of the pit would also change, making the stress state more complicated.

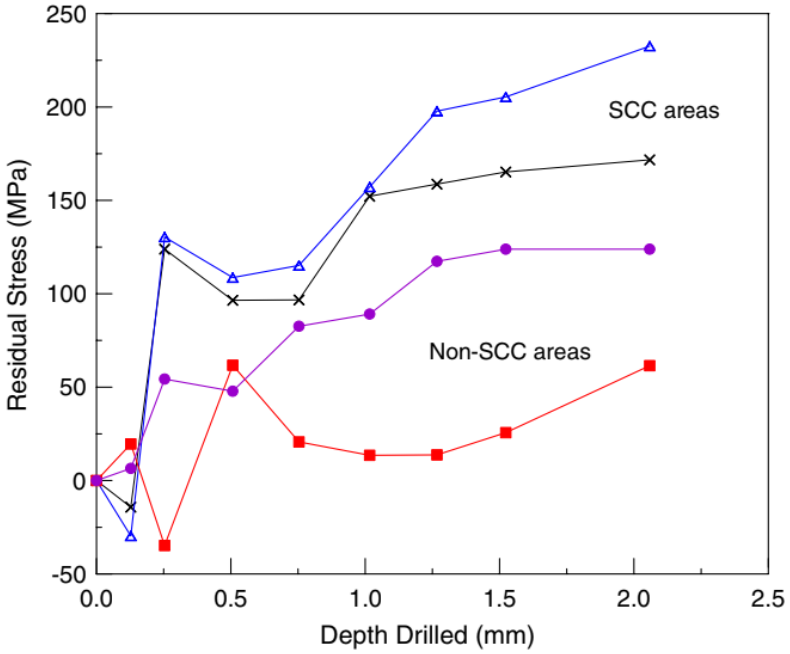

Figure 53: Residual stress in wall thickness using hole drilling technique [34].

4.6.2 Pits coalescence

The number of pits and cracks in this study is determined by manually counting them on the surface of the samples. However, in a corrosive environment, more scenarios can occur to surface pitting causing errors in counting and hence, a shift in the experimental results. Pit coalescence is a common phenomenon in corrosion, where two smaller pits merge into one another, creating a pit with a larger opening. Because the surface is directly exposed to the corrosive environment, the corrosion rate at the surface is a lot faster compared to anywhere inside

the material. This explains the high width to depth ratio commonly seen in NNpHSCC pits. With less exposure to corrosive environments, the speed of pit growth at the bottom of pits decreases, and with mechanical stress, cracking takes over and becomes the main mechanism at stage II NNpHSCC.

Pit coalescence is seen on all samples in this study, especially at highly dense pitting locations. Figure 54 shows an example of pit coalescence found in this study. There are three smaller pits merging in this Figure. When more time and mechanical loading is allowed, the three small pits will coalesce, creating only one large pit. The evidence of pits with large openings is shown in Figure 55. When pit coalescence happens, it is difficult to accurately determine the number of pits initiated from the original surface. Therefore, pitting occurrences change slightly with longer test durations, making it difficult for counting pits on the surface.

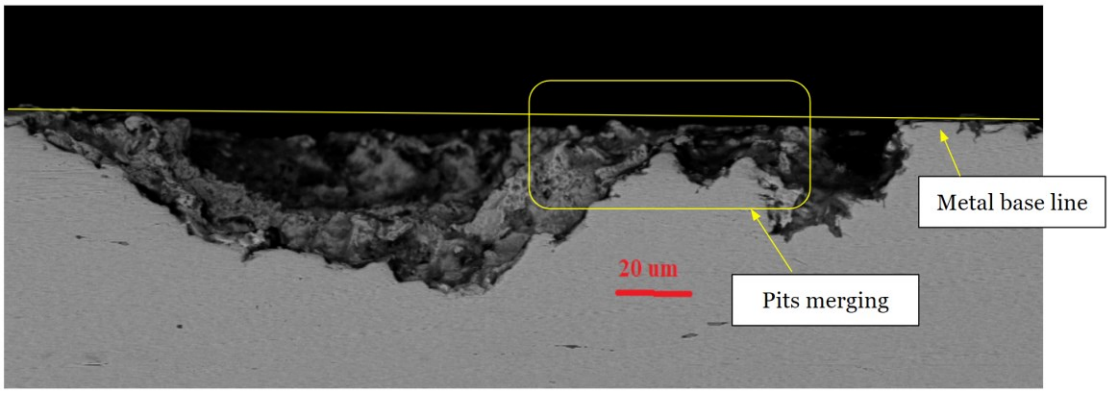

Figure 54: Pits merging.

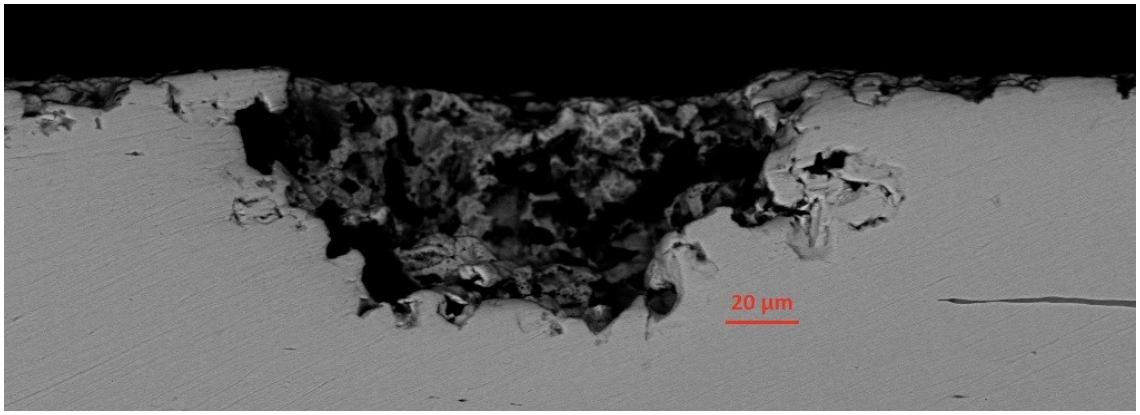

Figure 55: Large pit as a result of pit coalescence. There are a few smaller pits around the large pit, indicating a high pit concentration area.

Moreover, as cracks are observed in 2D, many cases can happen instead of crack initiating into the material in the depth direction. Pitting can extend in any direction on the surface, and crack can grow on the surface to connect pits [45]. Similarly, crack growth in the width direction inside the specimen body is also not considered. These growth directions are still possible in mode I fracture mechanics, because the cyclic loading direction is perpendicular to the possible cracking directions.

4.6.3 Effect of mill scale on SCC

Mill scale is a thin oxide layer formed on the steel surface as a result of steel forming or treatment process, including hot rolling, forging, and heat treatment [51]. Mill scale consists of hematite (Fe_2O_3), magnetite (Fe_3O_4) and wustite (FeO), varying depending on the steel type and the temperature of the process, but is generally porous and defected [51-53]. Steel pipelines found in the field typically have a mill scale covered surface, and the mill scale layer forms a galvanic cell with the steel underneath [27,51,52]. Because of this, the corrosion process in pipeline steel is accelerated, and areas with defected mill scale show signs or severe localized corrosion [52]. After

a period of corrosion in the NNpH solution, the mill scale will flake off, revealing the hidden steel surface.

Wang et al.'s study discusses the corrosion process on an as-received mill scale covered surface, shown in Figure 56 [51]. Wang et al. show that there are 3 stages of corrosion in mill scale covered surfaces. During the first stage, the outer layer of mill scale, consisting of **γ**-FeOOH, is removed by dissolution, and the layer following, which is unstable, can be broken off, causing breakage in the mill scale and hence localized corrosion. The second stage begins after some time of corrosion, where more steel underneath is exposed to the corrosive environment and more mill scale gets washed off. At this stage, the precipitation of $FeCO_3$ - the main corrosion product found in NNpHSCC - becomes more prominent. When most of the mill scale has flaked off, stage 3 begins. Stage 3 is mostly general corrosion on the exposed surface, with little to no barrier between the steel surface and the corrosive environment [51].

Mill scale plays an important role in how NNpHSCC is initiated on steel surface. As the surface of the samples in this study is not polished, a thin layer of mill scale is found on the as received sample (sample #1). Figure 57 shows the mill scale layer found in sample #1. The mill scale layer is about 20 μm thick, and can be of different thickness at various locations. When the mill scale layer is present, it can act as a protective layer on top of the sample. With short duration immersion tests, mill scale does not fully dissolve, and the steel surface remains untouched underneath the mill scale layer. In order for corrosion to occur, firstly, the mill scale layer needs to be broken or defective to expose the metal underneath.

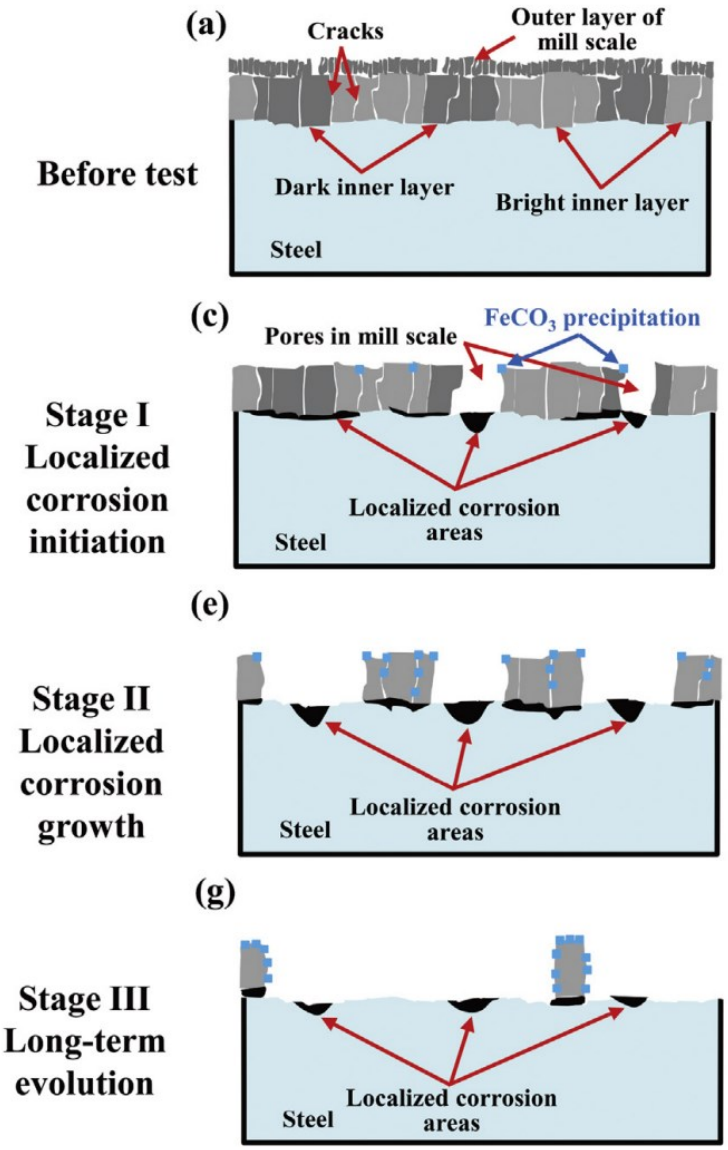

Figure 56: The 3 stages of corrosion on mill scale covered steel surface [51].

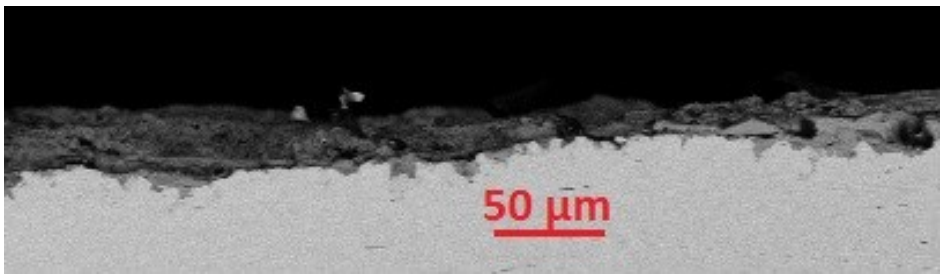

Figure 57: Mill scale covering the surface of sample #1.

During bending, the brittle mill scale is cracked, particularly at the center of outward bending. As outward bending occurs, the top surface is stretched out, and the mill scale layer adhere to the surface is broken off. The breaking of mill scale creates a more open surface for corrosion at the center of bend, and the corrosive solution gets to the steel underneath more readily than any point along the surface. Therefore, more pitting is seen at the center of bend for samples, even though the center of bend undergoes a more compressive residual stress. This also explains the peak seen in corrosion without cyclic loading samples. Without cyclic loading to change the residual stress distribution, the samples still show a significant number of corrosion pits. These pits occur as a result of the cracking of the mill scale layer, making mill scale a crucial factor in stage I NNpHSCC.

It is evident that many pits found are covered in mill scale, showing that mill scale remains covering pits in many locations. Figure 58 shows a mill scale covered pit. The mill scale adheres to the bottom of the pit, indicating that the pit has been there before hot rolling. It is also seen that the mill scale is cracked, making a galvanic cell with the steel underneath, and the corrosive solution is allowed to flow underneath the mill scale layer. When more time is allowed, the pit will grow deeper into the material, and the mill scale will also dissolve in the solution.

There are also many pits without mill scale covering, as seen in Figure 59. However, it remains unclear if these pits are present before hot rolling and their mill scale is removed during the experiment, if they are a result of galvanic corrosion just before the mill scale is removed, or purely from pitting on the surface. Regardless of the corrosion mechanism, the effect of mill scale needs to be taken into account when studying NNpHSCC on the as-received, mill scale covered surface.

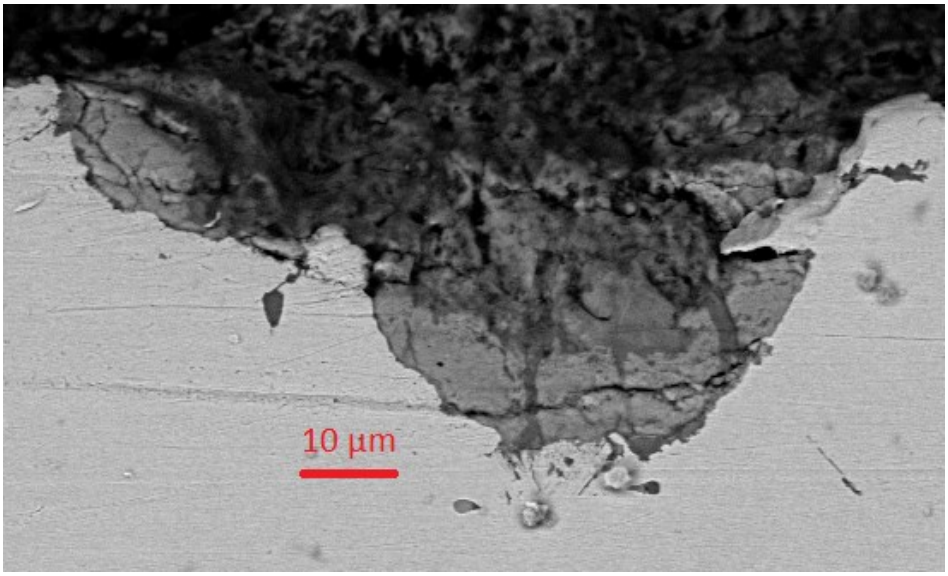

Figure 58: A mill scale covered pit found in the experiment.

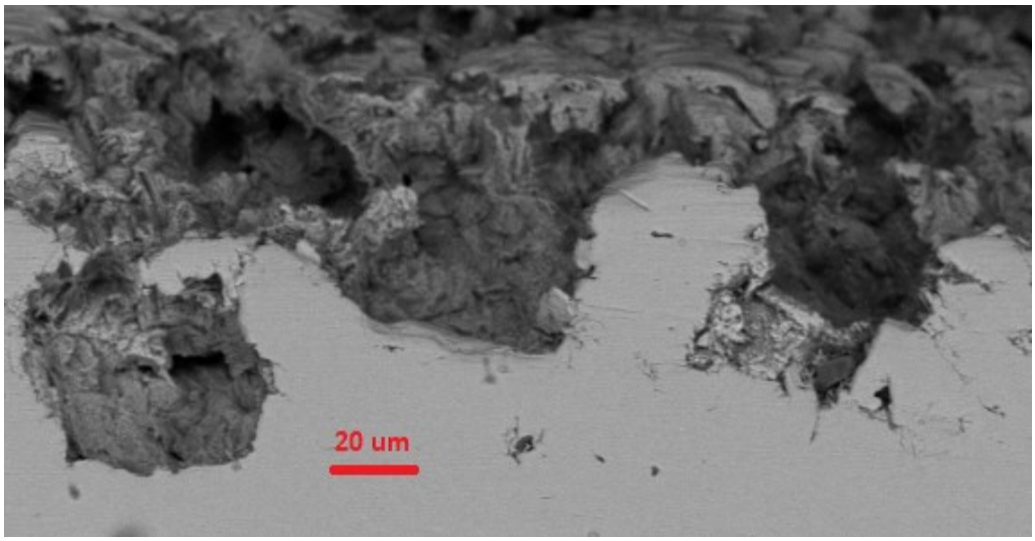

Figure 59: Pitting areas without mill scale protection.

CHAPTER 5

CONCLUSIONS

Different mechanical loading conditions are introduced to study the effect of maximum load on the crack initiation and growth in NNpHSCC at bends in pipelines. The crack initiation and growth mechanism is a pitting and pit-to-crack-transition mechanism, and cyclic loading modifies the residual stress distribution near the bending point. It was determined that in outward bending conditions where the center of bend experiences a compressive stress, pit and microcracks are still observed. Moreover, a lower maximum load causes pitting to concentrate at the center of bend in outward bending samples. It was discovered that higher maximum stress causes a higher compressive stress at the center of outward bending, therefore, pitting is minimized when higher maximum loads are applied.

The effect of bending angles was also discussed. While +20 degree bending provides a more aggressive condition for pits to form, +40 degree bending supports the growth of larger pits and microcracks. The +40 degree bending angle has a more compressive residual stress at the surface, therefore the residual stress profile within the depth direction is more profound, causing pit and crack growth.

The cut edge was found to experience a higher stress than the other surfaces, causing more pitting to occur along the edge. However, this condition is not considered in the field environment, and edging does not pose a threat to field pipelines. Excluding the edge might provide a more accurate analysis on the number of pits, but the effect is minimal when all the surfaces are considered. Moreover, as pipe curvature and springback are considered, modelling using FEM becomes challenging as there are many limitations with this method.

The localized residual stress was found to play a key role in pit growth and crack initiation. While the specimen surface experiences a compressive residual stress, pitting can still occur, but as pitting grows into the material, the localized residual stress at the pit tip can be in the "cracking range", and hence cracking can still occur. Predicting the crack shape and morphology is challenging, and blunt cracks are difficult to distinguish from growing pits. Pit coalescence can also happen, changing the results of the study. Moreover, pitting behaviour is a 3D phenomenon, and the growth direction cannot be predicted with this study.

Deeper pits are generally found on sample edges, as edging provides a stress concentrator similar to grain boundaries. Edging should be removed to correctly assess the number of larger pits developed on testing specimens. However, edging does not change how pits and cracks are distributed along the sample length, indicating that the role of cyclic loading and residual stress overcomes the edging effect.

Lastly, mill scale needs to be considered when studying the pits and crack initiation in NNpH environments. Surface defects aid in stage I NNpHSCC, but mill scale changes the surface exposure, as well as produces galvanic corrosion. In outward bending samples, the mill scale layer is broken at the center of bend, making the area more susceptible to pitting compared to anywhere else along the surface. Without the breakage of mill scale, the steel underneath is not exposed to NNpH environment, and SCC will not occur.

This work has provided significant insights in the study of C-SCC. By combining the residual stress factor from bending and different mechanical loading conditions, the study provides an understanding of the interaction between applied tensile stress and compressive residual stress. Studies on bending stress and NNpHCF cracks in the circumferential direction are still limited, and crack initiation and growth depends on many factors. This study provides an understanding

on how bending and applied stress factors interact with each other, causing pit and crack initiation. By understanding how applied stress changes the residual stress distribution, a resulting stress can be predicted in similar cases, and the pit and crack behaviour of the material can also be determined.

CHAPTER 6

FUTURE WORK

This study has provided the first step in studying how pits and cracks behave in bend sections with changes in cyclic loading conditions. In order to further investigate the NNpHCF behaviour, crack growth study in bent pipelines would be sufficient. Moreover, to understand how tensile stress changes the residual stress distribution within the samples during and after stress is applied, stress distribution modeling and residual stress measurements can be done on test specimens. Modeling would provide a general idea of how applied cyclic loading changes the stress profile in the sample, while residual stress measurements provide the actual stress after any applied stress is removed.

While the study of stress factor on NNpHCF is important, the geometry factor of pits can also be considered with change in bending angle and mechanical loading. As pits grow deeper into the material, the stress state at the bottom of the pit also changes, and more research needs to be done on how pitting affects residual stress and NNpHCF. Pitting study can also be done on polished surface, which removes surface defect and mill scale factor to purely understand the effect of dissolution and mechanical loading. However, the results would need to be modified to closely represent the field conditions.

The study is performed on outward bending samples, which has a compressive stress at the center of bend on the surface. Applying tensile mechanical loading increases the stress in the samples. However, with inward bending samples that experience a tensile residual stress, an applied tensile mechanical loading will decrease the stress in the samples. Because of the different interacting mechanisms, a study on inward bending conditions would be supportive to this study. It is also important to note that only the outer surface of the original pipeline is exposed to the

corrosive environment. Even though the inner surface experiences a tensile residual stress, the surface is not exposed to NNpH solution for a more accurate depiction of the condition seen in the field. If a similar study is done on inward bending angles, the outer surface would be bent inwardly, and the inner surface with compressive residual stress would be covered.

From the results of this study, a lower maximum applied stress shows more pit and crack initiating at the center of bend. The lowest maximum stress condition in this study is 15% of SMYS. It is still unclear whether a further decrease in maximum load would follow a similar trend, or if 15% of SMYS approximates the stress threshold for pit and crack initiation. Therefore, more experimental data with lower maximum load would be extremely helpful in the mechanical loading study of NNpHCF.

REFERENCES

[1] R. Goodfellow and K. Jonsson, "Pipeline Integrity Management System (PIMS)," in *Oil and Gas Pipelines: Integrity and Safety Handbook*, 1st edition, 2015, John Wileys & Sons, Inc. Edited by R. W. Revie.

[2] National Energy Board, "Public Inquiry Concerning Stress Corrosion Cracking on Canadian Oil and Gas Pipelines," *National Energy Board*, MH-2-95, Nov 1996.

[3] Y. F. Chen, "Fundamentals of Stress Corrosion Cracking," in *Stress Corrosion Cracking of Pipelines*, 1st edition, 2013, John Wileys & Sons, Inc.

[4] V. S. Sastri, "Introduction and Forms of Corrosion," *Challenges of Corrosion: Costs, Causes, Consequences, and Control*, 1st edition, 2015, John Wileys & Sons, Inc.

[5] R. H. Jones, "Stress-Corrosion Cracking," *ASM Handbook, Corrosion: Fundamentals, Testing, and Protection*, vol 13A, 346-366, 2003.

[6] G. H. Koch, "Stress-Corrosion Cracking and Hydrogen Embrittlement," *ASM Handbook, Fatigue and Fracture*, vol 19, 483-506, 1996.

[7] Eliaz et al., "Characteristics of hydrogen embrittlement, stress corrosion cracking and tempered martensite embrittlement in high-strength steels," *Engineering Failure Analysis*, 9 (2002), 167-184.

[8] T. R. Jack and B. Erno, "Generation of Near Neutral pH and High pH SCC Environments on Buried Pipelines," in *Corrosion*, *NACE International*, 362, 2000.

[9] Yan et al., "Factors affecting the generation of high-pH environments required for stress corrosion cracking (SCC)," *International Pipeline Conference*, *ASME*. ICP 2012, 90515.

[10] J. A. Beavers and B. A. Harle, "Mechanisms of high-pH and near-neutral-pH SCC of underground pipelines," *International Pipeline Conference, ASME*. IPC 1996, 1860.

[11] Beavers et al., “High-pH SCC: Temperature and potential dependence for cracking in field environments,” *International Pipeline Conference, ASME*. IPC 1998, 2050.

[12] B. N. Leis and R. J. Eiber, “Stress-Corrosion Cracking On Gas-Transmission Pipelines: History, Causes, and Mitigation,” *First International Business Conference on Onshore Pipelines*, Berlin, Dec 1997.

[13] W. Chen, “Modeling and prediction of stress corrosion cracking of pipeline steels,” *Trends in Oil and Gas Corrosion Research and Technologies*, 30, 2017. https://doi.org/10.1016/B978-0-08-101105-8.00030-9

[14] L. Niu and Y. F. Cheng, “Corrosion behaviour of X-70 pipeline steel in near-neutral pH solution,” *Applied Surface Science*, 253 (2007) 8626-8631. doi:10.1016/j.apsusc.2007.04.066

[15] R. Singh, “Hazards and threats to a pipeline system,” in *Pipeline Integrity - Management and Risk Evaluation, Elsevier*. 2017, 35-88. https://doi.org/10.1016/B978-0-12-813045-2.00005-3

[16] Zheng et al., “Recent Progress in the Study of Transgranular SCC in Line Pipe Steels,” *Corrosion - Deformation Interactions CDI’96*, 28.

[17] Y. F. Cheng and R. Norsworthy, “Coating Failure and Pipeline Stress Corrosion Cracking,” in *Pipeline Coatings*, *NACE International*. 121-147, 05, 2016.

[18] Song et al., “Hydrogen Permeation Through the Passivation Film on Iron by Time-Lag Method,” *J. Electrochem Soc.* 137, 1703, vol 6, 1990.

[19] Colwell et al., “Crack initiation of line pipe steels in near-neutral pH environments,” in *Environment-Induced Cracking of Materials, Vol 2 - Prediction, Industrial Developments and Evaluation*. 233-242, 02 (2008).

[20] Shirazi et al., “A review on current understanding of pipeline circumferential stress corrosion cracking in near-neutral pH environment,” *Engineering Failure Analysis*. 148 (2023) 107215. https://doi.org/10.1016/j.engfailanal.2023.107215

[21] Chen et al., “Environmental effects on near-neutral pH stress corrosion cracking in pipelines,” in *Environment-Induced Cracking of Materials*. Vol 2 (2008) 211-220. https://doi.org/10.1016/B978-008044635-6.50059-5

[22] M. J. Wilmott, “Factors influencing stress corrosion cracking of gas transmission pipelines: detailed studies following a pipeline failure. Part 1: Environmental considerations,” *International Pipeline Conference, ASME*. Vol 1, IPC 1996, 1856.

[23] Gu et al., “Transgranular Stress Corrosion Cracking of X-80 and X-52 Pipeline Steels in Dilute Aqueous Solution with Near-Neutral pH,” *Corrosion, NACE International.* Vol 55, 03, 0010-9312, 1999.

[24] *Line Pipe*, API Specification 5L, 46th edition, 2018.

[25] M. Baker Jr., “Understanding Stress Corrosion Cracking (SCC) in Pipelines,” *OPS TTO8 - Stress Corrosion Cracking Study Final Draft*. R8_GMP, 2004.

[26] Kushida et al., “Effects of Metallurgical Factors and Test Conditions on Near-neutral pH SCC of Pipeline Steels,” *Corrosion, NACE International*. 2001, 01213.

[27] Y. F. Cheng, “Understanding Pipeline Stress Corrosion Cracking,” in *Stress Corrosion Cracking of Pipelines*, 1st edition, 2013, John Wileys & Sons, Inc.

[28] G. H. Koch, “Stress-Corrosion Cracking and Hydrogen Embrittlement,” *ASM Handbook, Vol 19: Fatigue and Fracture*. 483-506, 1996. DOI: 10.1361/asmhba0002388

[29] R. R. Fessler and M. Sen, “Characteristics, causes, and management of circumferential stress-corrosion cracking,” *Proceedings of the 2014 10th International Pipeline*

Conference, ASME. ICP 2014, 33059.

[30] Parkins et al., "Transgranular Stress Corrosion Cracking of High-Pressure Pipelines in Contact with Solutions of Near-Neutral pH," *Corrosion, NACE International*. 0010-9312, 1994.

[31] W. Chen, "Modeling and prediction of stress corrosion cracking of pipeline steels," *Trends in Oil and Gas Corrosion Research and Technologies, Elsevier*. 2017. https://doi.org/10.1016/B978-0-08-101105-8.00030-9

[32] Zhao et al., "Statistical Analysis on Underload-Type Pipeline Spectra," *Journal of Pipeline Systems Engineering and Practice, ASCE*. ISSN, 1949-1190. (2016), 7(4) 04016007. DOI: 10.1061/(ASCE)PS.1949- 1204.0000241.

[33] Van Boven et al., "The role of residual stress in neutral pH stress corrosion cracking of pipeline steels. Part I: Pitting and cracking occurrence," *Acta Materialia, Elsevier*. 55 (2007) 29-42. doi:10.1016/j.actamat.2006.08.037

[34] Chen et al., "The role of residual stress in neutral pH stress corrosion cracking of pipeline steels - Part II: Crack dormancy," *Acta Materialia, Elsevier*. 55 (2007) 43-53. doi:10.1016/j.actamat.2006.07.021

[35] Chen et al., "Transgranular crack growth in the pipeline steels exposed to near-neutral pH soil aqueous solutions: The role of hydrogen," *Acta Materialia, Elsevier*. 57 (2009) 6200-6214. doi:10.1016/j.actamat.2009.08.047

[36] Wang et al., "Pre-cyclic-loading-enhanced Stage-1b stress corrosion crack growth of pipeline steels," *Corrosion Science, Elsevier*. 208 (2022) 110693. https://doi.org/10.1016/j.corsci.2022.110693

[37] Wang et al., "On the formation of stress corrosion crack colonies with different crack

population," *Corrosion Science, Elsevier*. 168 (2020) 108592. https://doi.org/10.1016/j.corsci.2020.108592

[38] D. W. Hoeppner, "Model for Prediction of Fatigue Lives Based Upon a Pitting Corrosion Fatigue Process," *ASTM*. 1979.

[39] Katona et al., "A Review of the Governing Factors in Pit-to-Crack Transitions of Metallic Structures," *Corrosion*. ISSN 0010-9312, 1938-159X. (2023) 79 (1): 72-96. https://doi.org/10.5006/4179

[40] Fang et al., "Pit to crack transition in X-52 pipeline steel in near neutral pH environment Part 1 - formation of blunt cracks from pits under cyclic loading," *Corrosion Engineering, Science and Technology. The International Journal of Corrosion Processes and Corrosion Control*. ISSN: 1478-422X. 1743-2782, 45:4, 302-312. https://doi.org/10.1179/147842208X386304

[41] Turnbull et al., "Challenges in modelling the evolution of stress corrosion cracks from pits," *Engineering Fracture Mechanics, Elsevier*. 76 (2009) 633-640. doi:10.1016/j.engfracmech.2008.09.004

[42] Balbin et al., "Pit to crack transition and corrosion fatigue lifetime reduction estimations by means of a short crack microstructural model," *Corrosion Science, Elsevier*. 180 (2021) 109171. https://doi.org/10.1016/j.corsci.2020.109171

[43] Chen et al., "A coupled mechano-chemical peridynamic model for pit-to-crack transition in stress-corrosion cracking," *Journal of the Mechanics and Physics of Solids, Elsevier*. 146 (2021) 104203. https://doi.org/10.1016/j.jmps.2020.104203

[44] *Fitness-for-service*, API 579-1/ASME FFS-1, 2021.

[45] *Manual for Determining the Remaining Strength of Corroded Pipelines*, ASME B31G,

2012.

[46] Nelson et al., “Temperature and loading frequency effects in the mechanism for NNpH SCC of pipeline steel,” *Proceedings of the 14th International Pipeline Conference*. IPC 2022, 87794.

[47] Najjar et al., “Influence of critical surface defects and localized competition between anodic dissolution and hydrogen effects during stress corrosion cracking of a 7050 aluminium alloy,” *Materials Science and Engineering, Elsevier*. A238 (1997) 293-302. PII S0921-5093(97)00369 -9

[48] M. Vasquez and B. Zinn, “Physics,” in *Applied Mathematics for Safety Professionals - Tips, Tools and Techniques to Solve Everyday Problems*. American Society of Safety Professionals (ASSP). 2010.

[49] Chu et al., “Stress Corrosion Cracking of an Aluminum Alloy under Compressive Stress,” *Metallurgical Transactions A*. Vol 16A, 1985.

[50] Z. Xu, “Introduction of Project of Circumferential Cracking Management,” *University of Alberta*. 2021. Internal presentation, not published.

[51] Wang et al., “Near-neutral pH corrosion of mill-scaled X-65 pipeline steel with paint primer,” *Journal of Materials Science and Technology, Elsevier*. 49 (2020) 166-178. https://doi.org/10.1016/j.jmst.2020.01.016

[52] Been et al., “The role of hydrogen in EAC of pipeline steels in near-neutral pH environments,” *SCC and Hydrogen Embrittlement of Pipeline Steels: Prediction, Industrial Developments and Evaluation*. Vol 2, 2008, 255-266. https://doi.org/10.1016/B978-008044635-6.50063-7

[53] Ghods et al., “Microscopic investigation of mill scale and its proposed effect on the

variability of chloride-induced depassivation of carbon steel rebar," *Corrosion Science, Elsevier*. 53 (2011) 946-954. doi:10.1016/j.corsci.2010.11.025

APPENDIX

A1. Effect of edging on pits and cracks distribution

The effect of edging is not significant when the pits and cracks distribution along the surface length is considered. Figure A1-3 show how removing the edge slice from analysis can affect the distribution. Little to no difference is observed between the two, which confirms that the effect of maximum load and residual stress are more significant to the pits and cracks distribution along the sample length.

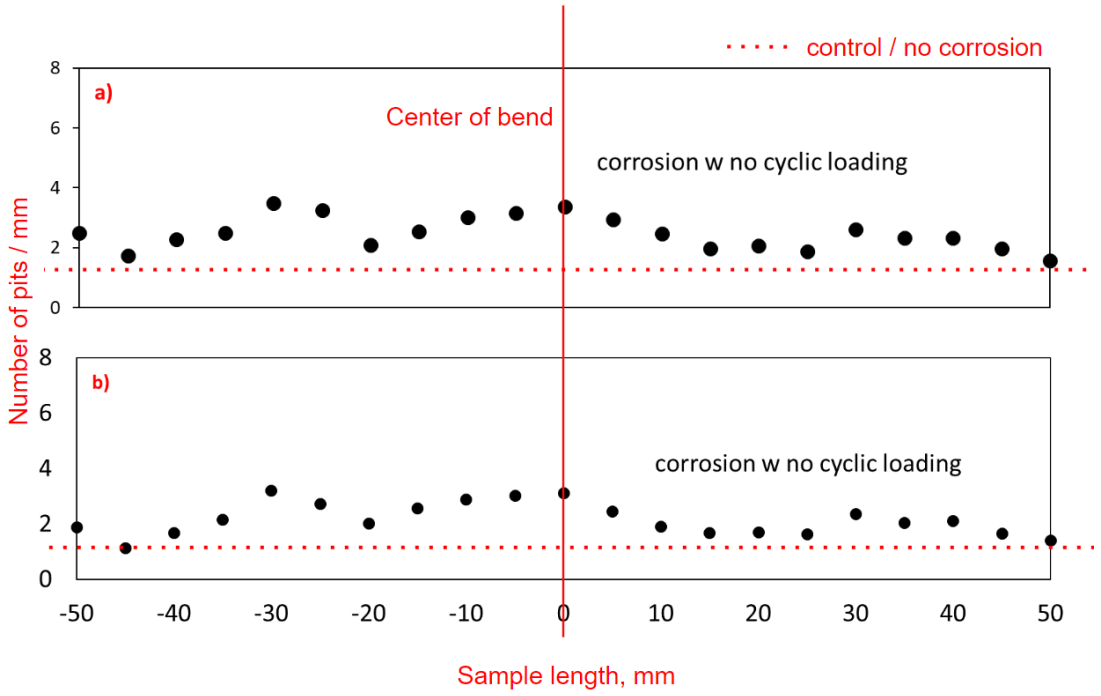

Figure A1: Pits distribution along sample length in sample #2: +20 degree bending corrosion without cyclic loading, a) including edge, b) excluding edge.

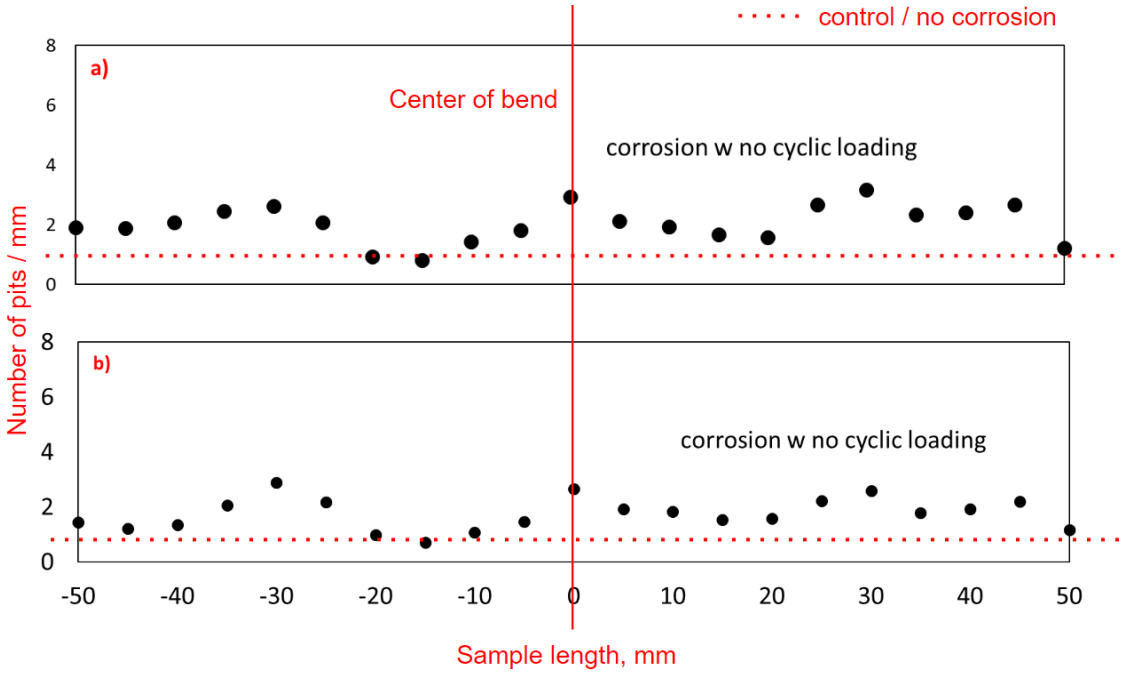

Figure A2: Pits distribution along sample length in sample #3: +40 degree bending corrosion without cyclic loading, a) including edge, b) excluding edge.

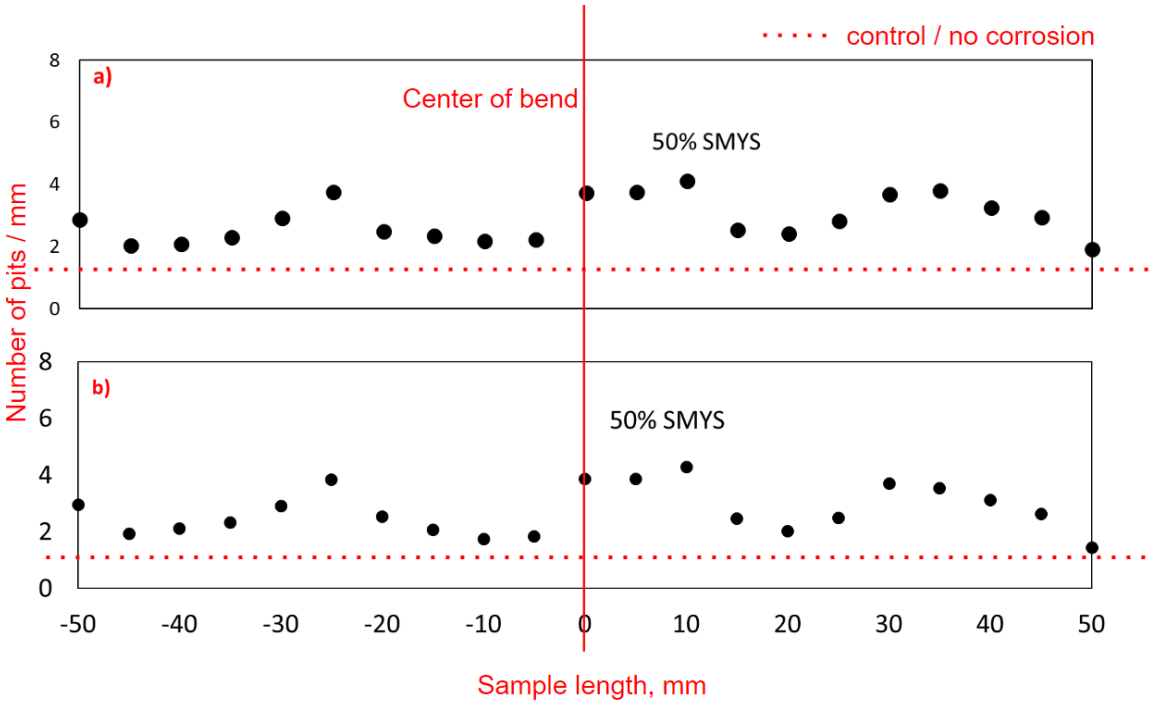

Figure A3: Pits distribution along sample length in sample #4: +20 degree bending, 50% of SMYS cyclic loading, a) including edge, b) excluding edge.

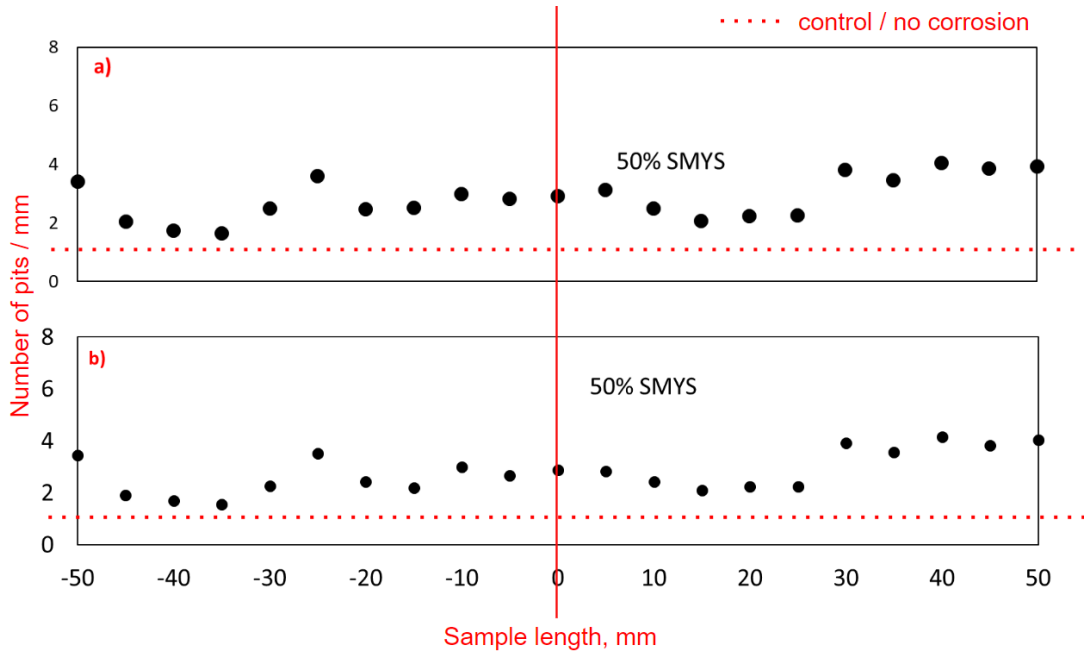

Figure A4: Pits distribution along sample length in sample #5: +40 degree bending, 50% of SMYS cyclic loading, a) including edge, b) excluding edge.

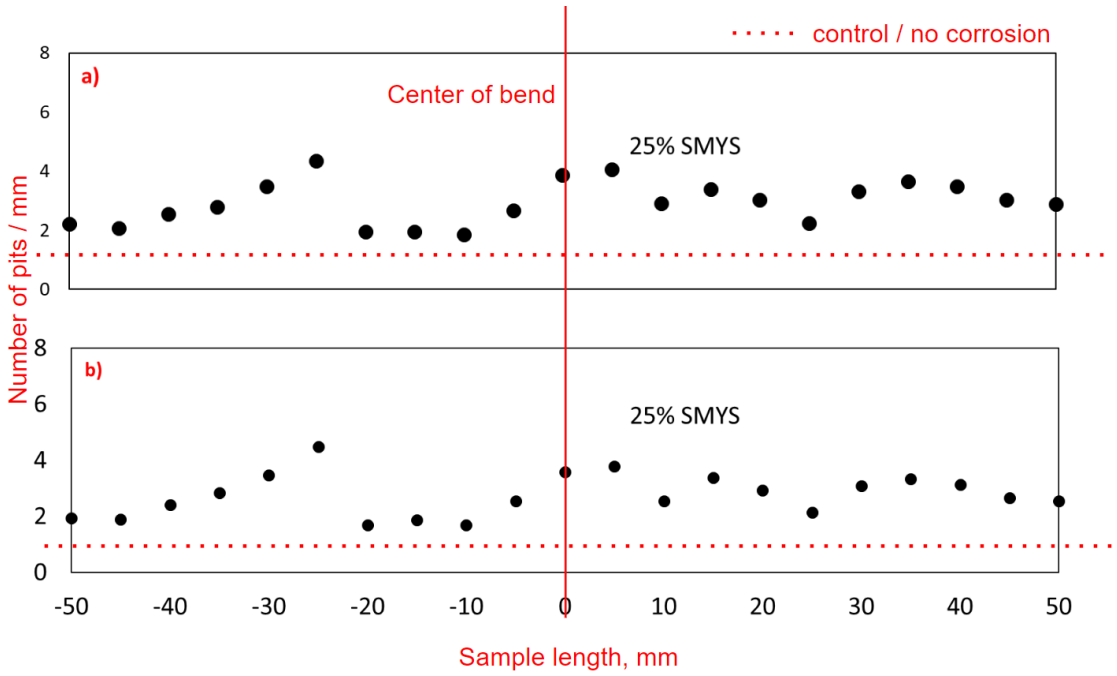

Figure A5: Pits distribution along sample length in sample #7: +40 degree bending, 25% of SMYS cyclic loading, a) including edge, b) excluding edge.

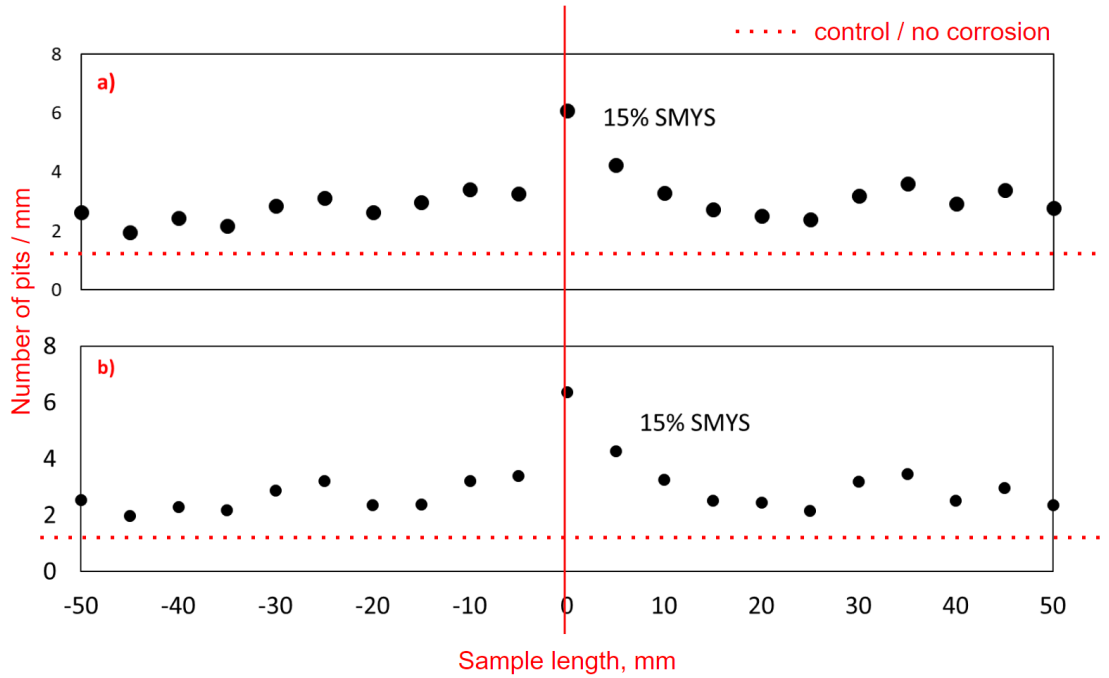

Figure A6: Pits distribution along sample length in sample #8: +20 degree bending, 15% of SMYS cyclic loading, a) including edge, b) excluding edge.

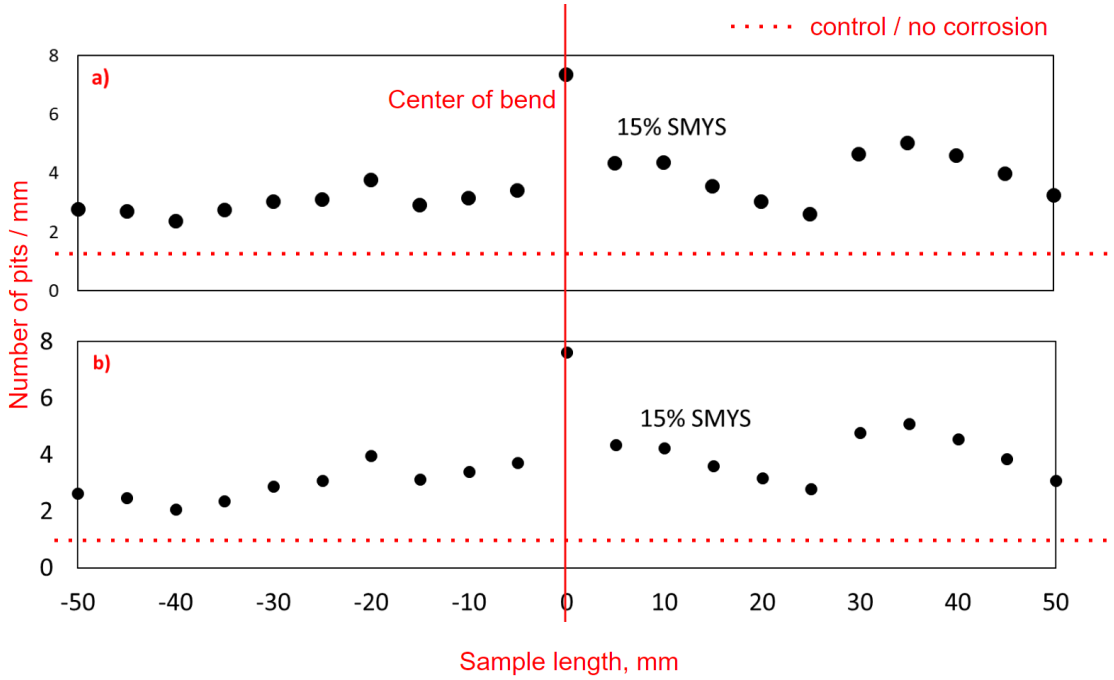

Figure A7: Pits distribution along sample length in sample #9: +40 degree bending, 15% of SMYS cyclic loading, a) including edge, b) excluding edge.